NOTICE

The quality of this microform is heavily dependent upon the quality of the original thesis submitted for microfilming. Every effort has been made to ensure the highest quality of reproduction possible.

If pages are missing, contact the university which granted the degree.

Some pages may have indistinct print especially if the original pages were typed with a poor typewriter ribbon or if the university sent us an inferior photocopy.

Reproduction in full or in part of this microform is governed by the Canadian Copyright Act, R.S.C. 1970, c. C-30, and subsequent amendments.

AVIS

La qualité de cette microforme dépend grandement de la qualité de la thèse soumise au microfilmage. Nous avons tout fait pour assurer une qualité supérieure de reproduction.

S'il manque des pages, veuillez communiquer avec l'université qui a conféré le grade.

La qualité d'impression de certaines pages peut laisser à désirer, surtout si les pages originales ont été dactylographiées à l'aide d'un ruban usé ou si l'université nous a fait parvenir une photocopie de qualité inférieure.

La reproduction, même partielle, de cette microforme est soumise à la Loi canadienne sur le droit d'auteur, SRC 1970, c. C-30, et ses amendements subséquents.

Canada

Neutral Plane of single Piles in Clay Subjected to Surcharge Loading

Hossam Esmail

A Thesis In
The Department of Civil Engineering

Presented in Partial Fulfillment of the Requirements
for the Degree of Master of Applied Science at
Concordia University
Montreal, Quebec, CANADA

March 1996

ISBN 0-612-10844-9

ABSTRACT

Neutral Plane of Single Piles in Clay Subjected to Surcharge Loading

Hossam Esmail

Numerical model was developed to analize the negative skin friction and the location of the neutral plane on a single pile embedded in clay. The clay layer was allowed to consolidate under the effect of surcharge loading. Finite element technique together with the soil models of the Modified Cam Clay and the Mohr-Coulomb were used in developing the numerical model. The numerical model was compared well with the available field data. The model was then used to conduct parametric studies in order to determine the sensitivities of the governing factors affecting the location of the neutral plane and accordingly the pile capacity.

Based on the results of the present investigation, design charts and design procedures for the Modified Cam Clay and Mohr-Coulomb soil models are presented. Conclusion and recommendations for future work are given.

ACKNOWLEDGEMENTS

I would like to express my sincere gradtitudes to my supervisor, professor ***A. M. Hanna***, for his valuable guidance, constant support and encouragement that he provided me throughout the course of this work, which made it possible to complete this research. I am honored to carry out the present investigation under his supervision.

The financial support from Natural Science and Engineering Research Council of Canada, NSERC is highly appreciated.

I wish also to thank my family, my wife and children for their patience and support during the preparation of this thesis.

TABLE OF CONTENTS

CHAPTER 4
RESULTS AND ANALYSIS

LIST OF SYMBOLS

SYMPOL	REPRESENTS
A	Area.
CSL	Critical State Line.
Cu	Ultimate shear stress.
D or d	Pile Diameter.
du	Excess pore water pressure.
ESP	Effective Stress Path.
E	Young's Modulus.
e	Voids Ratio of Soil.
fn	Factor of safety on drag load.
fp	Factor of safety on the permanent load.
f_Q	Factor of safety on ultimate bearing capacity.
fs	Frictional Stress Along Pile Shaft.
f_t	Factor of safety on the transient load.
ecs	Critical State Voids Ratio.
H	Height.
κ	Slope of the Swelling Line.
Ko	Coefficient of Earth Pressure at rest.
Kp	Coefficient of permeability.
L	Length.
M	Frictional Coefficient of Soil.

n	number of piles.
N	Value of v when P' = 1 on the NCL.
N_o	Vesic Coefficient.
NCL	Normal Consolidation Line.
o	Circumference of Pile.
P' or P_o	Mean Normal Effective Stress.
P'c	Size of Current Yield Locus.
Pn	Downdrag force.
Pp	Permanent load.
Pt	Transient load.
q	Deviator stress.
Q_f	Negative Friction.
Qu	Maximum Drag Force.
s	Spacing between piles.
S	Surcharge Load.
SSBS	Stable State Boundary Surface.
Su	Undrained shear strength.
v	Specific Volume of soil.
v_k	Value of v when P' = 1 on the Swelling Line.
α	Coefficient for undrained stress method.
β	Coefficient for drained stress method.
γ	Unit weight.
ϕ	angle of Shearing Resistance.

ψ &ω	Relative settlement
τ	Shear stress.
τ_s	Skin friction.
δ	Angle of pile-soil Friction.
μ	Poisson ratio.
λ	Slope of the Critical State Line in P'-v Space.
σ_1	Major Principal Effective Stress.
σ_3	Minor Principal Stress.
σ_v'	Vertical Effective Stress.
Γ	Value of v when P' = 1 on the CSL.
η	Stress Ratio.

LIST OF TABLES

LIST OF FIGURES

CHAPTER 1

INTRODUCTION

1.1 PREFACE

Pile foundations are usually recommended for structures founded on deep soft deposits. Although these piles are normally designed to be directly loaded through their caps, it is quite often that they could be indirectly loaded through the surrounding soils.

The design theories for pile foundations dictates that, under direct loading condition, the pile moves downward while the surrounding soils remain in location. This mechanism will generate skin friction along the shaft which will be positive in sign and further it will contribute to the increase of pile capacity. On the other hand, if the surrounding soil was subjected to direct loading, this will cause consolidation of the soil and consequently settlement or downward movement of the soil layer surrounding the pile. Depending on the resulting relative movement of the soil/pile system, pile may be subjected to a negative skin friction on a portion or the full length of its shaft.

The downward movement of the surrounding soils can arise from one or more of the following:

1. Settlement of soils under its own weight.

2. Settlement of soil due to primary cosolidation under the influence of direct loading such as embankments or surcharge fills, grading fills for surface drainage or other reasons.

3. Secondary consolidation of soils.

4. Philological creep of soils.

5. Subsidence of an area caused by an increase of effective stresses in soils due to lowering of the groundwater table or extraction of subsurface fluids such as oil.

6. Settlement of the surrounding soils following pile driving. This is mainly due to remolding, heave and displacement of piles.

7. Compression of soils due to stresses imposed by shallow footings of a new adjacent structures (Young and Thorburn, 1981).

8. Subsidence resulting from disposal materials.

9. Compaction of a loose cohesionless surface layer by means of vibrating equipment or traffic (Chellis 1961).

This negative drag load could be large enough to overstress the pile, cause excessive settlement of the surrounding layer and even shear failure in the entire mass.

The negative skin friction depends on the type of soil into which the pile is installed, the manner of installation and the amount and rate of relative movement between the soil and the pile.

Negative skin friction is induced in the upper portion of the pile, resulting in an increase of the pile load from zero at the pile head to a maximum at the depth of equilibrium, below which the load decreases by being transferred to the soil by means of the positive shaft resistance.

The plane at which the skin resistance changes its direction, i.e from a negative friction to a positive one is called the neutral plane.

The neutral plane is the depth at which the shear stress along the pile changes from negative skin friction to positive shaft resistance. It is also the depth where no relative displacement occurs between the pile and the soil.

1.2 RESEARCH OBJECTIVES

The objective of this research program is directed to the determination of the depth of the neutral plane and accordingly the evaluation of the negative and positive skin friction contribute to the pile capacity, specifically:

a- To conduct a literature review on negative skin friction and the location of the neutral plane.

b- To develop a numerical model, using finite element technique.

c- To compare the theoretical values produced by the numerical model with those obtained from the existing theories and available laboratory and field data.

d- To conduct a parametric study on the factors affecting the depth of the neutral plan. These factors are pile diameter, pile length, magnitude of surcharge and soil parameters.

e- To simulate the soil strength using the critical state and Mohr-Coulomb soil models.

f- To develop a design procedure together with design charts for the determination of the neutral plane and the negative skin friction.

1.3 SCOPE OF THE THESIS

A review of the literature for the negative skin friction is given in chapter 2. Chapter 3 describes the formulation of the finite element proposed for the numerical model with a brief review of the critical state soil mechanics theory. The results and the analysis are given in chapter 4. Finally the conclusion and recommendations are presented in chapter No. 5.

CHAPTER 2

LITERATURE REVIEW

2.1 GENERAL

In literature several reports can be found to deal with skin friction of pile foundations. While the majority of them evaluating the positive skin friction, little or non were published with respect to the evaluation of the negative skin friction and its contribution to pile capacity., However no theories were developed to predict the distribution and accordingly the neutral plane for pile foundations subjected to indirect loading.

2.2 REVIEW OF PREVIOUS WORK

Terzaghi and Peck (1948) suggested that the shear strength of the soil is mobilized along the full length of the individual piles or along the perimeter of pile groups thus assuming that the neutral point is located at the bearing stratum as shown in (Fig. 2.1)

In case of a single pile, downdrag is the perimeter area multiplied by the shear strength.

$$P_u = f_s \cdot \pi \cdot D \cdot L \quad \text{..... (2.1)}$$

where D is the pile diameter and f_s is the frictional stress along the pile shaft.

In case of a group of piles, it is assumed that the entire weight of the fill within the cap is carried by the piles in addition to the perimeter shear within the fill and the clay

$$Q_1 = \gamma_f \cdot a \cdot b \cdot H_f / n \quad \text{..... (2.2)}$$

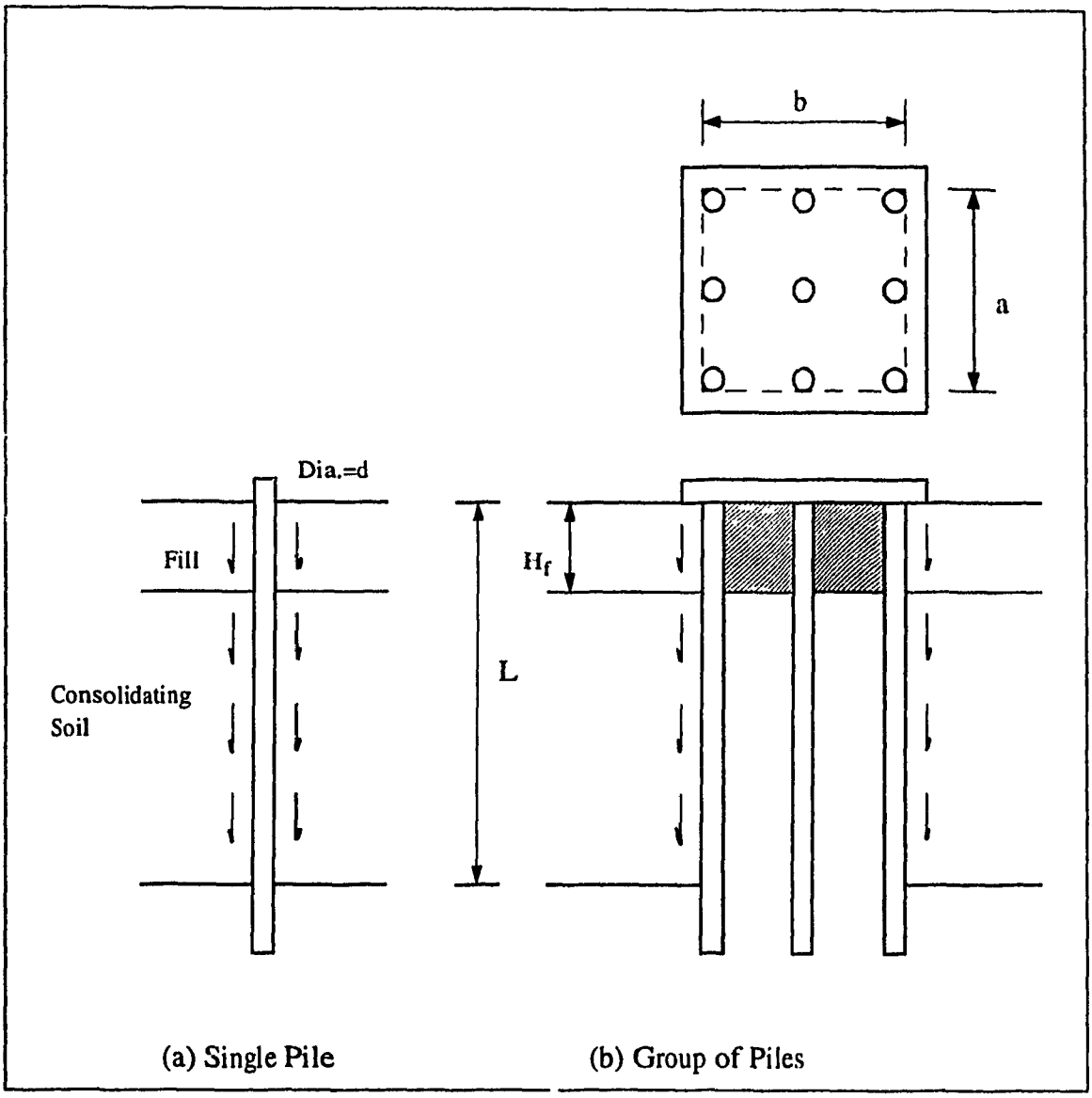

Fig. 2.1 Negative skin friction on piles.
(After Terzaghi and Peck, 1946)

$$Q_2 = f_s \cdot 2\,(a + b) \cdot L / n \quad \text{..... (2.3)}$$

$$Q_{total} = Q_1 + Q_2 \quad \text{..... (2.4)}$$

where

Q_1: downdrag force caused by the fill

Q_2: downdrag force due to perimeter shear within the fill and the clay

L : depth of embedment of pile

n : number of piles in a group

H_f : height of fill

γ_f: unit weight of fill

In order to reduce negative skin friction on the pile group a maximum distance of 2.5 the pile diameter between piles centre to centre was suggested.

Hansen (1968) proposed a method to calculate the skin friction for a single pile and pile groups. A general theory was developed for floating piles lightly loaded and allowed to settle a finite amount which is sufficient to mobilize friction. The theory was extended to cover negative skin friction where surcharge was placed directly on the surrounding soils. Due to this load the vertical stress throughout the layer was increased due to hang-up tendency caused by the presence of the pile. The vertical effective stress was accordingly reduced close to the pile shaft and the reduction in stress was given by the expression ($4f_s$) where f_s is the frictional stress along the pile shaft for a single pile determined from a dimensionless coefficient. In case a pile groups he proposed the relation [$4f_s$ (1+1.7 d/s)] where "d" is the diameter of the pile and "s" is the spacing between piles centre to centre. Since the compression of the soil would change to expansion (if the resulting

vertical stress decreased) the actual negative skin friction at any point of the pile will be limited by the following expression

$$f_s < S/(4+6.8d/s) \quad \text{.....} \quad (2.5)$$

Concerning the effects of pore water pressure change on negative skin friction Hansen postulated that a ground water lowering in clay will have the same effect as a surcharge load. Consequently the resulting negative skin friction can be calculated by means of the preceding expression. Excess pore water pressures, "du" existing before the execution of the piles (or induced as a result of the driving of the piles) will dissipate and accordingly will increase the effective stresses which may produce negative friction. However a negative friction will reduce the vertical stresses, and when this reduction is everywhere equal to du, the negative friction cannot increase further, thus giving un upper limit of f_s as **du/(4+6.8 d/s).**

Endo et al (1969) cited the existence of a neutral point, (Fig. 2.2) who conducted tests on unloaded piles at a site at Tokyo. The soil was approximately 43m thick alluvium whose undrained shear strength varied from 89 kPa to 178 kPa at 40m below the ground. Four types of piles were used in order to determine the downdrag load difference between open and closed, friction and end-bearing piles.

Piles of 609.6 mm diameter were driven at 10 m spacing to avoid group action. It was reported that driving stresses were measured using wire strain gauges, yet under the test conditions "differential transformer type gauges" were used because of reliability for long durations. Settlement records, started after the piles were driven, indicated the maximum surface settlements of 120mm/yr reducing to 30mm/yr after 3.5 years [from time of

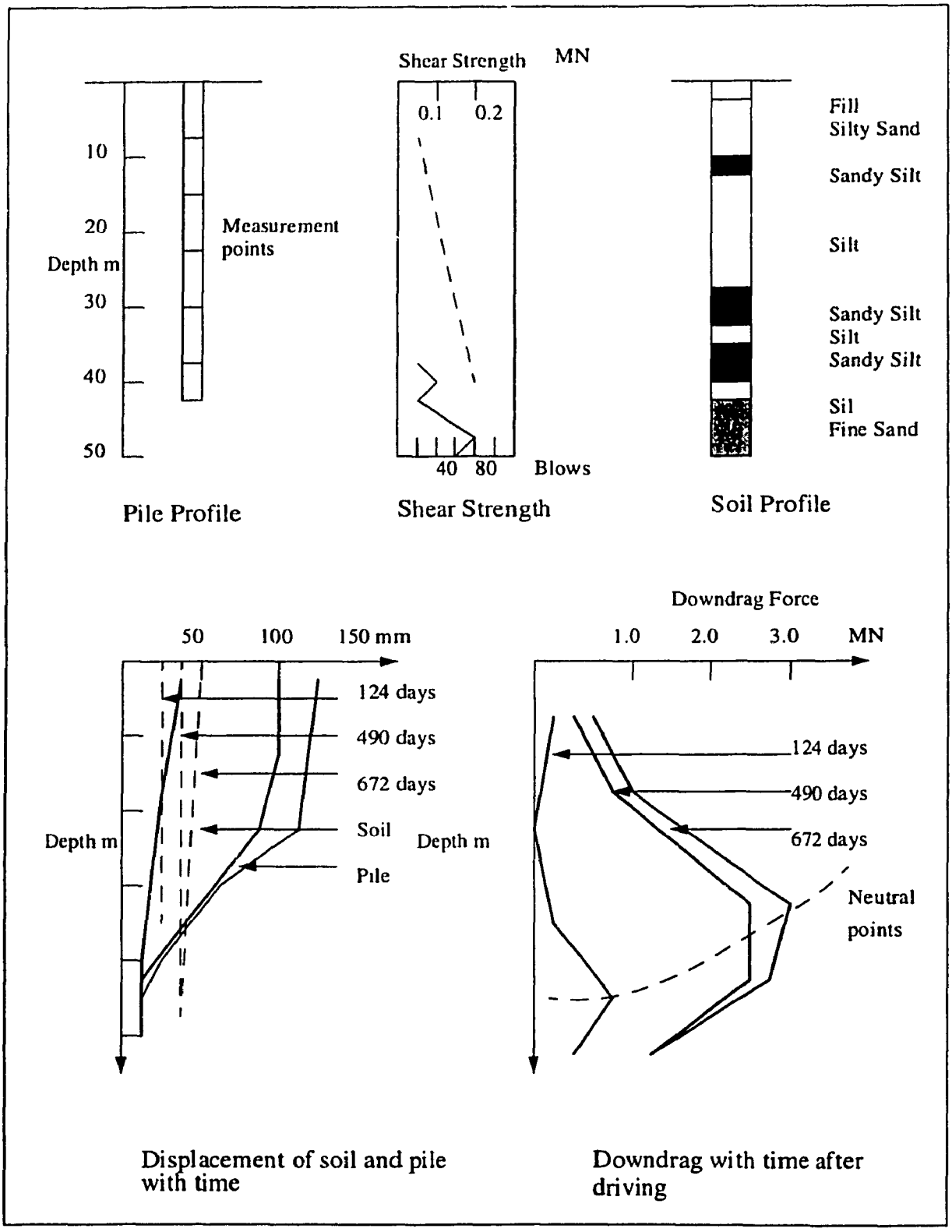

Fig. 2.2 Pile test at Tokyo.
(After Endo et al, 1969)

piling). Considerable settlement as explained by the authors, must have occurred during pile driving because of the loose fine sand stratum (standard penetration test-value of 10). Test results showed that the soil at each pile settled 118mm as compared to 172 mm. which was measured at a distance of 1.0m from the pile surface. This difference in settlement was attributed to the hanging-up effect of the soil around the pile. Pile head settlement were given, but no records were made of the settlement of sand at the toe level. It would have been interesting to have known the settlement in the lower soil deposits. The settlement at toe level are of great interest when considering the relative displacement of the pile-soil interface. Initially one would have expected a neutral point to have existed almost at that level and then decreased in depth as the low region became more compressed due to the process of consolidation.

Fellenius (1972) carried out a test program in Sweden on two instrumented precast concrete piles driven through 40m of soft clay and 15m into underlying silt and sand. The program consisted of two phases of study, The first phase was to study the influence of the driving and the following reconsolidation of the clay. The duration of this phase was 495 days started immediately after pile driving and up to the stage of pile loading. The second phase was to study the influence of load applied on the head of the pile which took 800 days started after load application up to the end of the measurements.

It was noticed tl at immediately after pile driving, the forces in the pile increased rapidly and the rate of load increase became linear after 5-7 months. The total downdrag load after 495 days was 55 tones. 30 tones of which corresponded only to reconsolidation of the clay due to pile driving and the rest was due to regional settlement.

The negative friction was compared with the shear strength as being 30% of the undrained shear strength or about 10% of the effective overburden pressure as shown in (Fig. 2.3). After completion of the 495 days, the piles were loaded by 44 tons which was followed a year later by an additional 36 tons thus making a total load of 80 tones. In both load increments the negative skin friction in the upper two thirds of the piles was eliminated while the load at the bottom of the clay layer was only slightly affected. The force at the pile tip was not affected and that was attributed to the existence of positive skin friction near the pile tip in the silt and sand layers.

Fellenius therefore presented a design approach which takes negative skin friction into consideration in determining the allowable load on single piles. The main feature of the recommended approach is that the permanent and transient working loads should be treated in connection with negative skin friction.

The bearing capacity of a single pile consists of a tip resistance $Q_{u\ tip}$ and a positive skin resistance $Q_{u\ skin}$ in the non-settling soil layer as shown in (Fig. 2.4). After determining the ultimate bearing capacity Q_u the maximum drag load $P_{n\ max.}$ can be estimated from the known strength properties of the settling soil without applying the usual reduction of the shear strength. If a transient load P_t on the pile head is smaller than twice the drag load $P_{n\ max.}$ i.e $\mathbf{P_t < 2\ P_{n\ max.}}$, the transient load will not be added to the load in the lower portion of the pile. Thus only the permanent load P_p on the pile head has to be considered. i.e the following equation applies:

$$\mathbf{P_p < Q_{u\ tip} + Q_{u,\ a\ skin} - P_n} \quad \text{.....(2.6)}$$

Fellenius recommended partial factors of safety to be applied due to the different nature of the factors and the above equation becomes

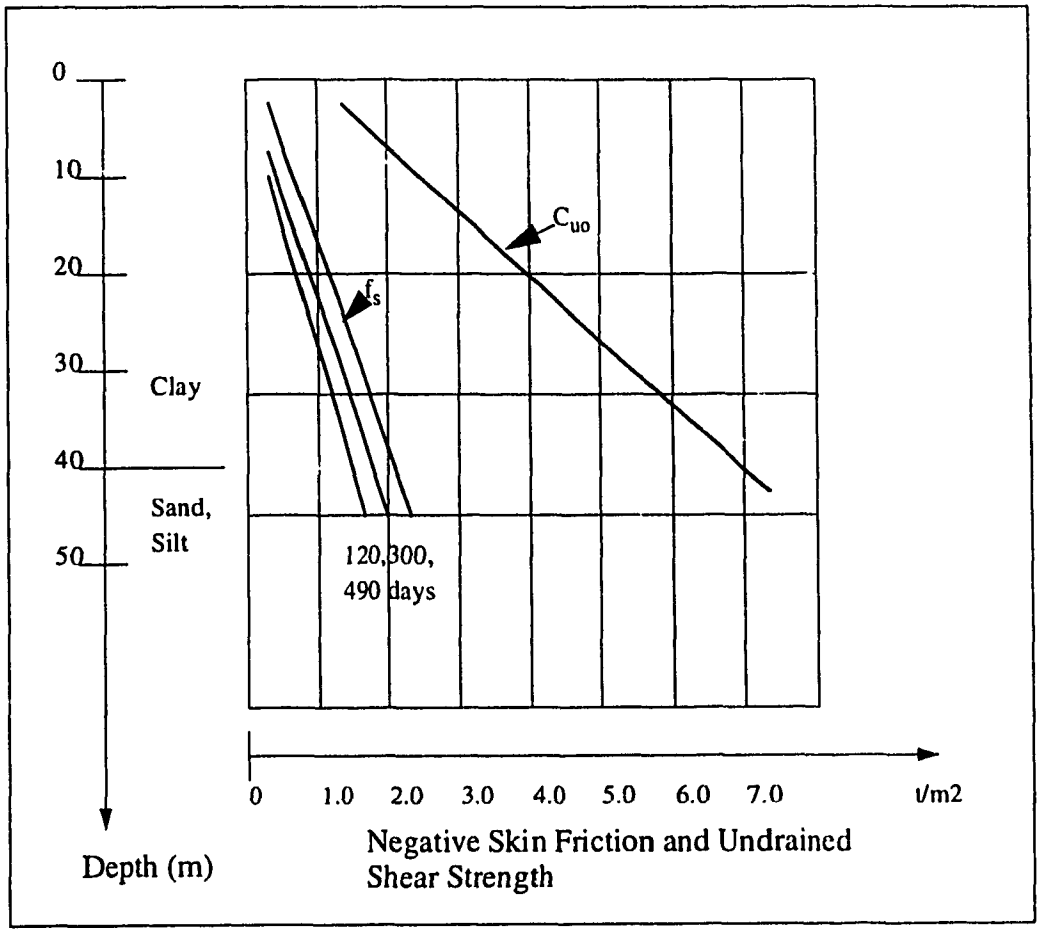

Fig. 2.3 Negative skin friction of a single pile versus the undrained shear strength of clay .(After Fellenius, 1972)

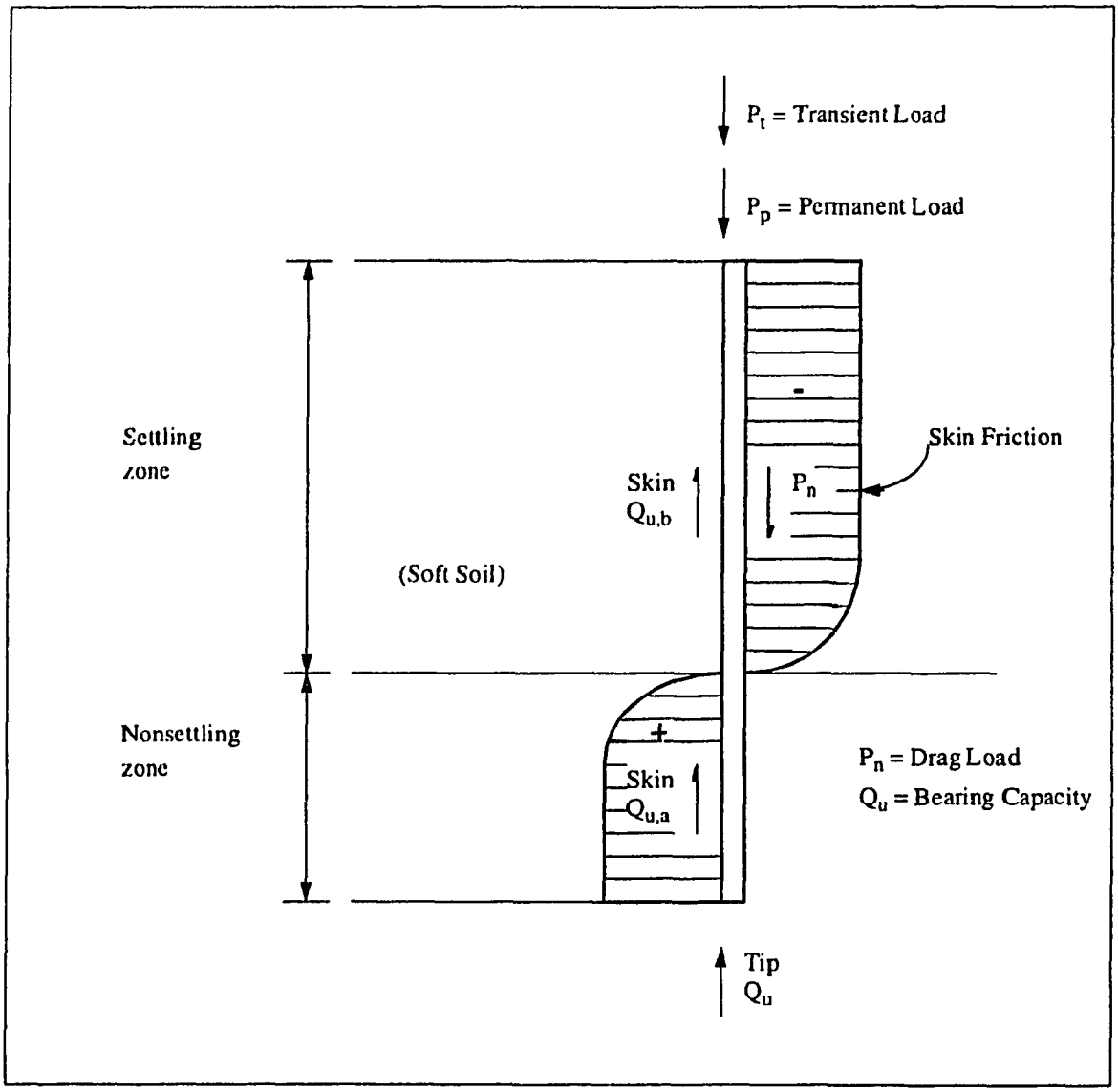

Fig. 2.4 Unit Skin Friction Along a Single Pile in an upper Layer of Soft Settling Soil and a Layer of Nonsettling Soil. (After Fellenius,1972)

$$f_p \cdot P_p < (1/f_Q) \cdot (Q_{u\ tip} + Q_{u,\ a\ skin}) - f_n \cdot P_n \quad \text{..... (2.7)}$$

where

fp: factor of safety on the permanent load, Pp.

f_Q: factor of safety on the ultimate bearing capacity of the pile, Qu.

fn: factor of safety on the drag load, Pn.

when 2 Pn max. < Pt, positive skin friction will then develop along the entire length of the pile and the equation 2.7 becomes

$$f_t \cdot P_t + f_p \cdot P_p < (1/f_Q) \cdot Q_u \quad \text{..... (2.8)}$$

where

ft: factor of safety on the transient load, Pt.

Bozozuk (1973) carried out an investigation using a 300mm diameter and 49m deep hollow steel pipe pile which was instrumented and driven vertically on the centre line of 9m high by 27m wide granular approach fill into an underlying marine clay. The size and distribution of skin friction generated in the floating pile over a period of 5 years was reported and compared with the predicted values which based on the insitu horizontal effective stresses and the influence of embankment loading. The unit skin friction exerted along the surface of the pile was determined from the load distribution curve and compared with the strength of the surrounding soil. Assuming plane strain conditions and using the linear elastic theory proposed by Perloff et al (1967), both vertical and horizontal stresses exerted on the foundation clay under the center line of the embankment were determined.

Observation on the behavior of the foundation soil under the embankment were

made of six settlement gauges and four piezometers which provided measurements of settlement from the ground surface up to a depth of 44m and excess pore water pressures from 6m to 27m respectively. In carrying out the prediction analysis Bozozuk introduced the following equations

$$f_s = M \cdot K_o \cdot \sigma_v' \cdot \tan \phi' \quad \text{..... (2.9)}$$

where

f_s : frictional stress along pile shaft

M: friction factor for the soil acting on the pile surface,

$M = \tan \delta' / \tan \phi'$ (a value of 0.7 was selected for the type of soil at site)

K_o:coefficient of earth pressure at rest

σ_v':vertical effective stress

ϕ' : effective friction angle of the soil

δ' : effective friction angle between pile and soil.

At the end of cosolidation, the total negative skin friction load accumulated up to a depth D from the ground surface is given by the following equation

$$P_u = \beta_1 \cdot o \cdot D^2/2 \quad \text{..... (2.10)}$$

Where

D : depth from ground surface to neutral plane.

$\beta_1 : M \cdot K_o \cdot \gamma_{sub} \cdot \tan \phi'$

γ_{sub}: submerged unit weight of soil.

o : circumference of pile.

The above load will be resisted by the positive friction which is generated in the

zone from the depth D to its tip level, hence

$$P_{pos} = \beta_2 . o . (L^2 - D^2)/2 \quad \text{..... (2.11)}$$

Where

$$\beta_2 = \beta_1/[(L/D)^2 - 1] \quad \text{..... (2.12)}$$

To determine the location of neutral plane, Bozozuk assumed that the pile carried no load at end-bearing, then for equilibrium conditions, $P_{neg} = P_{pos}$, moreover and letting $\beta_1 = \beta_2$, then

$$D = L/\sqrt{2} \quad \text{..... (2.13)}$$

Regarding skin friction loads generated by the embankment the following expressions were obtained:

$$P_u = M . \tan \phi' . o . D . d\sigma_h' \quad \text{..... (2.14)}$$

$$P_{pos} = M . \tan \phi' . o . (L-D) . d\sigma_h' \quad \text{..... (2.15).}$$

Where

$d\sigma_h'$: average change in horizontal effective stress due to the embankment load for the required depth. (Fig. 2.5) shows the distribution of the stresses under center line of embankment.

During the 5 years period the ground surface settled 540 mm which was reduced to 18 mm at 44 m depth. The excess pore water pressure had completely dissipated at a depth of 15 m, showing it was still high at 27 m depth. The relative movements of the pile as compared to the one of soil has indicated small values in the upper part where the excess pore pressure had dissipated, then reducing to zero at a depth of 15 m. Below 21 m where the excess pore pressure were high, relative movement were very large increasing to 430

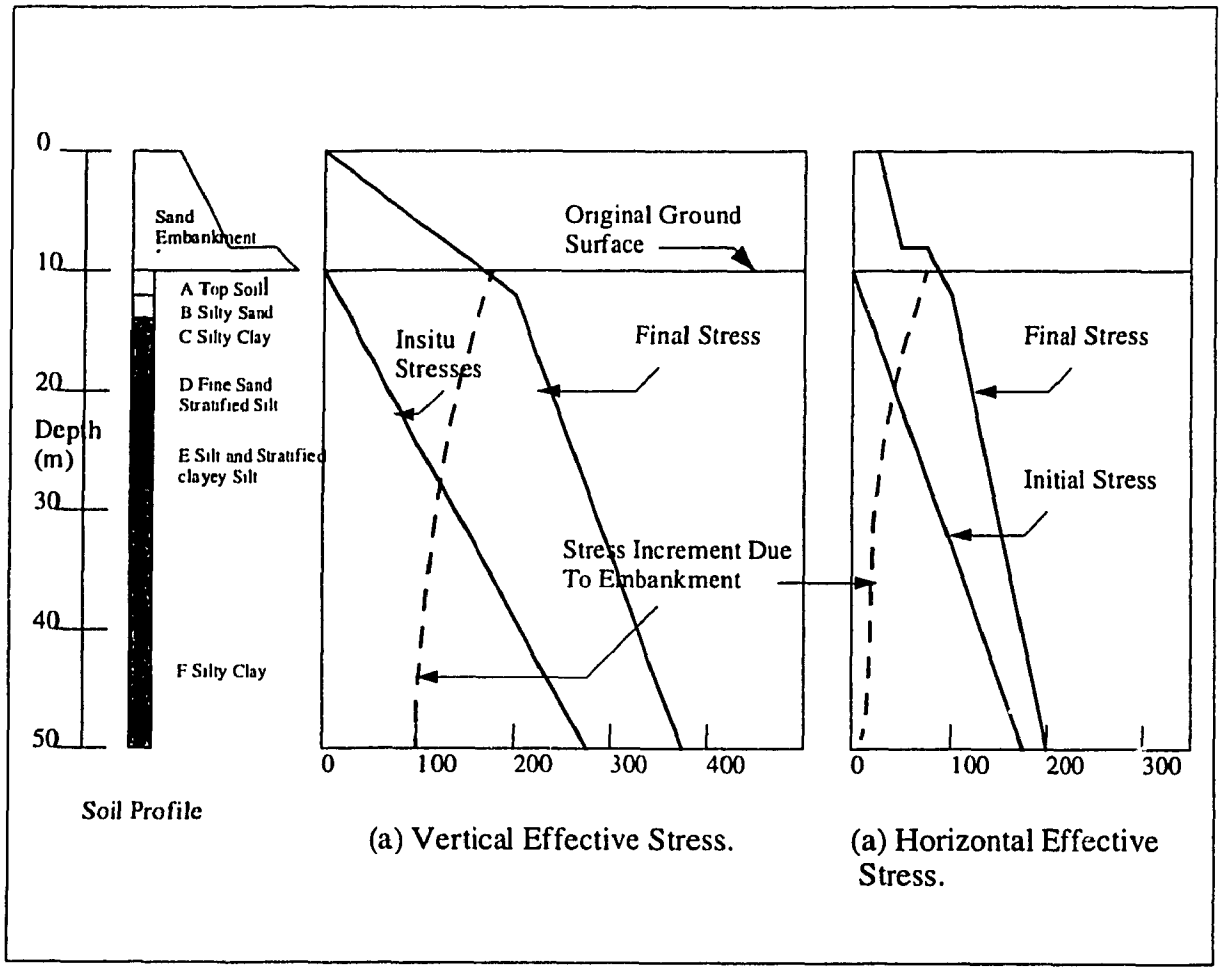

Fig. 2.5 Distribution of Vertical and Horizontal Stresses Under Centreline of Embankment
(After Bozozuk 1972)

mm at the bottom of the pile.

Bozozuk has compared the theoretical values of the skin friction to the experimental values, see Figure (2.6). It can be seen from this Figure that at 23-30 m from the top of the pile, the loads were transferred to a positive skin friction at a greater rate than was predicted, indicating that the values assumed for the friction factor, M, and the effective angle of shearing resistance, ϕ' were probably too small. However, Bozozuk attributed this to the 100% cosolidation assumed in the prediction analysis, i.e. as the 100% consolidation condition is approached, the family of positive skin friction curves will fan out and reach the predicted curves.

A comparison made between the skin friction and soil strength analysis indicated that there was little relation between the negative skin friction exerted on the pile and the in-situ shear strength of the soil. In fact where relative movements between pile and the soil were small and excess pore water pressure had dissipated, skin friction had approached but did not exceed the drained strength. On the other hand, where relative movements and excess pore water pressures were large, skin friction had decreased to the remolded strength.

Garlanger and lambe, (1973) made a comparison between the different methods of predicting negative skin friction on a steel H-pile for the cutler circle bridge in Revere, Massachusetts. The piles of one of the abutments was under duress from downdrag due to the compression of soft soils beneath the approach fill behind the abutment. Evidence that the piles had been subjected to downdrag included a 46 mm differential settlement of the approach slab, settlement and cracking of the slope protection beneath the bridge and

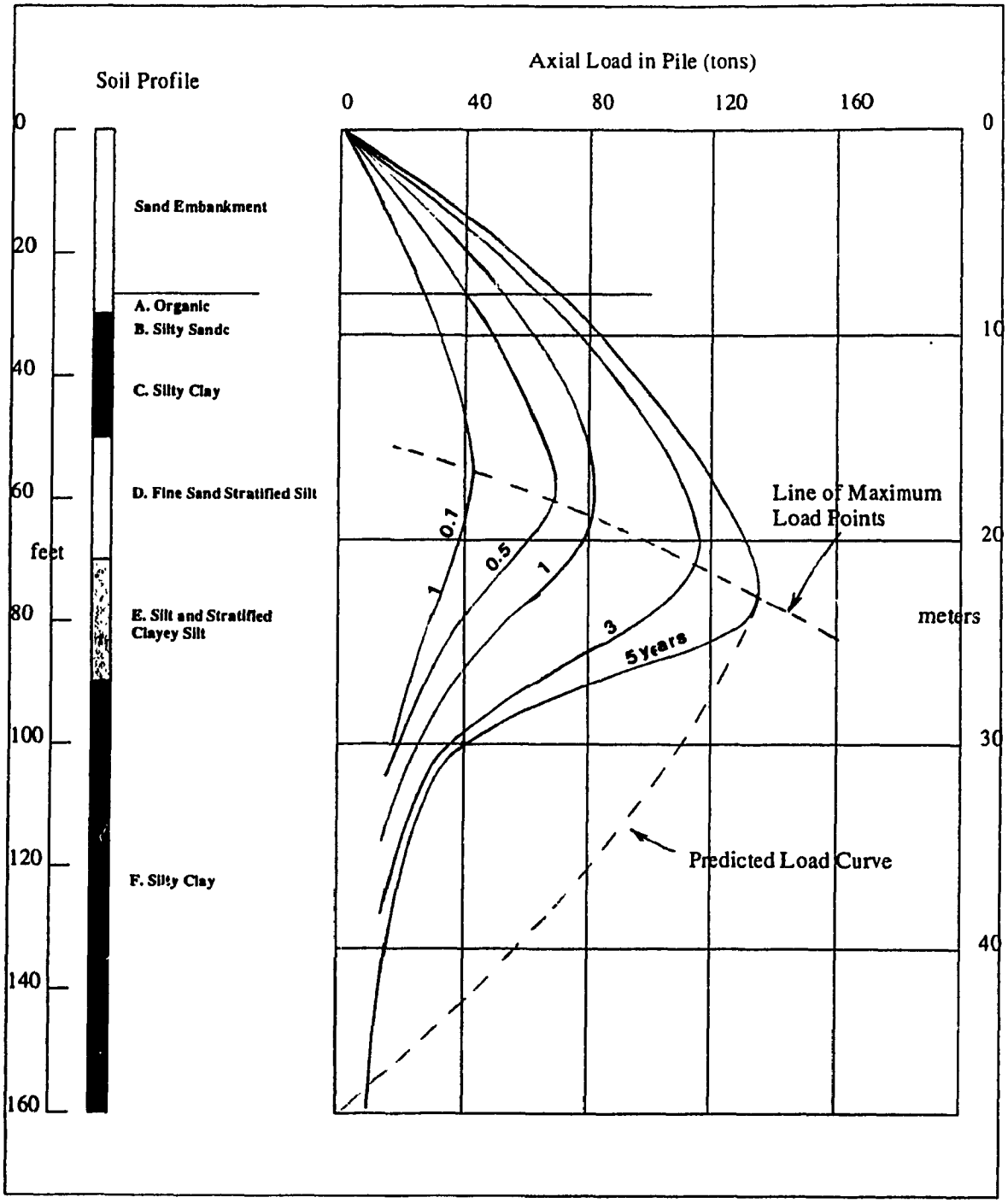

Fig. 2.6 Variation of Skin Friction Load in 300 mm Diameter Steel Pipe Pile with Time. (After Bozozuk 1972)

backward tilting of the abutment. The soil profile consisted of 7.6 m high approach fill overlying 4.0 m of sand followed by 15.2 m of soft clay and a dense glacial till.

Due to the fact that the piles were not instrumented prior to driving, a detailed program was planned and carried out to measure the downdrag load indirectly. One of these piles was cut from the pile cap, the negative skin friction in the pile was released by breaking the soil-pile bond through electro-osmosis. The elastic rebound of the pile was recorded and used to back-figure the downdrag that had been in the pile.

Given the data that were available regarding the project, and before the pile downdrag was measured, six engineers (D. J. D'Appolonia, Dr. M. I. Esrig, Mr. G. Perez Guerra, Dr. E. H. Davis with H. G. Poulos, Dr. J. E. Garlanger and Mr. J. A Focht) were asked to predict the elastic rebound and downdrag load and the total load in the pile in several levels. The field results were sealed and were not revealed until after the prediction had been presented at the symposium. It was noticed that all of the predictors used the same approach, however, there were differences of opinion related to the determination of the structural load, maximum negative skin friction, the vertical effective stress and the behavior of the bearing layer. Results of the prediction were as follows:

1. The measured load at the pile top was two to three times greater than the predicted loads. Other predictions agreed more closely with the measured results.

2. The predictions of the structural and downdrag loads were substantially different from the measured results.

3. Regarding the predictions of movements, a wide variation as much as plus or minus 100% from the measured value was noticed.

4. The effect of the till bearing layer was only considered by two of the predictors, and none of the predictors considered horizontal movements.

Tables 2.1 and 2.2 present a summary of comparisons of both predicted and measured values.

Table 2.1 Summary of predicted and measured loads, Cutler circle bridge

Prediction	D'Appolonia	Davis	Esrig	Focht	Garlanger	Guerra	Measured
Load at top of Pile, kN	268	357	401	535	250	357	780
ϕ or E tanϕ_0 for fill	0.58	0.30	0.15		0.33	0.20	0.30-0.40
ϕ or E tanϕ_0 for sand	0.58	0.30	0.15		0.33	0.20	0.30-0.40
ϕ or E tanϕ_0 for O.C. clay	0.33	0.30	0.25		0.20	0.25	0.20-0.25
ϕ or E tanϕ_0 for N.C. clay	0.23	0.30	0.21		0.20	0.12	0.20-0.25
Downdrag due to sand &fill kN	980	327	254	598	375	272	312-446
Load in pile at bottom of sand kN	1250	682	624	1128	624	629	
Elev. of Neutral point, m	-13.7	-14.0	-14.0	-14.2	-13.7	-14.1	
Down-drag due to clay kN	1160	954	1012	482	580	615	580-713
Load in pile at Neutral point kN	2408	1636	1668	1605	1204	1244	
Load at pile tip, kN	0	31	245	459	624	660	
Load in pile before cutting kN	258	433	458	535	392	445	1017

Table 2.2 Summary of predicted and measured movements, Cutler circle bridge.

Prediction	D'Appolonia	Davis	Esrig	Focht	Garlanger	Guerra	Measured
Strain @ A after cutting, μ	100	150	160	190	140	155	365
Movement of pile after cutting, mm	1.52	2.95	4.39	4.90	3.66	3.94	
Rebound of till after cutting, mm	0	0.08	0	14.27	0	0	
Movement of A after cutting, mm	1.52	3.02	4.39	19.18	3.66	3.94	10.18
Movement of pile after excavating sand, mm	6.10	1.63	1.57	4.11	1.22	2.33	
Rebound of till after excavating sand, mm	0	0.05	0	0	0	0	
Movement of A after excavating sand, mm	6.10	1.67	1.57	4.11	1.22	2.39	2.46
Movement of pile after electro-osmosis, mm	4.57	3.30	3.43	2.03	2.97	2.34	
Rebound of till after electro-osmosis, mm	0	0.25	0	0	0	0	
Total movement of pile, mm	12.19	8.25	9.40	25.15	7.85	8.66	16.64

Garlanger (1973) proposed an empirical estimation of the negative skin friction and it was recommended for use in the foundation and earth structures manual (1982)

Table 2.3 Empirical values of negative skin friction. (After Garlanger 1973)

Soil Type	Negative Skin Friction
Sand	0.35 to 0.50 σ'_v . A
Silt	0.25 to 0.35 σ'_v . A
Clay	0.20 to 0.25 σ'_v . A

Where

σ'_v = average effective stress

A = area of shaft in the zone of settlining soil

Tomlinson (1975) proposed a design method concerning negative skin friction of single piles. Two cases were reported as shown in Fig. 2.7. The first case, where a pile is driven into a relatively incompressible layer, as shown in Fig. 2.7 (a), while in Fig. 2.7(b), into a compressible layer. The settlement at the ground surface is assumed to be of an appreciable amount in order that the maximum negative skin friction can be mobilized. The relative movement between the soil and the pile, for soft clays, required to initiate maximum negative skin friction was, approximately 1% of the pile diameter. The maximum negative skin friction in Fig. 2.7 (a) is assumed to be fully mobilized at a distance 0.1H above the incompressible stratum.

The pile in Fig. 2.7 (b) was driven into a compressible stratum. Only the top part of the pile will then be subjected to negative skin friction. Tomlinson suggested that a pile

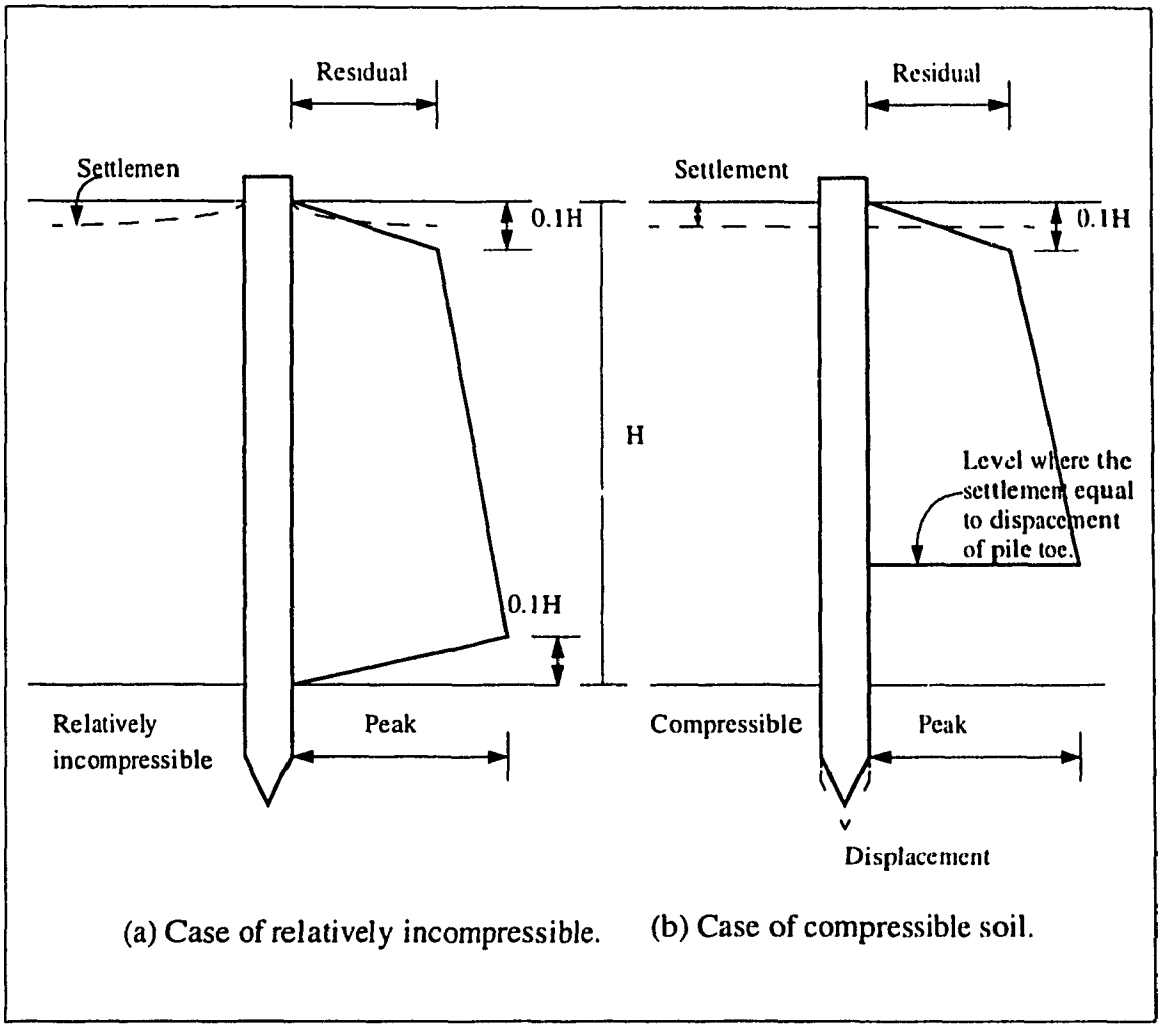

Fig. 2.7 Negative skin friction on single piles.
(After Tomlinson, 1975)

should be designed for negative skin friction down to a depth where the settlement of the soil corresponds to the axial displacement of the pile, i.e., down to the neutral point.

It should be noted here that the work described by Tomlinson was based on the mobilization of skin friction with depth due to the relative movement between pile and soil and this can be visualized as follows: When surcharge pressure is applied to the soil, the movement of the ground surface will mobilize the peak skin friction whereas the movements at lower levels would not have been as such to mobilize the peak value. If however a load is superimposed on the pile above ground level the pile will compress elastically and the peak skin friction, at the top, will then drop into a "residual" value. This suggests that the peak value of negative skin friction will not at any time act on the whole length of the pile. However, as the magnitude of downdrag mobilized along the pile shaft is time dependent.

Auvinet and Hanell (1981) have studied the development of negative skin friction and its variation with time during four years period at the well known regional subsidence of the subsoil of the Mexico valley and the large settlement registered, mainly due to water pumping, which makes negative skin friction an important factor to be considered in deep foundations design in that region.

Instrumented precast concrete piles were driven through 32 m of highly compressible clay affected by intense pumping-induced consolidation. Two piles were used, a 30.5 m friction pile and a 32 m point bearing pile which rested on a thin sandy layer. The piles, which comprised three sections each, of triangular cross section, were built and instrumented with eleven load cells. The load cells consisted of steel pipes 152 mm in diameter

welded to two triangular 16 mm steel plates. On the pipes, strain gauges were welded as shown in (Fig. 2.8). Measuring devises were installed before the piles were driven, included benchmarks for recording vertical settlement at different elevations and piezometers. Test results showed that in each year, during the rainy season, a significant heave of the surface was observed which caused the soil to move upwards with respect to the upper part of the piles. The authors argued that this would affect the negative skin friction distribution by developing a second neutral point. Regarding the friction pile, the effect of the periodic behavior was observed as the downdrag loads increased during the dry seasons and decreased during the rainy seasons. A maximum downdrag load of 210 kN was registered in the middle of the pile nearest to the neutral plane. It is of interest to note that a small but clear reduction of downdrag loads (about 20% of the maximum load) was registered as a consequence of an earthquake.

Concerning the point-bearing pile, and as shown by settlement records, the pile penetrated through the sand layer and behaved as a friction pile. A maximum downdrag load of 320 kN was registered, however the authors indicated that a great similarity existed between the behavior of the point bearing pile and the friction pile. The periodic reductions and final vanishing of the downdrag loads were also similar for both piles. The reduction of the downdrag loads due the effect of the earthquake was larger for point bearing pile.

The maximum friction per unit area in both piles was registered during the dry seasons and figures were compared to three different formulas by different authors, for negative skin friction estimation, i. e., 1- Kerisel (1965), 2- Zeevart (1973) and 3- Kerisel (1976). It was concluded that when predicting negative skin friction values according to

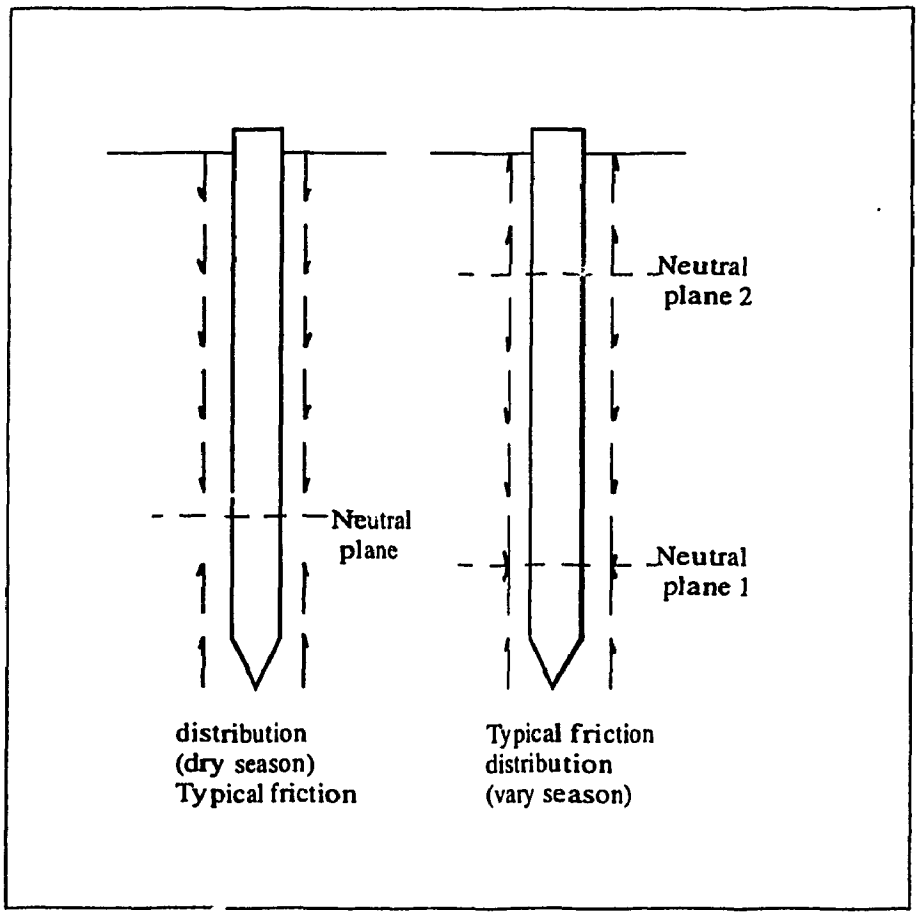

Fig. 2.8 Skin friction distribution.
(After Auvinet and Hanell, 1981)

the total stress method, $f_s = \alpha \cdot C_u$, an adhesion factor value (α) of 0.8 would be in good agreement with the measured values.

Vesic (1977) explained the neutral plane and showed that the neutral plane can be located higher or lower than 0.75 L.

Vesic (1979) introduced an equation to estimate the negative skin friction

$$(Q_f)_{neg.} = N_o \cdot P_o \cdot A \quad \text{.....(2.16)}$$

Where

N_o = nontraditional factor that can be obtained from table 1.

P_o = the mean normal effective stress.

A = the area of the shaft in the zone of settling soil

.Table 2.4 Values of N_o for various conditions. (After Vesic, 1979)

Soil & pile Condition	N_o
(a) Uncoated pile 1- In soft compressible layers of silt and clay 2- In loose sands	 0.15 - 0.30 0.30 - 0.80
(b) Pile coated with bitumen or bentonite	0.01 - 0.05

Bozozuk (1981) reported in his paper "Bearing Capacity of Pile Preloaded By Downdrag" further work relating to the first one published in 1972. In the first paper he reported the results of an instrumented 49 m long steel pipe pile driven through a highway embankment into a deep compressible marine clay. Ten years after pile driving the accumulated peak downdrag load on the pile was 1.52 MN. After the pile was filled with con-

crete, a comprehensive load-testing program was carried out to examine the load-carrying capability of the pile. Bozozuk suggested, and then showed, that the locked-in negative skin friction can be considered as stored energy that support transient or short-term live loads. The test program was divided into three phases:

1. Investigation of performance of the prestressed friction pile loaded to Pn/3, 2Pn/3 and Pn (Pn = 1.52MN), over a period of 11 days.

2. Investigation of the performance of the pile loaded to 2Pn/3, 4Pn/3 and 2Pn over a period of 7 days.

3. Subjecting the pile to a series of cyclic loads to investigate the effect on shaft friction.

Considering number one above the first and second loading increments were applied and maintained for 17 and 19 hours respectively since no additional settlement were detected over those periods of times. The third loading increment was applied and maintained for 6 days. Results showed that all the load increments were carried by the prestress in the pile. For the 3rd load increment (1.52 MN), there was an indication of development of positive skin friction in the upper portion, see (Fig.2.9). It should be noted here that the rate of settlement, at this last load, was greatly increased indicating that if this load was applied for a long period of time. Positive skin friction could eventually be mobilized along the whole length of the pile. On applying the load increments in number two above., it was noticed that the load increment of 2Pn = 3.06 MN could not be maintained without causing excessive settlement of the pile. At this stage of loading it was also clear that positive skin friction was mobilized down to the neutral plane, see (Fig. 2.9). Regarding the

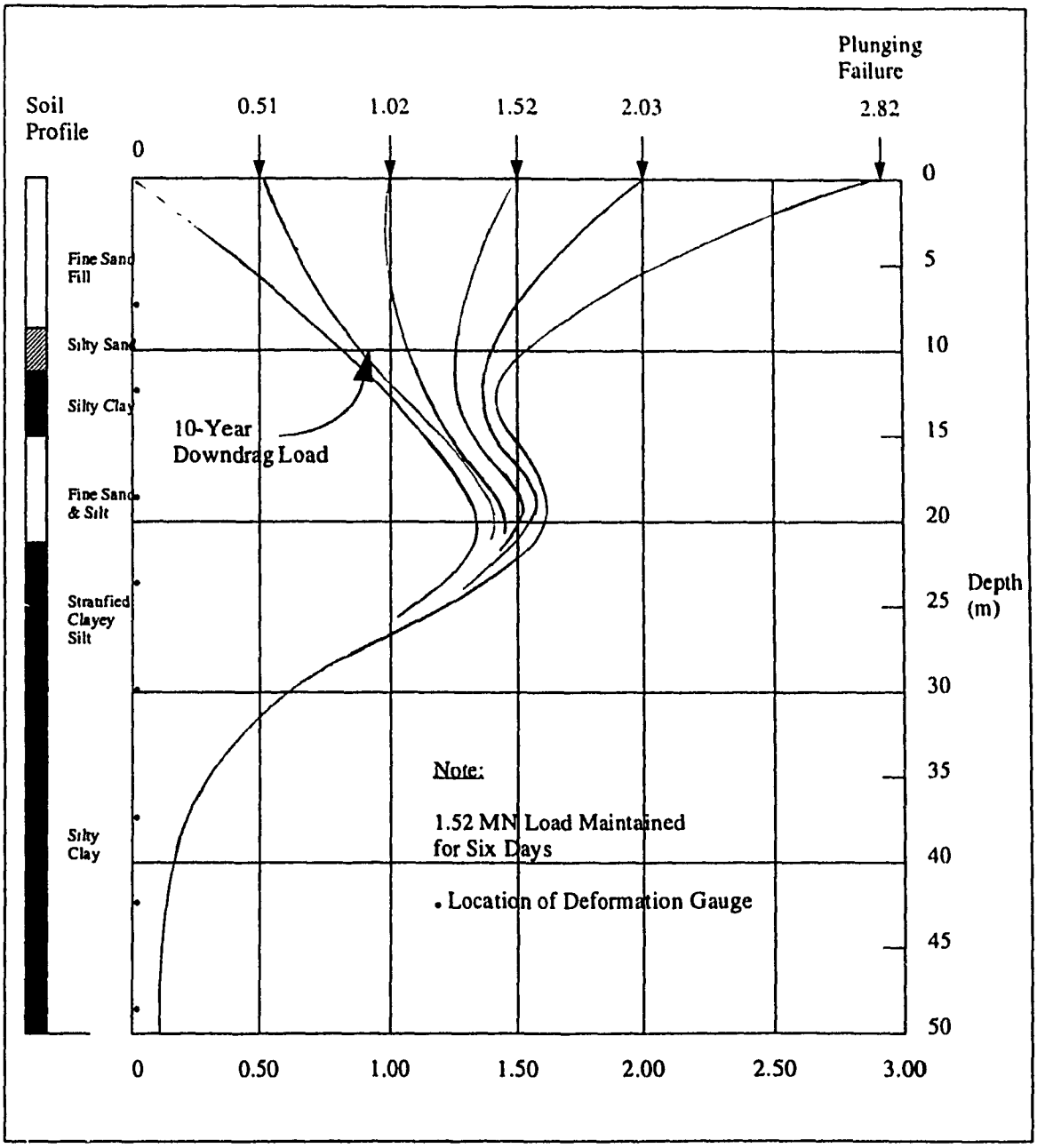

Fig 2.9 Load Distribution in Test Pile. (After Bozozuk,1981)

third loading phase given in number three above., it appeared that cycling the load 10 times within a stress range of +1/3 of Pn had very little destructive effect on the load carrying capacity of the preloaded friction pile.

Based on these observations Bozozuk concluded that:

1- The 1.52 MN downdrag load which developed in the floating friction pile over a period of 10 years could be considered as prestress that is capable of responding to transient, cyclic and short-term live loads.

2- Applied axial loads equal to or less than Pn, where Pn is the maximum downdrag carried by the pile, can be supported for one month if a displacement to pile diameter ratio of 1.25 is acceptable.

3- To support applied loads varying from Pn to 2Pn, positive skin friction must be mobilized in the upper cosolidating soil.

Bozozuk therefore presented an interesting investigation of the negative skin friction by considering downdrag on piles as a stored energy which is capable of supporting transient or short-term live loads for different times depending on the magnitude of the applied load on the pile.

Clement (1984) established a field testing program in Honolulu to investigate negative skin friction and downdrag on prestressed concrete piles in highly plastic underconsolidated silty-clay. The ability of bitumen coating to reduce negative skin friction was also investigated. The clays were soft and compressible to a depth of 43 m. The rate of ground settlement due to self weight of soil was about 12-18 mm/year.

Five, 420 mm diameter piles were employed in a comparative field study. Three of the piles were coated with different grades and thicknesses of bitumen to reduce downdrag while the other two piles acted as uncoated reference piles to measure the full downdrag. A 3.7m high embankment was placed over the piles to accelerate the cosolidation process. Pile compression data were obtained from multi-rod extensometers installed in a central hole in each pile. From these data the distribution of downdrag forces acting along each pile was established. After six months of observations the peak downdrag values on the uncoated piles were 1620 kN. After 42 months the peak values were 3335 kN and 3380 kN. These values exceeded the predicted ones. This was based on a total stress utilizing the undrained strength and on an effective stress analysis, (the Beta method). The bitumen coatings were very effective in minimizing the development of negative skin friction. In one pile with 4.8 mm thick coating, the increase in the downdrag load in the length of the pile through the soft clay was nearly zero. Another pile with 1.6 mm coating also exhibited a low rate of load increase with depth. On a third pile, a less viscous coating, 3.2 mm thick, was also effective in reducing downdrag. The results from the uncoated piles exceeded the predictions of negative skin friction based on the semi-empirical Beta method. Values of β of 0.47 and 0.31 were calculated from the measured load distribution.

The wide variation of β values (about 52%) was attributed to the difference in the two piles considered with respect to their lengths, location of neutral points, different average pore water pressures and effective stresses acting on the piles. However, Clement summarized his conclusions by reporting that β values may vary significantly from one site to another and even within the same site. Regarding the effectiveness of the bitumen

on downdrag reduction, the author recommended bitumen coating thicknesses ranging from 1.6 mm to 5.0 mm depending on the environmental conditions above and below ground provided that coating remains on the pile during installation.

Fellenius (1989) shows that the neutral plane develops in all piles not just those in soils that settle significantly and it lies below the midpoint of the pile and if the soil below the neutral plane is strong, the neutral plane lies near the pile toe and the extreme case is for a pile on rock where the location of a neutral plane is at bedrock elevation., For a floating pile in a homogeneous soil with linearly increasing shear resistance, the neutral point lies at the lower third point of the pile embedment length.

Fellenius shows also that the larger the toe resistance, the deeper the elevation of the neutral plane into the soil and if an increased dead load is applied to the pile head, the elevation of the neutral plane moves up as shown in (Fig. 2.10) He shows also that the neutral plane is located at the intersection of two load distribution curves, the first curve is drawn from the pile head and down, with the load value starting with the applied dead load and increasing with the load because of negative skin friction taken as acting along the entire length of the pile. The second curve is drawn from the pile toe and up starting with the value of the toe resistance and increasing with the positive shaft resistance as shown in (Fig. 2.11)

B. Indraratna et al (1992) studied the development of negative skin friction on driven piles in soft Bangkok clay. They studied the results of short-term pullout tests and long-term full-scale measurements of negative skin friction on driven piles in Bangkok

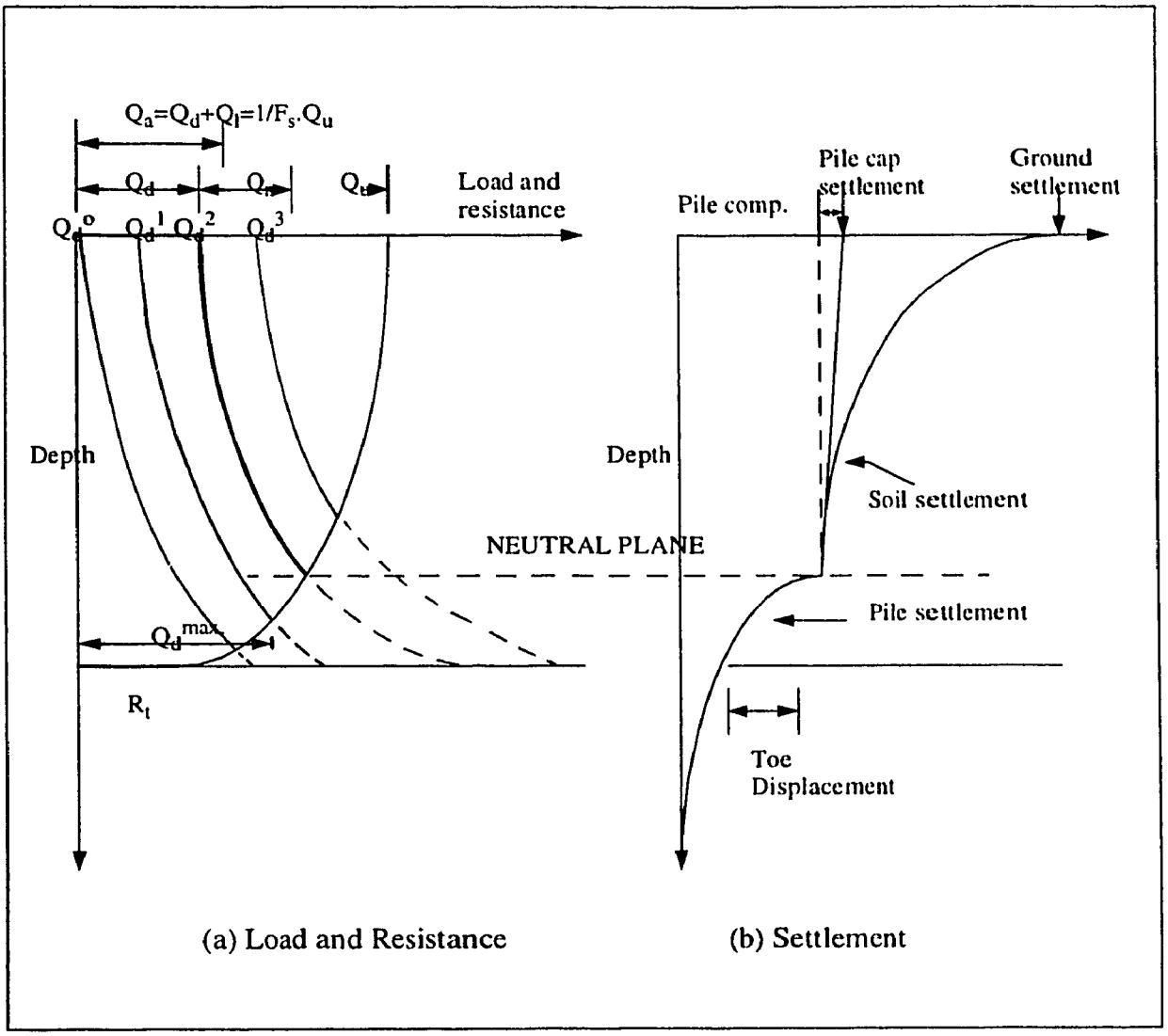

Fig. 2.10 Unified Design for Bearing Capacity, Negative Skin Friction and Settlement. (After Fellenius, 1989)

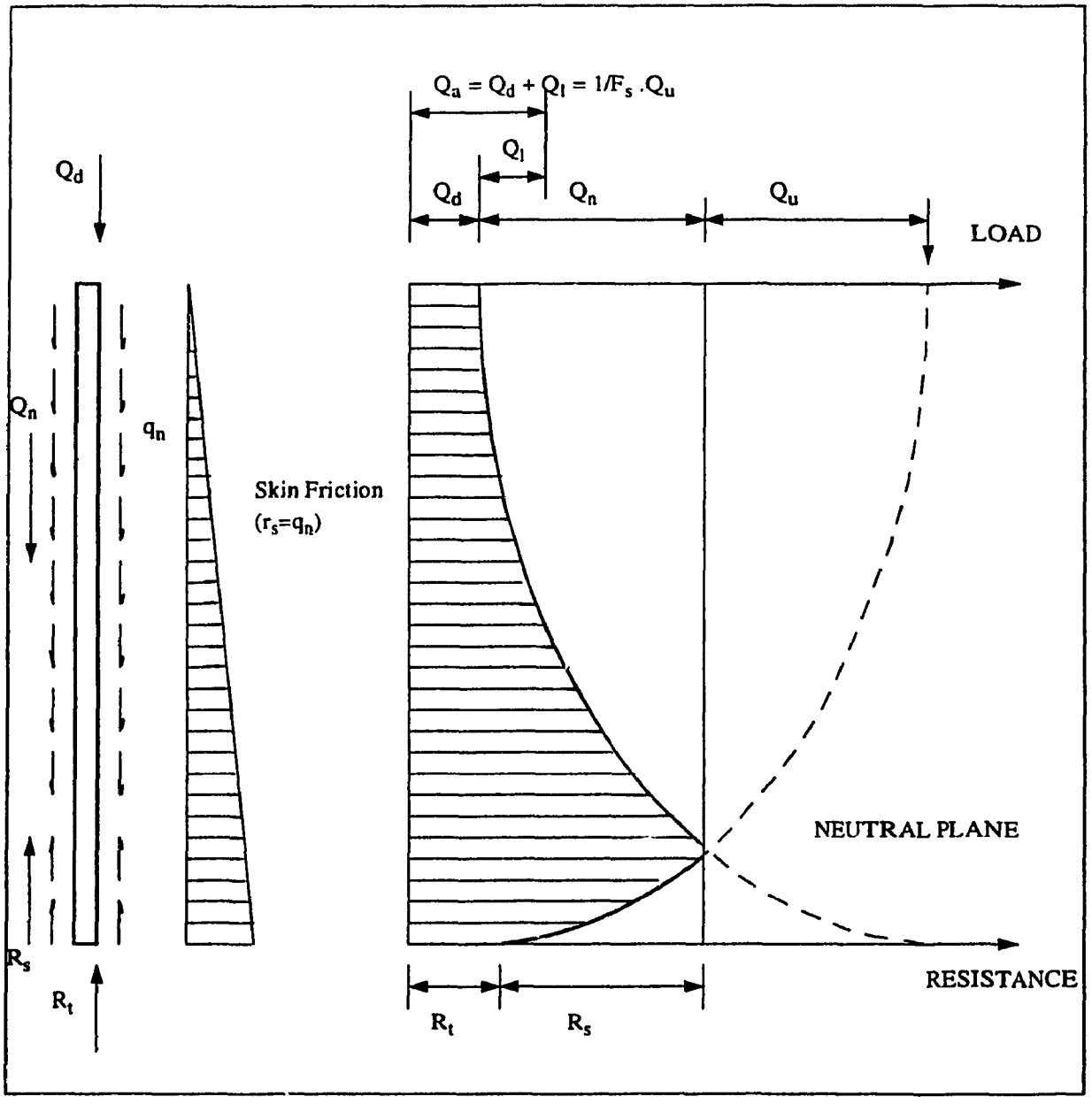

Fig. 2.11 Definition and Construction of the Neutral Plane.
(After Fellenius,1989)

subsoils. They proved that the α and β parameters obtained from short-term tests agreed closely with the long-term measurements for the soft clay layer. They found that the negative skin friction can be predicted well by the effective stress approach using values of β between 0.1 and 0.2. They have preesented a finite-element analysis simulating the development of downdrag in the pile caused by placing an embankment on the ground surface. They obtained values of α for the so-called total stress method of predicting the shaft capacity of driven piles in soft clays (Brenner and Balasubramaniam 1984) correlating the limiting skin friction (τ_s) with the undrained shear strength of the soil (S_u) $\tau_s = \alpha \times S_u$

Burland (1973) conducted a long term analysis for negative skin friction can be made with the effective stress approach $\tau_s = \beta x \sigma'_v$ where the parameter β depends on the friction between the pile and the soil as well as the ratio of the horizontal to vertical stress. The calculated β by Indraratna within the soft clay layer indicated a range of 0.15 - 0.2 for the uncoated pile and 0.05 - 0.1 for the coated piles and based on this results the negative skin friction on driven piles may be predicted using the short-term pullout test results to some degree of accuracy.

Elmer L. Matyas and J. Carlos Santamarina (1994) presented an elastic-plastic closed form solution that permits an estimate of down-drag forces and the location of the neutral plane. He shows that the conventional rigid-plastic solution may overestimate down drag forces by as much as 50% and may also overestimate the depth of the neutral plane. He assumed that the relative displacement profile is linear, with maximum value at the ground surface and decreasing with depth and he assumed that the pile is rigid. The solution permits an estimate of negative skin friction in terms of the most relevant param-

eters, where δ_{sy} is the displacement of the soil relative to the pile that is required to yield the shaft resistance, and δ_{ty} is the displacement that yields the toe resistance. Subscripts s, t, y, and m are used to indicate shaft, toe, yield, and mobilized respectively. The dimensionless ratios to the total relative settlement $S = \delta_h + \delta_t$ wnere δ_h is the settlement of the pile head relative to the ground Surface, and δ_t is the relative settlement of the pile toe, $\psi = \delta_{ty}/S$, $\omega = \delta_{sy}/S$, $\lambda = \delta_h/S$. The settlement S is given by the integral of the vertical strain in the soil mass within the depth of embedment D.

$$\lambda = \frac{-(\alpha-1) + \sqrt{(\alpha-1)2 + 8\psi(\alpha-1) + 8\psi 2\left(1 - \frac{\alpha}{Fs} - \frac{2\omega 2}{3}\right)}}{4\psi}$$

where

$\alpha = R_u/R_{su}$, $F_s = R_u/Q_d$.

2.3 DISCUSSION AND SCOPE OF PRESENT RESEARCH

Based on the above it can be concluded that beside a few empirical formulas, no acceptable solutions can be found for the determination of the neutral plane and accordingly the evaluation of the negative skin friction for piles subjected to surcharge loading.

The purpose of the present research program is to determine the depth of the neutral plane for friction piles in clays and accordingly it will allow an accurate assessment of the negative and positive skin friction contributes to the pile capacity.

CHAPTER 3

NUMERICAL MODELLING

3.1 GENERAL

Numerical analyses using finite element techniques have been particularly popular in recent years for solving many engineering problems. Based on the method described by Zienkiewicz (1977), a variety of finite element computer programs have been developed with different facilities to suit certain needs.

Since the behaviour of soil can be approximated by the use of an appropriate stress-strain law applied to discrete elements, the finite element method provides a valuable analytical tool for the interpretation of cases where unusual geometry or three dimensional effects are significant, and where realistic simplified models can be specified. It is particularly relevant when it is possible to compare or back analyses the performance of a well instrumented prototype, either full scale in the field or at model scale in the centrifuge. In calibrating these tests, design procedures may be developed and proven.

For analyses using critical state soil mechanics models, Phillips (1986) and Kusakabe (1982) have shown that good results can be achieved by providing a finite element mesh which is fine enough in the areas of high strain gradient, and where the loading increments were relatively small. Clearly, the choice of element and the mesh design has to reflect a compromise between an acceptable degree of accuracy and computing costs.

In order to develop a finite element model to represent the state of loading in the field of a single pile driven in clay, a group of assumptions must be made. The pile model will be assumed to be rigid, where no deformation takes place during loading. The soil will be assumed to be homogenous and isotropic. Figure (3.1) shows the common employed idealizations of soil material. In the present investigation, two soil models will be utilized namely the critical state model, where the soil will be assumed to have an elasto-plastic stress strain relationship as shown in Figure (3.1-c), and Mohr-Coulomb soil model, where soil will be assumed to have an elastic perfectly plastic stress strain relationship as shown in Figure (3.1-b).

3.2 NUMERICAL MODELING

Numerical analysis will be conducted on the pile/soil models utilizing the critical state soil mechanics and Mohr-Coulomb soil model, the analysis will be conducted using the finite element program "CRISP".

3.2.1 PROGRAM "CRISP"

This program was written and developed by Geotechnical Group in Cambridge University starting in 1975. It was initiated by Zytynski and developed further twice by Britto & Gunn (1987) and (1995).

The soil models which can be used in the program are: Anisotropic-elastic, unhomogeneous elastic, (properties varying with depth), critical state soil mechanics (cam-clay, modified cam-clay), and elastic perfectly plastic model.

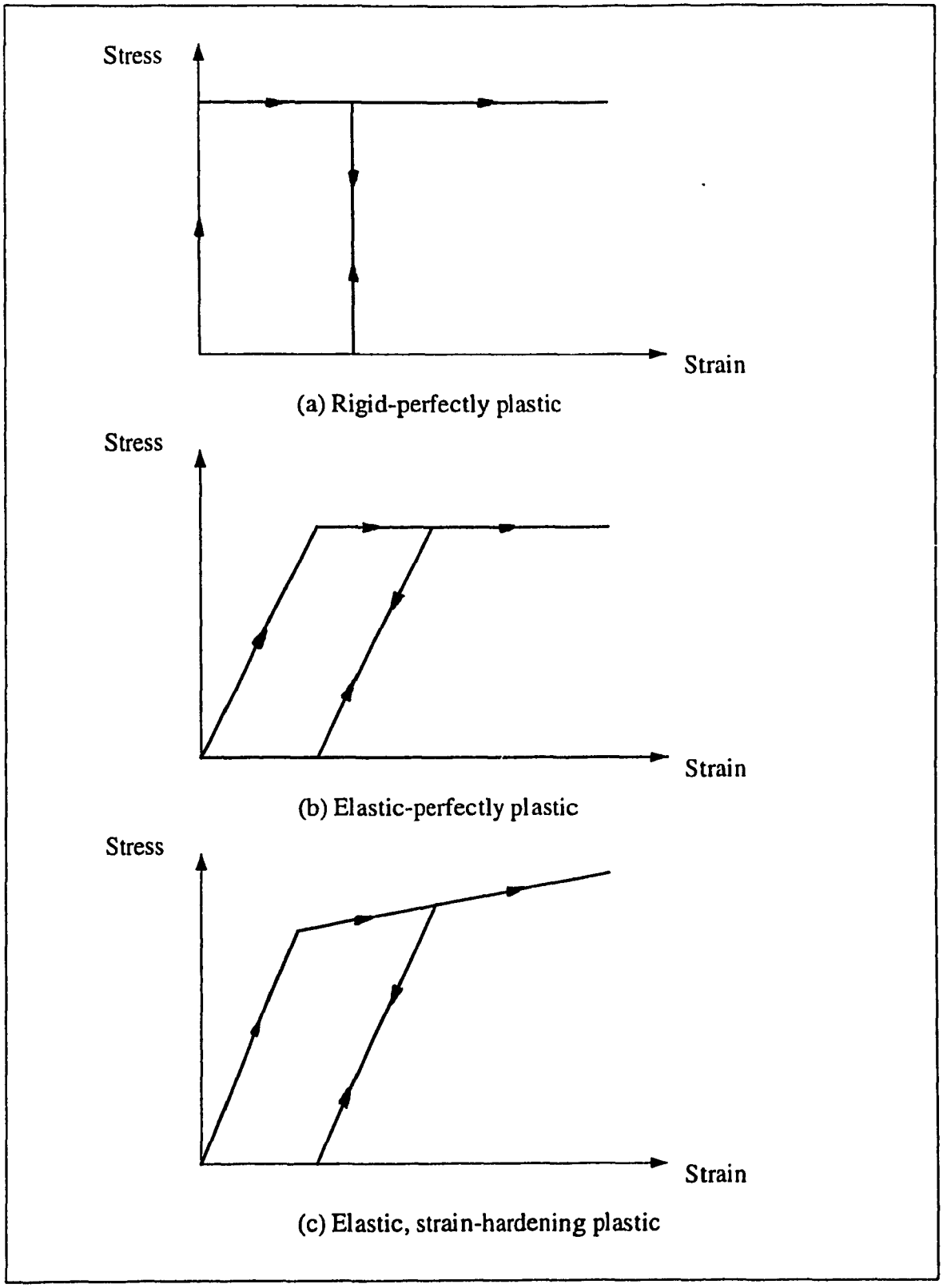

Fig. 3.1 Idealisation of Plastic Behaviour.

The programs consists of "geometry program" and "main program", the input data which must be supplied to the program are:

1. Information describing the finite element mesh, the number of super elements, the coordinate and number of super nodes, number of divisions of each side of the super elements etc. Several types of elements can be studied like: linear strain triangle, cubic strain triangle, linear strain quadrilateral and the 20-nodded brick element. Based on this information, the program generates the node and element numbering system.

2. Material properties associated with each super element.

3. In-situ stress and boundary condition of the region under investigation.

CRISP uses incremental stiffness approach for analyzing non-linear problem using finite elements. In this technique, the user divides the total load acting into a number of small increments and the program applies each of these incremental load in turn. During each increment, the stiffness properties appropriate for the current stress levels are used in calculations. The linear simultaneous stiffness equations are solved using the frontal solution method. In essence, this is just Gaussian elimination method but programmed in such a way as to minimize operations on zero terms and to use minimum computer memory for the stiffness matrix.

Furthermore, CRISP can perform different types of analysis. It supports undrained, drained, and fully coupled consolidation analysis of three dimensional and two dimensional plane strain or axi-symmetric (with axi-symmetric loading) solid bodies.

3.2.2 TYPE AND SIZE OF FINITE ELEMENT MESH

The type of mesh used in this investigation was determined according to the size of the pile and the amount of deformation expected during the analysis. Since the zone of interest which is limited to a few diameters around the pile, an axi-symmetric analysis for a mesh with axis coincides with the axis of the pile foundation was found to be the most efficient model. The choice of the number of elements and mesh design was determined to reflect a compromise between an acceptable degree of accuracy and computing time.

Tochanis, Bielak and Christiano (1988) suggested that the bottom of the mesh is to be located at a distance of 0.6 to 0.7 times the pile length from the pile tip to provide sufficient accuracy. Similarly the lateral boundary was placed at a distance more than 0.6 times the pile length from the pile centre axis. In the present investigation three different meshs were used corresponding to the three pile lengths 16, 24 and 32 m, Fig. (3.2)-(3.4) show element and node numbers for each pile length.

3.2.3 TYPE OF ELEMENT

Both the soil and the pile are modeled by an four noded Linear Strain Quadrilateral (LSQ) with a quadratic function of displacement. Figure (3.5) shows a schematic diagram of the used element.

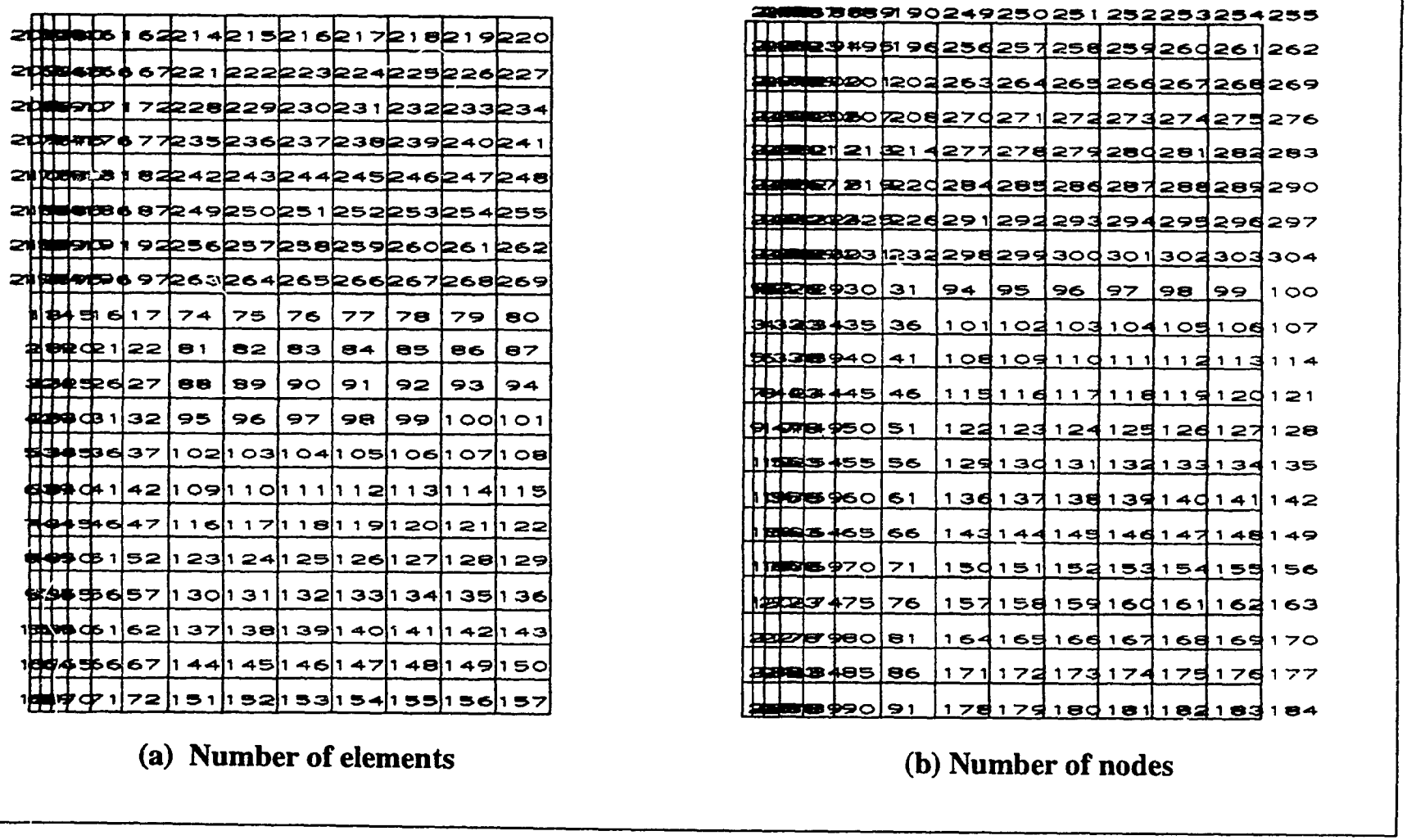

(a) Number of elements

(b) Number of nodes

Fig. 3.2 Finite Element Mesh for Pile Length = 16 m

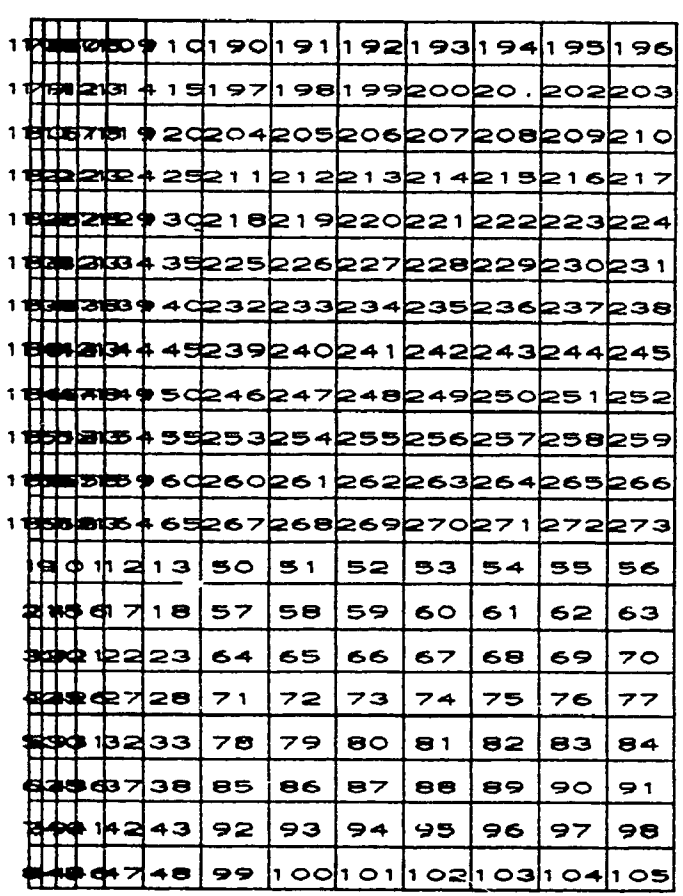

(a) Number of elements

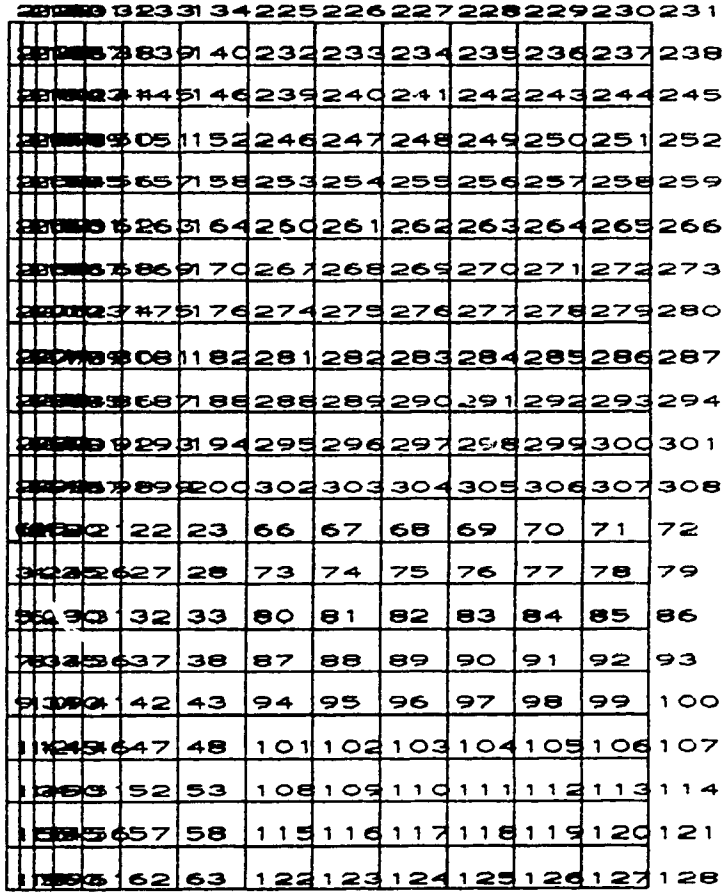

(b) Number of nodes

Fig. 3.3 Finite Element Mesh for Pile Length = 24 m

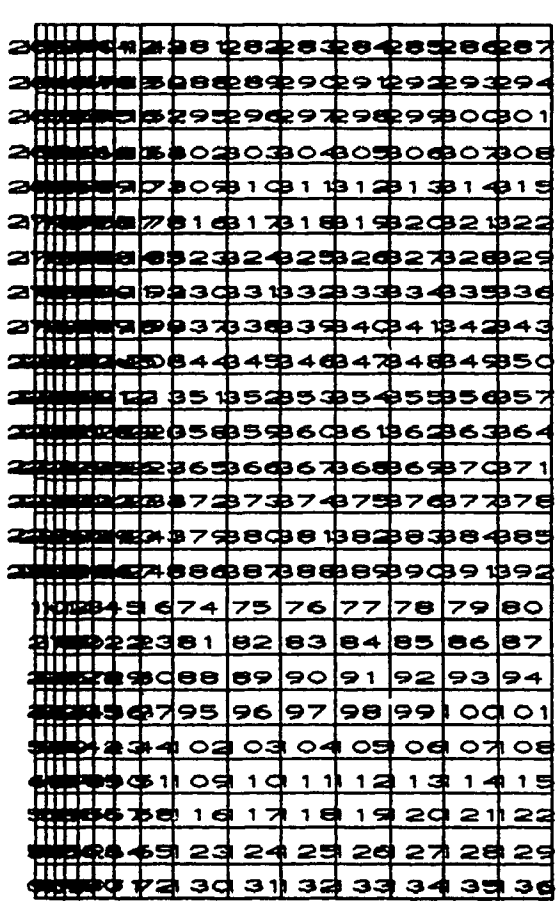

(a) Number of elements

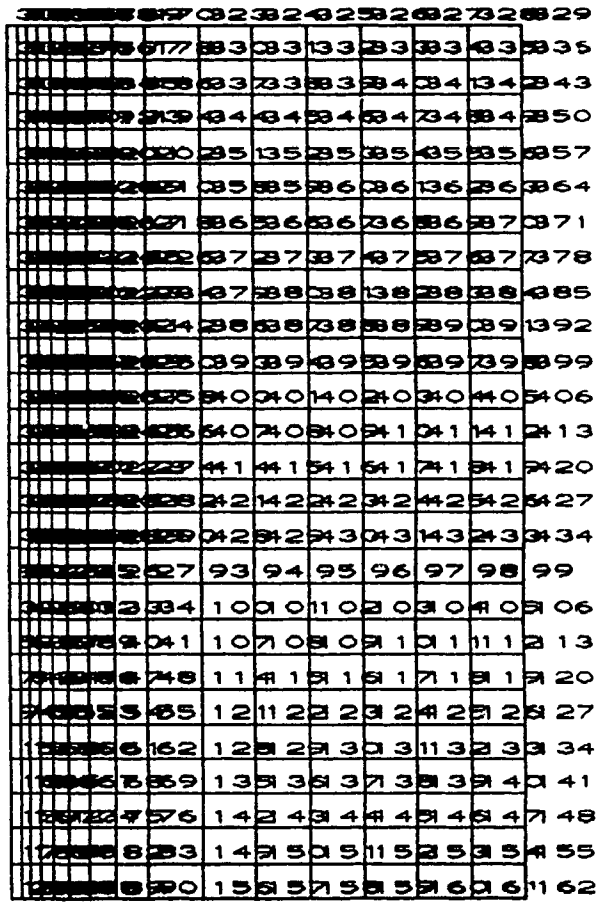

(b) Number of nodes

Fig. 3.4 Finite Element Mesh for Pile Length = 32 m

3.2.4 BOUNDARY CONDITIONS

In order to avoid any boundary conditions, the outer boundary was placed as far as possible, away from the zone which subjected to the changes in the loading.The height of the mesh as shown in the fig. (3.6) is 40m for the 16 m and 24 m piles and 50 m for the 32 m. long piles, in the direction of loading and the outer boundary in the other direction is 30 m. away from the centre of the pile. These dimensions were sufficient to eliminate any effect of the boundaries.

The outer vertical boundaries (left and right sides) are specified restrained in the (x) direction. This means that these boundaries are only free to move in the vertical (y) direction where clay may consolidate in the y direction. The base of the mesh is restrained in both (x) and (y) directions where it is believed that the boundary conditions are no longer affecting the results.

3.2.5 PILE MODEL

The elements constituting the pile model was assumed to behave elastically all the time. The basic properties used in the analysis are those corresponding to the pile material. The maximum stresses attained during this study did not exceed the yield limit of the chosen material, which support the assumption of elastic pile behavior. The pile characteristics in this study are:

E_p (Young's modulus) = 29,400,000 kN/m^2

μ_p (Poison ratio) = 0.33

γ_p (Unit weight) = 14.7 kN/m^3

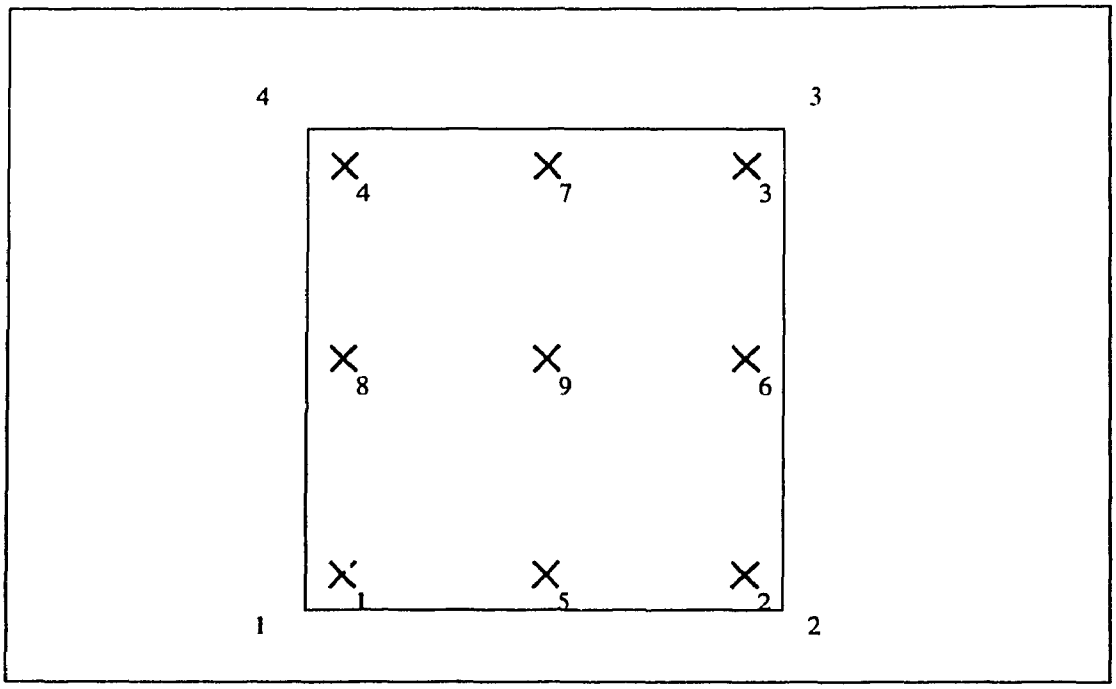

Fig. 3.5 Linear Strain Quadrilateral(9 Integration Points)

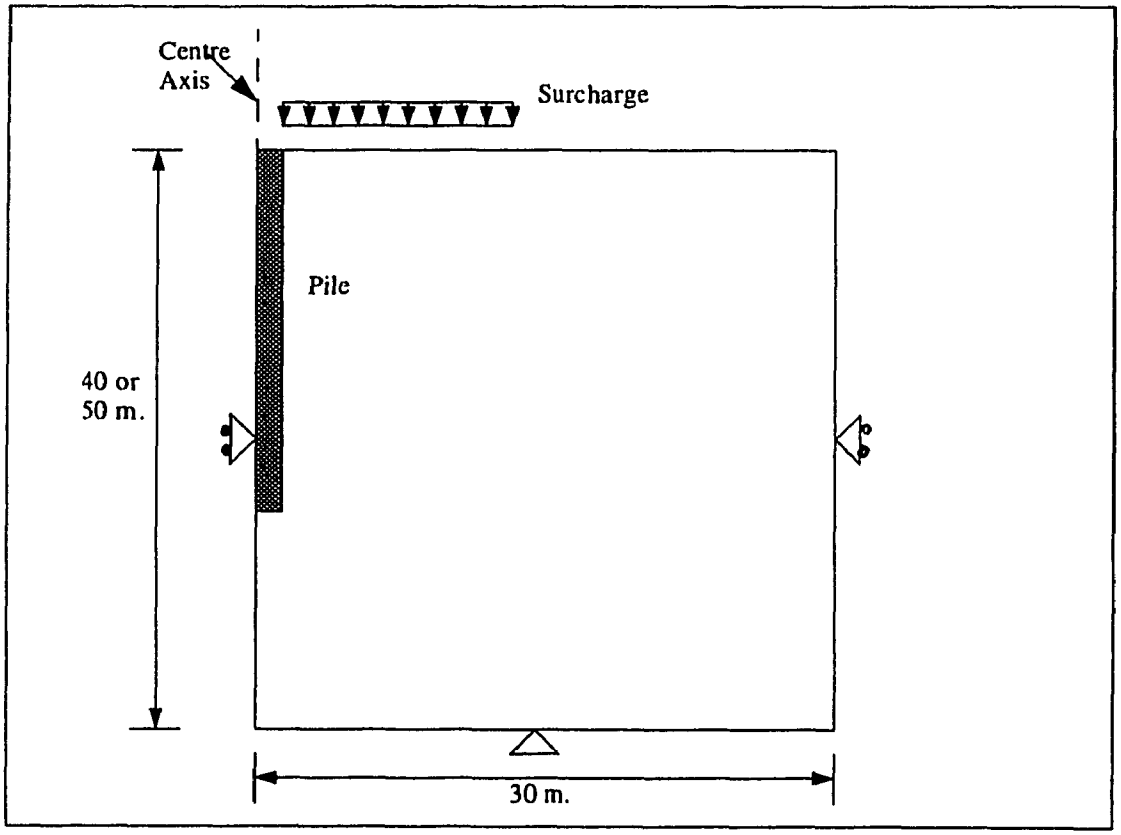

Fig. 3.6 The Outer Boundary Conditions.

K_{px} (Permeability in x direction) = 0.11 E^{-9} m/sec.

K_{py} (Permeability in y direction) = 0.11 E^{-9} m/sec.

Three different pile diameters are used namely; 0.4, 0.8 and 1.2m. and three different pile lengths 16, 24 and 32 m are also used in the study.

3.2.6 SLIP ELEMENT

A slip element was used in the analysis in order to simulate the interface between the pile and the soil. The following properties were assigned to this element:

δ (The angle of pile-soil friction) = $2\phi/3$

t (The thickness of slip element) = 3 cm

3.2.7 SOIL MODELS

In this investigation two soil models were used namely the modified cam clay and Mohr-Coulomb soil models.

3.2.7.1 MODIFIED CAM CLAY SOIL MODEL

The deformation of the soil was assumed to be elasto-plastic in the modified cam-clay soil model. It is an extension of the general concept of using a hardening plasticity model to describe the stress-strain behavior of soil which was first introduced by Drucker et al. (1957). The advantage of this model is that it manages to reproduce an appropriate description of volumetric response during shear.

The Modified Cam Clay parameters are: The slope of the Critical State Line (CSL),

λ, the slope of the swelling line k, the critical state void ratio, e_{cs} and Poisson ratio μ.

The theory of soil behavior known as critical state soil mechanic was developed from the application of the theory of plasticity to soil mechanics.

Three parameters, P' (the mean normal effective pressure), q (the deviator stress) and v (the specific volume) describe the state of a sample of soil during a triaxial test. The parameters are defined as:

$$P = \frac{\sigma_1 + 2\sigma_3}{3} \quad \text{.....(3.1)}$$

$$q = \sigma_1 - \sigma_3 \quad \text{.....(3.2)}$$

$$v = 1 + e \quad \text{.....(3.3)}$$

where

σ_1: the major principal effective stress

σ_3: the minor principal effective stress

e: the void ratio

The instantaneous state of a soil sample during a triaxial test can be represented by a point in a three dimensional space with axes P', v and q and the line joining all such points is called effective stress path (ESP). From the theory of plasticity, it is concluded that the ESP for a soil reaches a yield surface and moves on this surface until it reaches a final destination at which failure occurs, this final destination is called the critical state. A family of drained test in q-P' and v-P' space during a standard triaxial test is shown in Figure (3.7).

The single and unique line of failure points of both q-P' and v-P' spaces is defined as the critical state line.

In a standard drained triaxial test, the sample is subjected to:

i) isotropic compression pressure: During this part of the test the sample follows a stress paths in (P',v) plots, which called the Normal Consolidation Line (NCL), as shown in Figure (3.8-a). Its state may be moved to the left of the (NCL) by unloading along a swelling line. But it is not possible to move the state of the soil to the right of the NCL. In critical state theory the virgin compression, swelling and recompression lines are assumed to be straight line in v-ln(P'), plots with slops $-\lambda$ and -k respectively as shown in Fig. (3.8-b)

The equation of the isotropic virgin compression line is:

$$v = N - \lambda \ln P' \quad \text{.....(3.4)}$$

where N is a constant for a particular soil. It is the value of v when $\ln P' = 0$ or $P' = 1\ kN/m^2$.

The equation of the swelling or recompression line is

$$v = v_k - k \ln P' \quad \text{.....(3.5)}$$

The value of v_k depends upon which k line the soil is on, but it stays constant while the soil is moving up or down the same line.

ii) Increases of the axial stress: During this part, the ESP approaches the Critical State Line (CSL) as shown in fig. (3.7), as for NCL.

The CSL, in v-ln(P') plot is assumed to be a straight line lying on the right of the NCL and parallel to it. The CSL has the 2 following equation:

$$q = MP' \quad \text{.....(3.6)}$$

$$v = \Gamma - \lambda \ln P' \quad \text{.....(3.7)}$$

where M is the slope of CSL in q:P' space.

Γ is the value of v corresponding to P' = 1kN/m^2 on the CSL.

Thus, Γ locates the CSL in v:lnP' plane in the same way that N located the Normal Compression Line. Equations (3-6) and (3-7) together define the position of the CSL in q:P':v space. M and Γ, like N, λ, and k are regarded as soil constants.

Fig. (3.9) shows the critical state line in a three dimensional q:P':v space, the normal isotropic compression line is shown in the q=0 plane.

The distinction between elastic and plastic deformation is best illustrated by the behavior during isotropic compression. In fig. 3.8 (b) if the soil is unloaded from B, it moves along the swelling line BV_{k1}, if it is reloaded from V_{k1}, the soil retraces path V_{k1} to B, then when an additional compression occurs, the sample moves down the normal consolidation line to C. Similarly, if the sample is unloaded from C, it moves back along the swelling or k line to V_{k2}. The strain is elastic along any swelling or k lines such as $V_{k1}B$ and $V_{k2}C$, and is plastic along the Normal Consolidation Line.

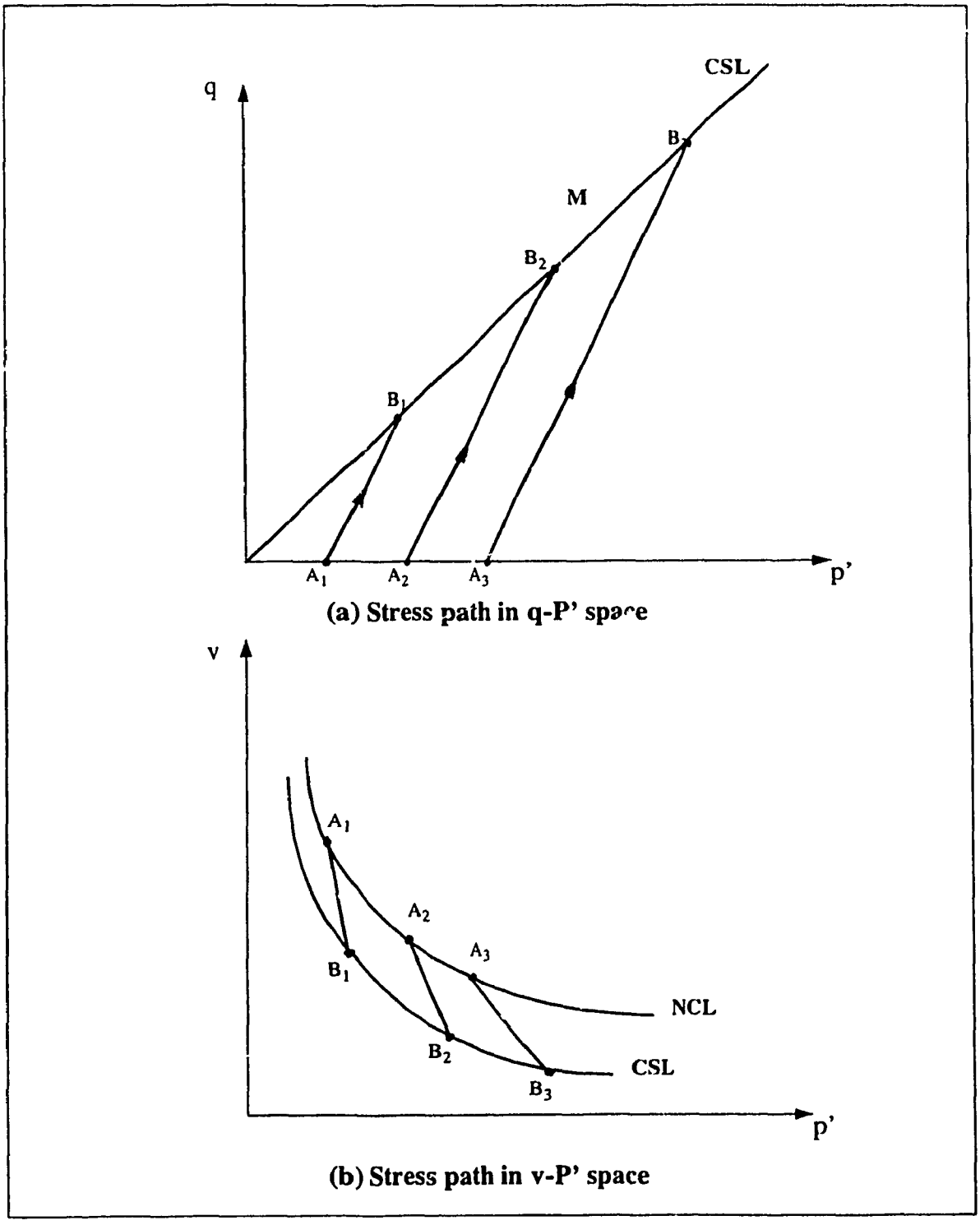

Fig. 3.7 Effective Stress Path for a Family of Drained Test

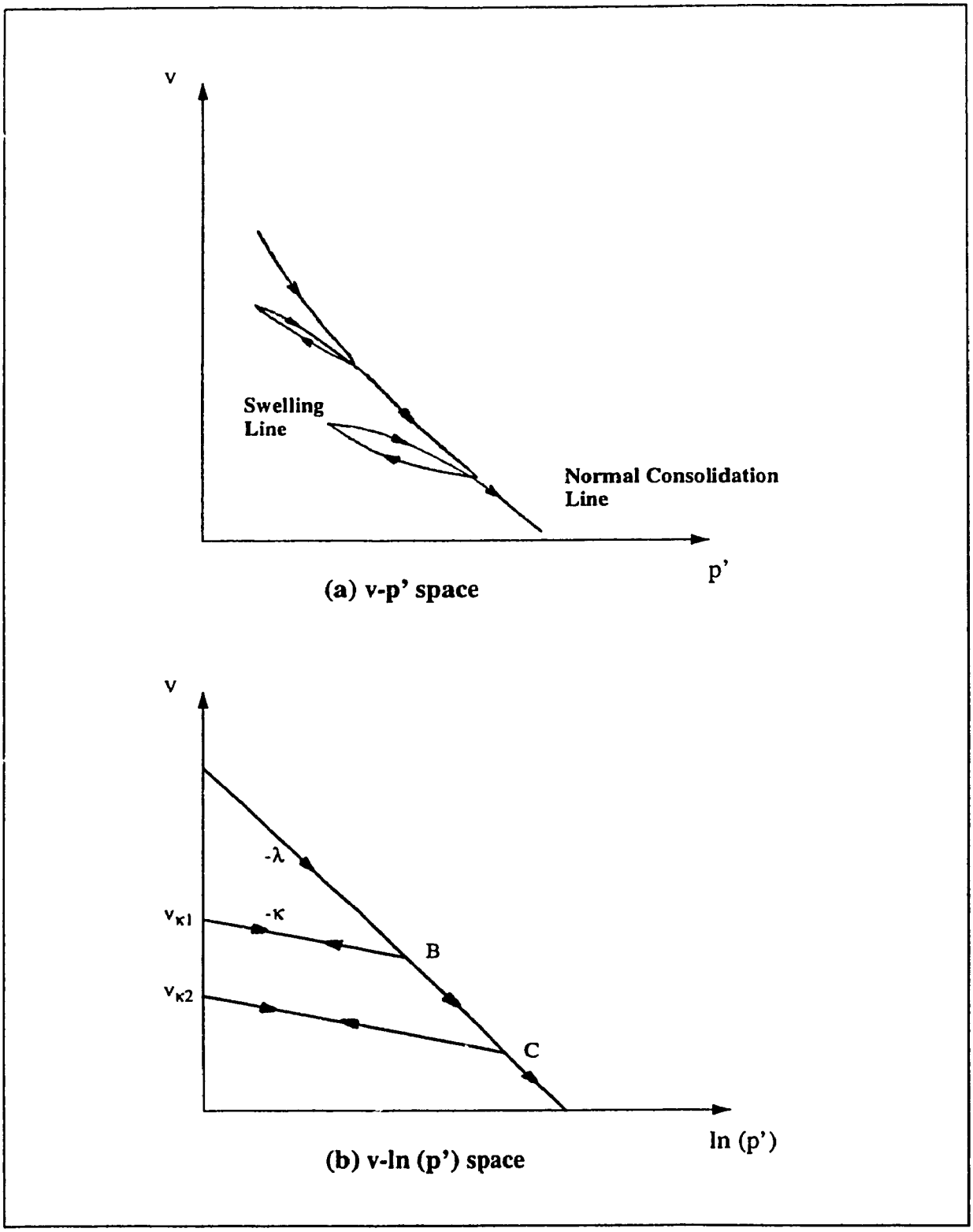

Fig. 3.8 Normal Consolidation Line

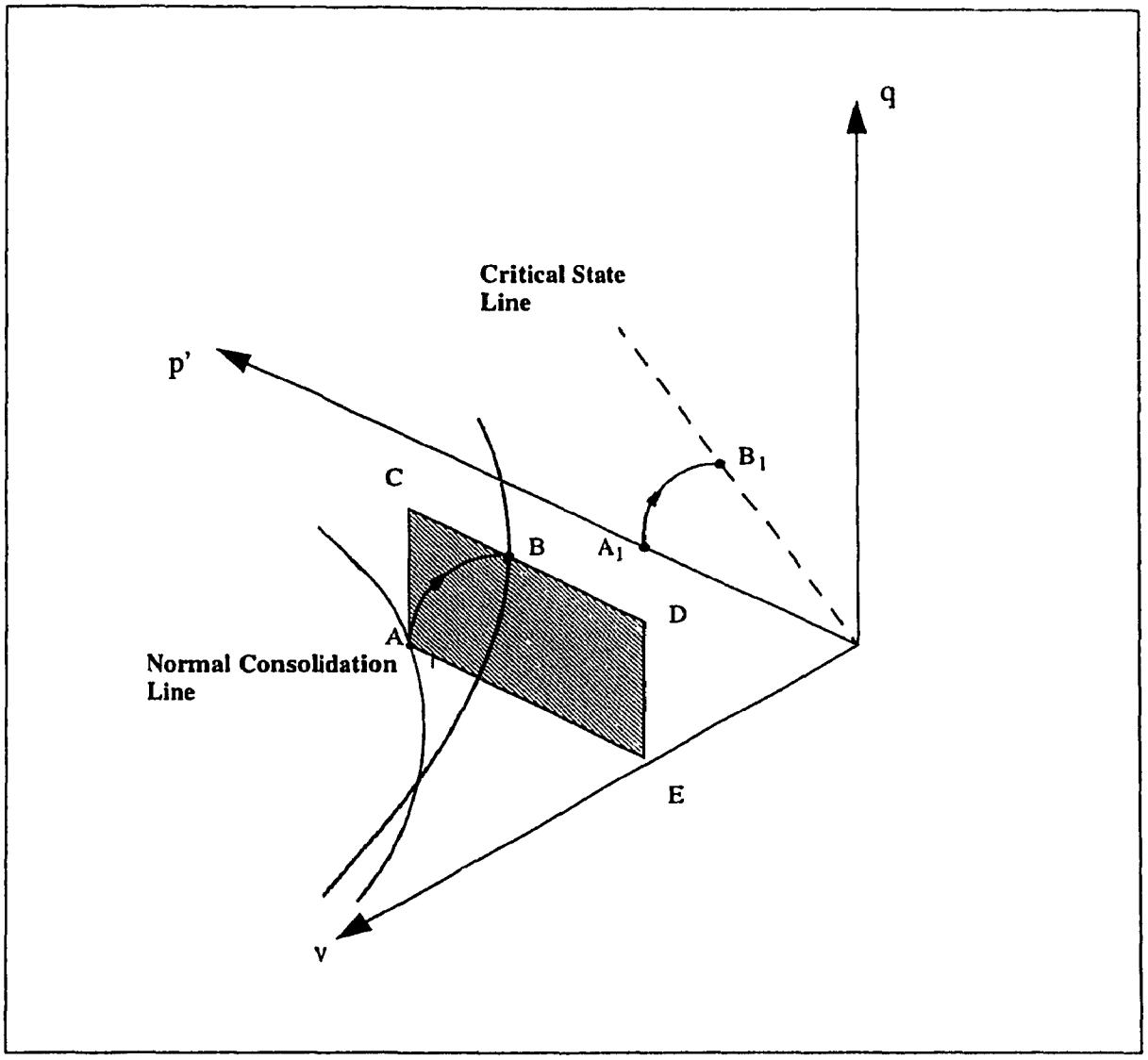

Fig. 3.9 Critical State and Normal Consolidation Line in Three Dimensional q-p'-v space

When a triaxial test is conducted on a sample of soil, the stress state of the sample can follow undetermined number of stress paths depending on two factors: The type of test (drained or undrained) and the variation of the principal major and minor stresses. Each stress path consists of 2 parts: elastic one, when the behavior of the soil is elastic and plastic one, when the soil is yielding. These two parts are separated by a point called the yield point.

The yield curve is defined as the link of yield points, in P':q plot, for all possible stress paths for samples having the same initial stress state.

Fig. (3.10) shows different yield curve, each one is associated with a particular initial stress state, a set of all yield curves, in P' :q:v space, forms a yield surface.This surface is considered as a Stable State Boundary Surface (SSBS) with the Critical State Line lying on it, when the stress state of the sample is inside this surface, its behavior is elastic, when the stress path moves on the surface, its behavior is plastic and the stress state cannot lie outside the surface.

Cam Clay is the name given to an elasto-plastic model of soil behavior. The Cam Clay equations developed at Cambridge University can describe many real soils if appropriate material parameters are chosen.

This theory was developed for Normally Consolidated and lightly Over Consolidated soil.

The Cam Clay State Boundary Surface equation as developed by the geotechnical group at Cambridge is as follows:

$$q = \frac{MP}{\lambda - k}(\Gamma + \lambda - k - v - \lambda \ln P) \quad \text{.....(3.8)}$$

Fig. (3.11) shows this equation in P':q:v space.

The state boundary surface intersects the v:P' plane along the normal consolidation line where eq=o and v = N- λ - k. Hence, from equation (3.8):

$$\mathbf{N = \Gamma + \lambda - k} \quad \text{.....(3.9)}$$

Equation (3.8) can also be written as:

$$\mathbf{v_\lambda = \Gamma + (\lambda - k)(1 - \eta/M)} \quad \text{.....(3.10)}$$

where η is the stress ratio.

Elastic straining underneath the SSBS corresponds to movement along a k-line, with a corresponding change in v. Thus when an elastic sample is brought to the point of yield it must simultaneously lie both on the k-line and on the SSBS. Therefore the intersection of the SSBS with the k-line equation gives the current yield surface:

$$\mathbf{q = MP' \ln(P_c/P')} \quad \text{.....(3.11)}$$

where P'_c is the size of the current yield locus. This point lies on the isotropic normal consolidation line.

The Modified Cam Clay model modifies essentially the shape of the yield locus, in the original Cam Clay model, to be an elliptical one. So the equation of the SSBS will change to:

$$\mathbf{v_\lambda = \Gamma + (\lambda - k)[\ln(2) - \lambda v(1+(\eta/M)^2]} \quad \text{.....(3.12)}$$

The equation of the isotropic NCL is the same as for Cam Clay

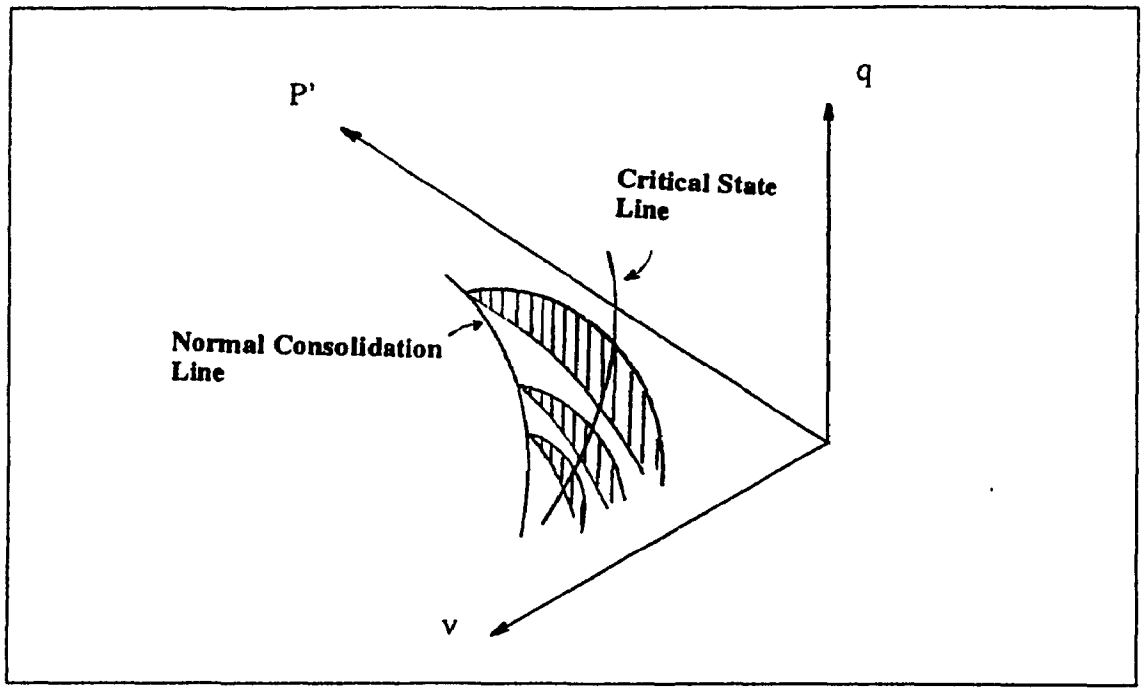

Fig. 3.10 Yield Curves in q-P'-v Space

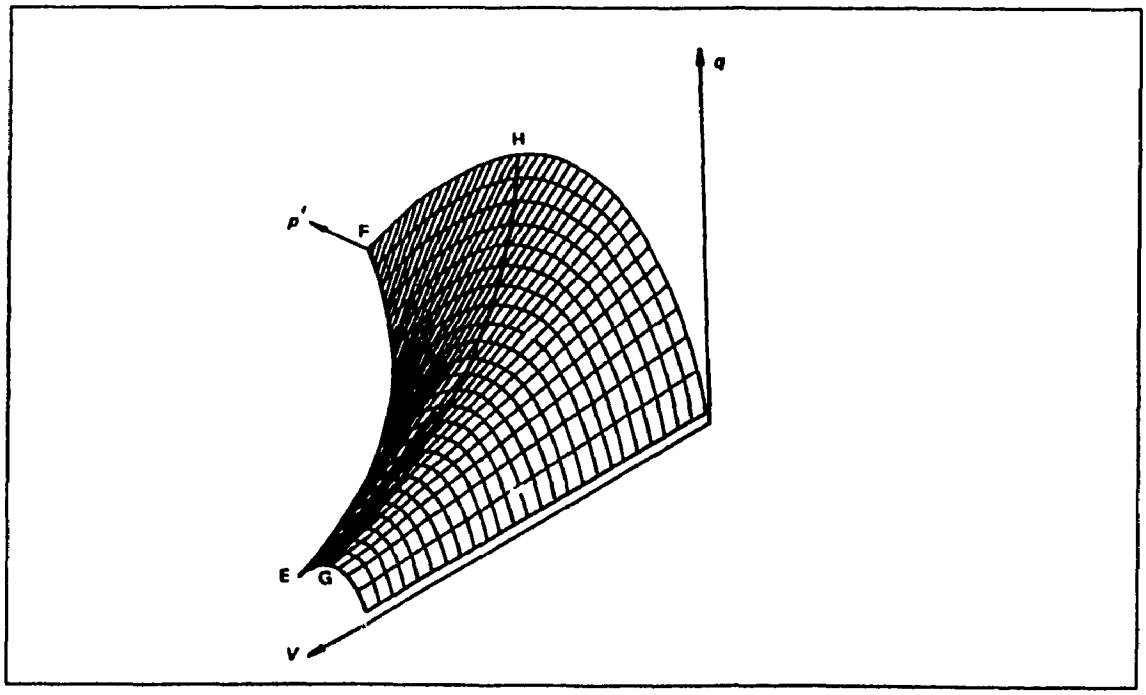

Fig. 3.11 The Stable State Boundary Surface in q-P'-v Space.

$$v = N - \lambda \ln(P')$$

$$\text{but } N = \Gamma + (\lambda - k)\ln 2 \quad \text{.....(3.13)}$$

and the current yield locus will be given by:

$$q^2 + M^2 P'^2 = M^2 P' P_c' \quad \text{.....(3.14)}$$

The critical state soil parameters can all be determined from the normal range of laboratory tests that are performed on a soil. These parameters are:

a. The frictional constant M

M is the slope of the CSL in q:P' space. Triaxial tests on isotropically consolidated samples can be used to obtain the frictional constant M. A number of tests need to be carried out with different consolidation pressures, for each test, P' and q have to be determined. The frictional constant M and the angle of shearing resistance ϕ are related with the following equation:

$$M = \frac{6\sin\varnothing}{3 - \sin\varnothing} \quad \text{.....(3.15)}$$

b. Slope of the normal consolidation line λ and swelling line k

These parameters can be obtained from odometer test or from triaxial tests on sample either isotropically or with K_0 normally consolidated conditions. λ is the slope of NCL or CSL in v-ln (P') plot. κ is the slope of the swelling line in the same plot.

c. ***Critical state void ratio*** e_{cs}

e_{cs} is defined as the void ratio on the critical state line for a P' = 1 or lnP'=0. This parameter determines the location of the CSL in v:lnP' space. e_{cs} is obtained from:

$$e_{cs} = \Gamma - 1 \quad \text{.....(3.16)}$$

d. ***Poison ratio*** μ

Poisson ratio may be evaluated from the ratio of the lateral strain to axial strain during a triaxial compression test in axial loading.

e. ***Size of the initial yield locus*** P'_c

Knowing the stress history of the ground, one can calculate P' and q as follows:

$$P' = (2\sigma'_x + \sigma'_y)/3 \quad \text{.....(3.17)}$$

$$q = \sigma'_y - \sigma'_x \quad \text{.....(3.18)}$$

$$\sigma'_x = k_o \cdot \sigma'_y \quad \text{.....(3.19)}$$

where

σ'_x and σ'_y are the normal and horizontal effective stress respectively

k_o: the coefficient of earth pressure at rest.

where

$$k_o = 1 - \sin(\phi) \quad \text{.....(3.20)}$$

Substituting these values in the expression for the Cam Clay or modified Cam Clay yield locus (equation 3-11 and 3-14), we obtain P_c' value for any point as:

For Cam Clay:

$$P_c' = P' * e^{(q/MP')} \quad \text{.....(3.21)}$$

For modified Cam Clay:

$$P_c' = P' + (q'/M)^2/P' \quad \text{.....(3.22)}$$

When the soil is subjected only to its own-weight, this stage is called the in-situ stage and the stresses are specified at the bottom and the top of the mesh as follows:

$$\sigma_y' = \gamma . y \quad \text{.....(3.23)}$$

$$\sigma_x' = \sigma_z' = k_0 \sigma_y' \quad \text{.....(3.24)}$$

$$\tau_{xy} = 0 \quad \text{.....(3.25)}$$

where y is the depth of the point (0 at ground level)

3.2.7.2 MOHR-COULOMB MODEL

The deformation of the soil was assumed to be elastic-perfectly plastic in the Mohr-Coulomb soil model, where in (1776) Coulomb introduced the failure condition for soil which called Mohr-Coulomb failure criterion, where the shear strength increases with increasing normal stress on the failure plane by a linear function

$$\tau = c + \sigma \tan \phi \quad \text{.....(3.26)}$$

where

τ : the shear stress on the failure plane

c : the cohesion of the material

σ : the normal effective stress on the failure surface

ϕ : the angle of internal friction

The Mohr-Coulomb failure criterion and the yield surface are shown in fig. (3.12) and (3.13).

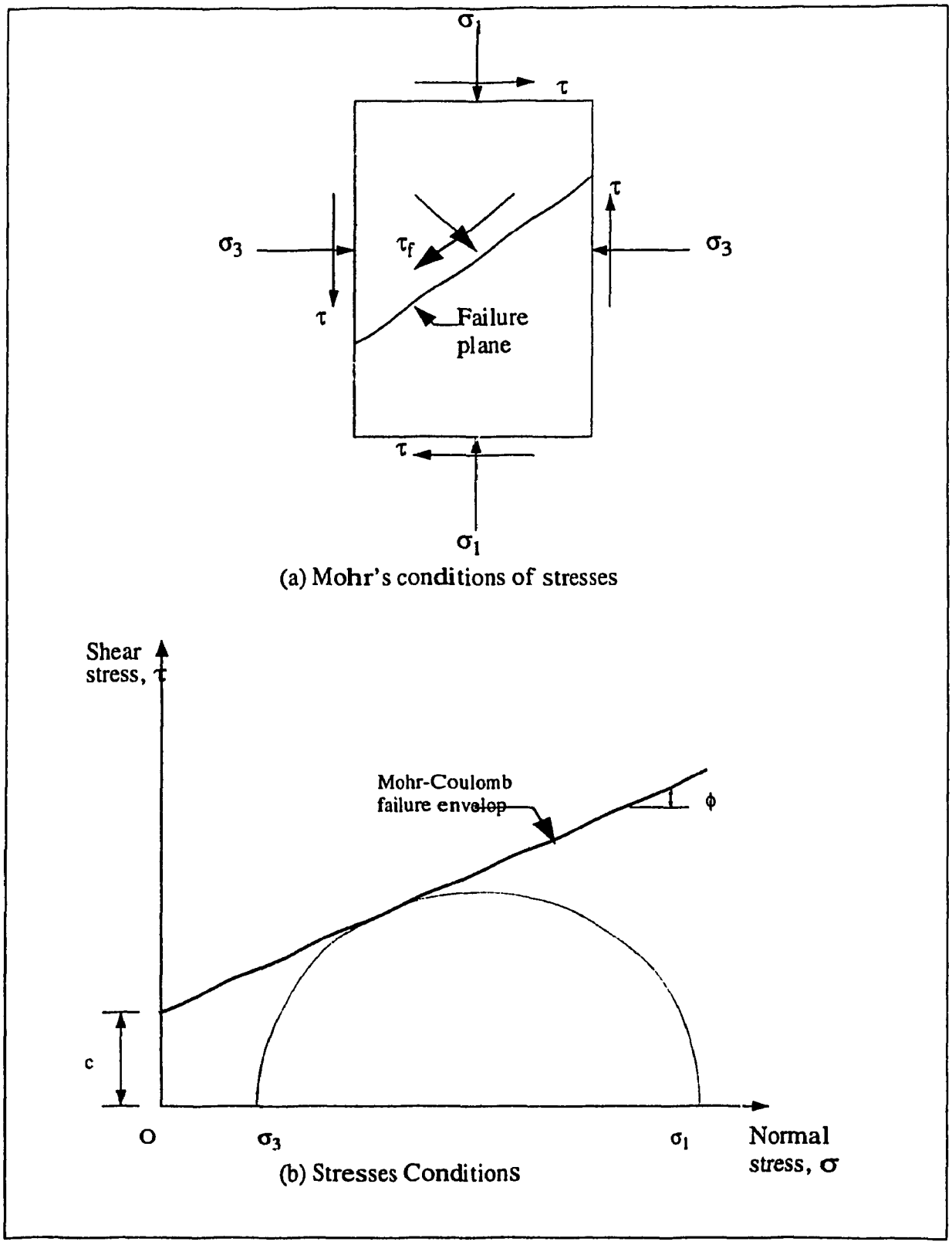

Fig. 3.12 Mohr and Mohr-Coulmb Failure Envelopes.

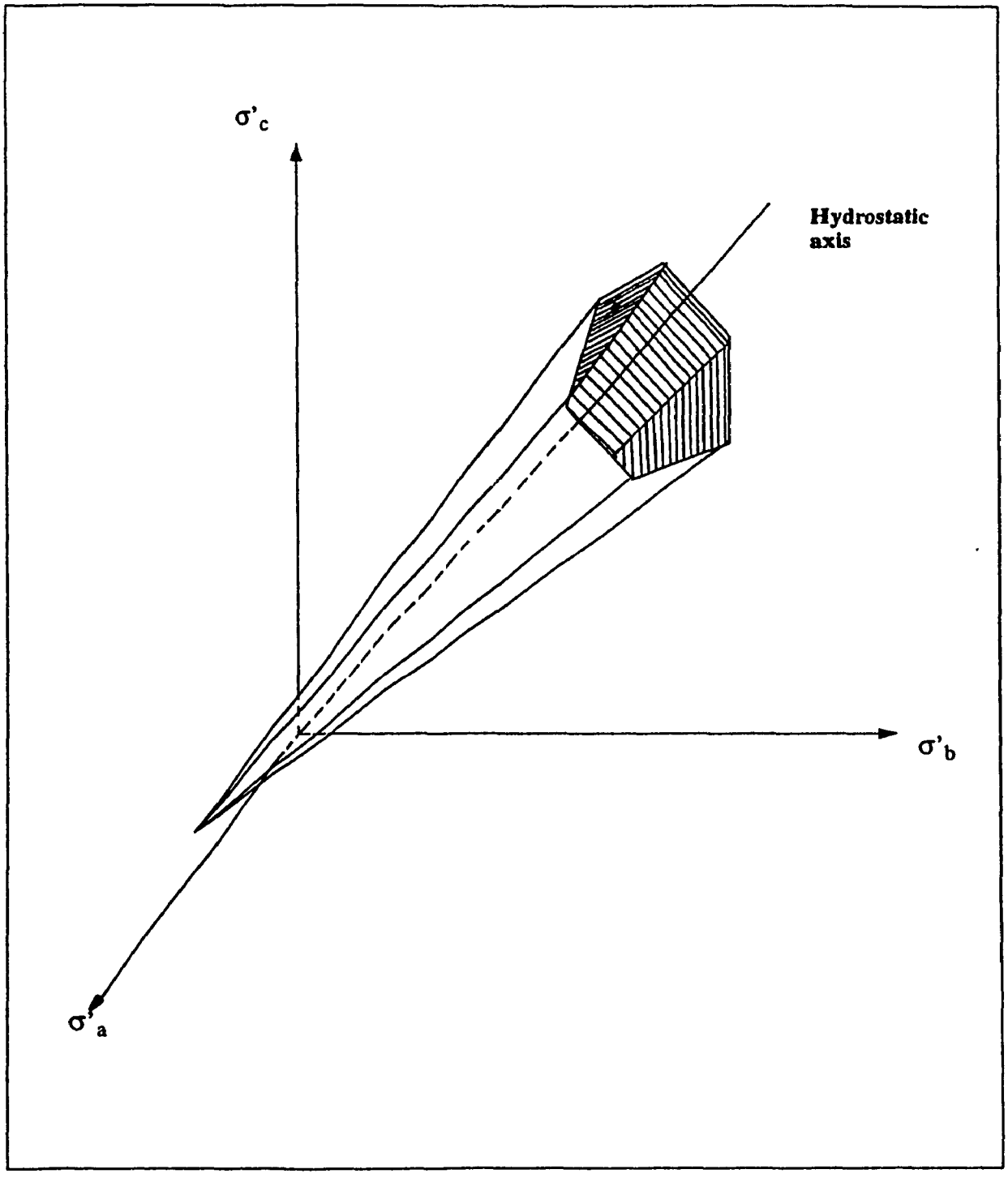

Fig. 3.13 The Mohr-Coulomb Yield Surface.

3.5 VARIABLES CONSIDERED

Table (3-1) summarizes the range of the different parameters in the present investigation for the critical state model and table (3.2) presents the different parameters which was used in Mohr-Coulomb soil model.

The range of the Critical State soil parameters: λ, k and e_{cs} used in the present investigation were taken from TAM Heng-Kong (Some Applications of Cam Clay in Numerical Analysis, 1992).

Table 3.1 Range of different parameters in Modified cam clay model

Surcharge (kN/m^2), S	5 to 15
Slope of the Critical State Line, λ	0.05 to 0.35
Slope of the swelling line, k	0.005 to 0.175
Critical State void ratio, ecs	0.71 to 3.47
Critical State frictional coefficient, M	0.77 to 1.4
Pile Length (meter), L	16 to 32
Pile Diameter (meter), D	0.4 to 1.2

Table 3.2 Range of different parameters in Mohr-Coulomb model

Surcharge (kN/m^2), S	5 to 15
Cohesion (kN/m^2), C	10 to 30
Pile Length (meter), L	16 to 32
Pile Diameter (meter), D	0.4

3.6 LOADING INCREMENTS

The entire loading was divided into 30 increments, these increments are grouped into 2 increments blocks. The first block consists of 20 increments of equal surcharge load which was sufficient to give a good accuracy to the results and the second block increment consists of 10 equal increments to represent the consolidation period of one year after applying the surcharge load.

The surcharge load was applied over 10 days period, and 20 load increments. After the application of all increments the clay was then allowed to consolidate for a period of one year.

Trial calculations were done for 10, 20 and 30 increments, the results showed no effect of the number of increments on the location of the neutral plane, see Fig. (3.14)

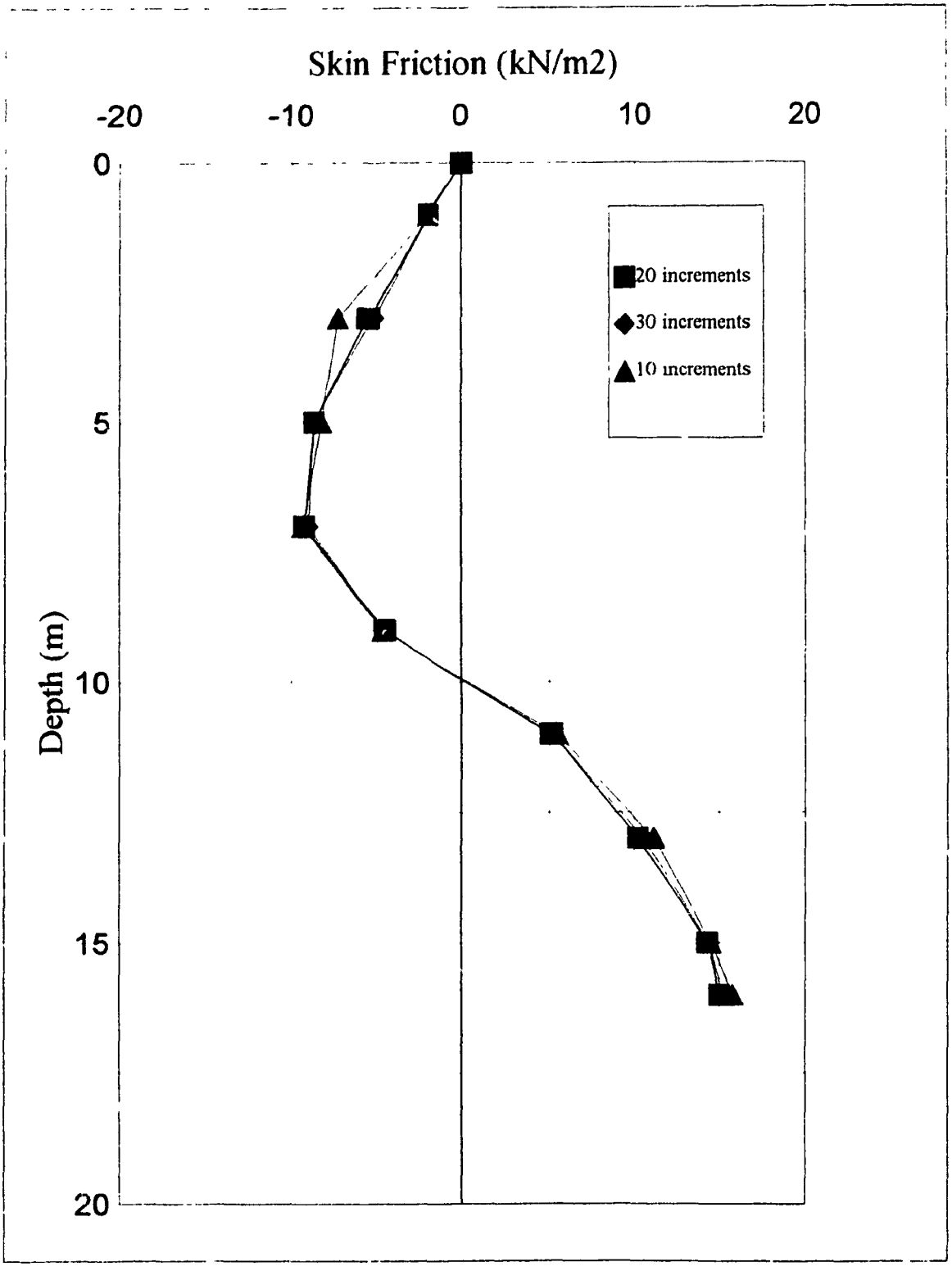

Fig. 3 14 Effect of Number of Increment Load on the location of the neutral plane.

CHAPTER 4

RESULTS AND ANALYSIS

4.1 GENERAL

In this chapter the numerical results of the finite element analysis using the modified cam clay model and Mohr-Coulomb model are presented. For each of these soil model the factors affecting the location of the neutral plane are examined and a design procedure is presented.

405 trial analysis divided into 5 groups were conducted in the present investigation using the numerical model developed in chapter 3. In the first 4 groups, the Modified Cam Clay was extensively used. In group number 5 the elastic perfectly plastic model of Mohr-Coulomb was used.

In order to examine the effect of different parameters on the determination of the depth of neutral plane, groups were divided to series where each parameter was isolated and examined individually.

Tables 4.1 to 4.18 present the test results using the Modified Cam Clay model (groups No. 1 to 4) and Table 4.19 present the test results for Mohr-Columb model (Group No. 5).

Table 4.1 Test Results for Group I-1, λ=0.05, D=0.4m, L=16m and e_{cs}=0.71

Test No.	Series No.	Surcharge KN/m2	κ/λ	Slope of Swelling Line, κ	Critical State Frictional Coefficient, M	Depth of Neutral Plane, ND
1	1	5	0.1	0.005	0.77	8.46
2					1.00	8.25
3					1.40	8.55
4			0.4	0.02	0.77	8.94
5					1.00	8.97
6					1.40	9.11
7			0.6	0.03	0.77	9.10
8					1.00	9.15
9					1.40	9.23
10	2	10	0.1	0.005	0.77	9.44
11					1.00	8.79
12					1.40	8.65
13			0.4	0.02	0.77	9.56
14					1.00	9.28
15					1.40	9.22
16			0.6	0.03	0.77	9.55
17					1.00	9.35
18					1.40	9.31
19	3	15	0.1	0.005	0.77	9.95
20					1.00	9.51
21					1.40	8.84
22			0.4	0.02	0.77	9.86
23					1.00	9.68
24					1.40	9.37
25			0.6	0.03	0.77	9.81
26					1.00	9.66
27					1.40	9.43

Table 4.2 Test Results for Group I-2, λ=0.05, D=0.4m, L=24m and e_{cs}=0.71

Test No.	Series No.	Surcharge KN/m2	κ/λ	Slope of Swelling Line, κ	Critical State Frictional Coefficient, M	Depth of Neutral Plane, ND
28	4	5	0.1	0.005	0.77	9.38
29					1.00	9.63
30					1.40	10.65
31			0.4	0.02	0.77	10.77
32					1.00	11.36
33					1.40	11.91
34			0.6	0.03	0.77	11.26
35					1.00	11.81
36					1.40	12.17
37	5	10	0.1	0.005	0.77	10.35
38					1.00	10.03
39					1.40	10.72
40			0.4	0.02	0.77	11.34
41					1.00	11.62
42					1.40	12.01
43			0.6	0.03	0.77	11.71
44					1.00	12.01
45					1.40	12.27
46	6	15	0.1	0.005	0.77	11.34
47					1.00	10.57
48					1.40	10.81
49			0.4	0.02	0.77	11.53
50					1.00	11.97
51					1.40	12.17
52			0.6	0.03	0.77	12.09
53					1.00	12.25
54					1.40	12.41

Table 4.3 Test Results for Group I-3, λ=0.05, D=0.4m, L=32m and e_{cs}=0.71

Test No.	Series No.	Surcharge KN/m2	κ/λ	Slope of Swelling Line, κ	Critical State Frictional Coefficient, M	Depth of Neutral Plane, ND
55	7	5	0.1	0.005	0.77	9.67
56					1.00	10.23
57					1.40	11.65
58			0.4	0.02	0.77	11.72
59					1.00	12.82
60					1.40	13.85
61			0.6	0.03	0.77	12.55
62					1.00	13.65
63					1.40	14.36
64	8	10	0.1	0.005	0.77	10.48
65					1.00	10.38
66					1.40	11.69
67			0.4	0.02	0.77	12.10
68					1.00	12.92
69					1.40	13.93
70			0.6	0.03	0.77	12.74
71					1.00	13.76
72					1.40	14.44
73	9	15	0.1	0.005	0.77	11.50
74					1.00	10.78
75					1.40	11.75
76			0.4	0.02	0.77	13.12
77					1.00	13.07
78					1.40	14.05
79			0.6	0.03	0.77	14.01
80					1.00	13.93
81					1.40	14.50

Table 4.4 Test Results for Group I-4, λ=0.05, D=0.8m, L=16m and e_{cs}=0.71

Test No.	Series No.	Surcharge KN/m2	κ/λ	Slope of Swelling Line, κ	Critical State Frictional Coefficient, M	Depth of Neutral Plane, ND
82	10	5	0.1	0.005	0.77	8.39
83					1.00	8.22
84					1.40	8.60
85			0.4	0.02	0.77	8.87
86					1.00	8.94
87					1.40	9.12
88			0.6	0.03	0.77	9.03
89					1.00	9.12
90					1.40	9.24
91	11	10	0.1	0.005	0.77	9 30
92					1.00	8.70
93					1.40	8.65
94			0.4	0.02	0.77	9.46
95					1.00	9.21
96					1.40	9.20
97			0.6	0.03	0.77	9.46
98					1.00	9.30
99					1.40	9.30
100	12	15	0.1	0.005	0.77	9.92
101					1.00	9.40
102					1.40	8.82
103			0 4	0 02	0.77	9.84
104					1 00	9.59
105					1.40	9.34
106			0.6	0.03	0.77	9 81
107					1.00	9 62
108					1.40	9.39

Table 4.5 Test Results for Group I-5, λ=0.05, D=0.8m, L=24m and e_{cs}=0.71

Test No.	Series No.	Surcharge KN/m2	κ/λ	Slope of Swelling Line, κ	Critical State Frictional Coefficient, M	Depth of Neutral Plane, ND
109	13	5	0.1	0.005	0.77	9.39
110					1.00	9.75
111					1.40	10.94
112			0.4	0.02	0 77	10.68
113					1.00	11.33
114					1.40	11.96
115			0.6	0.03	0.77	11.13
116					1.00	11.78
117					1.40	12.19
118	14	10	0.1	0.005	0.77	10.26
119					1.00	10.04
120					1.40	10.93
121			0.4	0.02	0.77	11.15
122					1.00	11.51
123					1.40	12.01
124			0.6	0.03	0.77	11.52
125					1.00	11.91
126					1.40	12.25
127	15	15	0.1	0.005	0.77	11.27
128					1.00	10.53
129					1.40	10.96
130			0.4	0.02	0.77	11.55
131					1.00	11.81
132					1.40	12.10
133			0.6	0.03	0.77	12.11
134					1.00	12.25
135					1.40	12.38

Table 4.6 Test Results for Group I-6, λ=0.05, D=0.8m, L=32m and e_{cs}=0.71

Test No.	Series No.	Surcharge KN/m2	κ/λ	Slope of Swelling Line, κ	Critical State Frictional Coefficient, M	Depth of Neutral Plane, ND
136	16	5	0.1	0.005	0.77	9.67
137					1.00	10.23
138					1.40	11.65
139			0.4	0.02	0.77	11.72
140					1.00	12.82
141					1.40	13.85
142			0.6	0.03	0.77	12.55
143					1.00	13.65
144					1.40	14.36
145	17	10	0.1	0.005	0.77	10.48
146					1.00	10.38
147					1.40	11.69
148			0.4	0.02	0.77	12.10
149					1.00	12.92
150					1.40	13.93
151			0.6	0.03	0.77	12.74
152					1.00	13.76
153					1.40	14.44
154	18	15	0.1	0.005	0.77	11.50
155					1.00	10.78
156					1.40	11.75
157			0.4	0.02	0.77	13.12
158					1.00	13.07
159					1.40	14.05
160			0.6	0.03	0.77	14.02
161					1.00	13.93
162					1.40	14.50

Table 4.7 Test Results for Group I-7, λ=0.[illegible], D=1.2m, L=16m and e_{cs}=0.71

Test No.	Series No.	Surcharge KN/m2	κ/λ	Slope of Swelling Line, κ	Critical State Frictional Coefficient, M	Depth of Neutral Plane, ND
163	19	5	0.1	0.005	0.77	8.32
164					1.00	8.19
165					1.40	8.65
166			0.4	0.02	0.77	8.81
167					1.00	8.90
168					1.40	9.12
169			0.6	0.03	0.77	8.97
170					1.00	9.10
171					1.40	9.25
172	20	10	0.1	0.005	0.77	9.18
173					1.00	8.[illegible]
174					1.40	8.66
175			0.4	0.02	0.77	9.37
176					1.00	9.13
177					1.40	9.25
178			0.6	0.03	0.77	9.37
179					1.00	9.25
180					1.40	9.30
181	21	15	0.1	0.005	0.77	9.89
182					1.00	9.27
183					1.40	8.80
184			0.4	0.02	0.77	9.84
185					1.00	9.49
186					1.40	9.28
187			0.6	0.03	0.77	9.82
188					1.00	9.62
189					1.40	9.36

Table 4.8 Test Results for Group I-8, λ=0.05, D=1.2m, L=24m and e_{cs}=0.71

Test No.	Series No.	Surcharge KN/m2	κ/λ	Slope of Swelling Line, κ	Critical State Frictional Coefficient, M	Depth of Neutral Plane, ND
190	22	5	0.1	0.005	0.77	9.40
191					1.00	9.97
192					1.40	11.23
193			0.4	0.02	0.77	10.61
194					1.00	11.29
195					1.40	12.00
196			0.6	0.03	0.77	11.01
197					1.00	11.73
198					1.40	12.20
199	23	10	0.1	0.005	0.77	10.18
200					1.00	10.04
201					1.40	11.14
202			0.4	0.02	0.77	10.96
203					1.00	11.39
204					1.40	12.01
205			0.6	0.03	0.77	11.32
206					1.00	11.79
207					1.40	12.22
208	24	15	0.1	0.005	0.77	11.07
209					1.00	10.48
210					1.40	11.13
211			0.4	0.02	0.77	11.55
212					1.00	11.65
213					1.40	12.06
214			0.6	0.03	0.77	12.09
215					1.00	12.25
216					1.40	12.37

Table 4.9 Test Results for Group I-9, λ=0.05, D=1.2m, L=32m and e_{cs}=0.71

Test No.	Series No.	Surcharge KN/m2	κ/λ	Slope of Swelling Line, κ	Critical State Frictional Coefficient, M	Depth of Neutral Plane, ND
217	25	5	0.1	0.005	0.77	9.67
218					1.00	10.23
219					1.40	11.65
220			0.4	0.02	0.77	11.72
221					1.00	12.82
222					1.40	13.85
223			0.6	0.03	0.77	12.55
224					1.00	13.65
225					1.40	14.36
226	26	10	0.1	0.005	0.77	10.48
227					1.00	10.38
228					1.40	11.69
229			0.4	0.02	0.77	12.10
230					1.00	12.92
231					1.40	13.93
232			0.6	0.03	0.77	12.74
233					1.00	13.76
234					1.40	14.44
235	27	15	0.1	0.005	0.77	11.50
236					1.00	10.78
237					1.40	11.75
238			0.4	0.02	0.77	13.12
239					1.00	13.07
240					1.40	14.05
241			0.6	0.03	0.77	14.01
242					1.00	13.93
243					1.40	14.50

Table 4.10 Test Results for Group II-1, λ=0.15, D=0.4m, L=16m and e_{cs}=1.63

Test No.	Series No.	Surcharge KN/m2	κ/λ	Slope of Swelling line	Critical State Frictional Coefficient, M	Depth of Neutral Plane, ND
244	1	5	0.1	0.015	0.77	8.69
245					1.00	8.37
246					1.40	8.63
247			0.4	0.06	0.77	9.10
248					1.00	9.11
249					1.40	9.21
250			0.6	0.09	0.77	9.22
251					1.00	9.27
252					1.40	9.28
253	2	10	0.1	0.015	0.77	9.52
254					1.00	8.90
255					1.40	8.76
256			0.4	0.06	0.77	9.70
257					1.00	9.41
258					1.40	9.32
259			0.6	0.09	0.77	9.67
260					1.00	9.46
261					1.40	9.39
262	3	15	0.1	0.015	0.77	10.05
263					1.00	9.61
264					1.40	8.97
265			0.4	0.06	0.77	10.11
266					1.00	9.79
267					1.40	9.47
268			0.6	0.09	0.77	10.21
269					1.00	9.75
270					1.40	9.55

Table 4.11 Test Results for Group II-2, λ=0.15, D=0.4m, L=24m and e_{cs}=1.63

Test No.	Series No.	Surcharge KN/m2	κ/λ	Slope of Swelling Line, κ	Critical State Frictional Coefficient, M	Depth of Neutral Plane, ND
271	4	5	0.1	0.015	0.77	9.71
272					1.00	10.07
273					1.40	10.91
274			0.4	0.06	0.77	11.01
275					1.00	11.6
276					1.40	12.15
277			0.6	0.09	0.77	11.46
278					1.00	12.00
279					1.40	12.33

Table 4.12 Test Results for Group II-3, λ=0.15, D=0.4m, L=32m and e_{cs}=1.63

Test No.	Series No.	Surcharge KN/m2	κ/λ	Slope of Swelling Line, κ	Critical State Frictional Coefficient, M	Depth of Neutral Plane, ND
280	5	5	0.1	0.015	0.77	10.09
281					1.00	10.78
282					1.40	12.23
283			0.4	0.06	0.77	12.19
284					1.00	13.35
285					1.40	14.13
286			0.6	0.09	0.77	12.84
287					1.00	14.03
288					1.40	14.72

Table 4.13 Test Results for Group III-1, λ=0.25, D=0.4m, L=16m and e_{cs}=2.55

Test No.	Series	Surcharge KN/m2	κ/λ	Slope of Swelling Line, κ	Critical State Frictional Coefficient, M	Depth of Neutral Plane, ND
289	1	5	0.1	0.025	0.77	8.73
290					1.00	8.51
291					1.40	8.70
292			0.4	0.10	0.77	9.12
293					1.00	9.13
294					1.40	9.23
295			0.6	0.15	0.77	9.25
296					1.00	9.29
297					1.40	9.32
298	2	10	0.1	0.025	0.77	9.56
299					1.00	9.01
300					1.40	8.88
301			0.4	0.10	0.77	9.72
302					1.00	9.44
303					1.40	9.33
304			0.6	0.15	0.77	9.70
305					1.00	9.46
306					1.40	9.42
307	3	15	0.1	0.025	0.77	10.14
308					1.00	9.66
309					1.40	9.09
310			0.4	0.10	0.77	10.15
311					1.00	9.81
312					1.40	9.49
313			0.6	0.15	0.77	9.48
314					1.00	9.80
315					1.40	9.57

Table 4.14 Test Results for Group III-2, λ=0.25, D=0.4m, L=24m and e_{cs}=2.55

Test No.	Series No.	Surcharge KN/m2	κ/λ	Slope of Swelling Line, κ	Critical State Frictional Coefficient, M	Depth of Neutral Plane, ND
316	4	5	0.1	0.025	0.77	9.97
317					1.00	10.57
318					1.40	11.25
319			0.4	0.10	0.77	11.12
320					1.00	11.65
321					1.40	12.10
322			0.6	0.15	0.77	11.45
323					1.00	12.11
324					1.40	12.34

Table 4.15 Test Results for Group III-3, λ=0.25, D=0.4m, L=32m and e_{cs}=2.55

Test No.	Series No.	Surcharge KN/m2	κ/λ	Slope of Swelling Line, κ	Critical State Frictional Coefficient, M	Depth of Neutral Plane, ND
325	5	5	0.1	0.025	0.77	10.47
326					1.00	11.20
327					1.40	12.61
328			0.4	0.10	0.77	11.97
329					1.00	13.42
330					1.40	14.14
331			0.6	0.15	0.77	12.95
332					1.00	14.29
333					1.40	14.77

Table 4.16 Test Results for Group IV-1, λ=0.35, D=0.4m, L=16m and e_{cs}=3.47

Test No.	Series No.	Surcharge KN/m2	κ/λ	Slope of Swelling Line, κ	Critical State Frictional Coefficient, M	Depth of Neutral Plane, ND
334	1	5	0.1	0.035	0.77	8.75
335					1.00	8.64
336					1.40	8.82
337			0.4	0.14	0.77	9.16
338					1.00	9.14
339					1.40	9.24
340			0.6	0.21	0.77	9.29
341					1.00	9.31
342					1.40	9.37
343	2	10	0.1	0.035	0.77	9.63
344					1.00	9.15
345					1.40	8.97
346			0.4	0.14	0.77	9.75
347					1.00	9.47
348					1.40	9.35
349			0.6	0.21	0.77	9.75
350					1.00	9.35
351					1.40	9.45
352	3	15	0.1	0.035	0.77	10.19
353					1.00	9.71
354					1.40	9.24
355			0.4	0.14	0.77	10.18
356					1.00	9.83
357					1.40	9.52
358			0.6	0.21	0.77	10.05
359					1.00	9.88
360					1.40	9.60

Table 4.17 Test Results for Group IV-2, λ=0.35, D=0.4m, L=24m and e_{cs}=3.47

Test No.	Series No.	Surcharge KN/m2	κ/λ	Slope of Swelling Line, κ	Critical State Frictional Coefficient, M	Depth of Neutral Plane, ND
361	4	5	0.1	0.035	0.77	10.27
362					1.00	11.16
363					1.40	11.56
364			0.4	0.14	0.77	10.65
365					1.00	11.72
366					1.40	12.08
367			0.6	0.21	0.77	11.43
368					1.00	12.20
369					1.40	12.37

Table 4.18 Test Results for Group IV-3, λ=0.35, D=0.4m, L=32m and e_{cs}=3.47

Test No.	Series No	Surcharge KN/m2	κ/λ	Slope of Swelling Line, κ	Critical State Frictional Coefficient, M	Depth of Neutral Plane, ND
370	5	5	0.1	0.035	0.77	10.78
371					1.00	12.34
372					1.40	12.93
373			0.4	0.14	0.77	11.81
374					1.00	13.50
375					1.40	14.16
376			0.6	0.21	0.77	13.06
377					1.00	14.49
378					1.40	14.82

Table 4.19 Test Results for Group V, D=0.4m,

Test No.	Series No.	Pile Length (m)	Surcharge KN/m2	Cohesion c	Depth of Neutral Plane, ND
379	1	16	5	10	8.76
380				20	8.52
381				30	8.47
382			10	10	9.21
383				20	8.59
384				30	8.37
385			15	10	9.59
386				20	8.94
387				30	8.5
388	2	24	5	10	11.71
389				20	11.13
390				30	11.04
391			10	10	12.63
392				20	11.35
393				30	10.94
394			15	10	13.3
395				20	12.06
396				30	11.31
397	3	32	5	10	14.00
398				20	13.15
399				30	13.03
400			10	10	14.91
401				20	13.62
402				30	12.92
403			15	10	15.93
404				20	14.43
405				30	13.57

4.2 SKIN FRICTION DISTRIBUTION

The finite element results deduced from the present investigation are presented in graphical forms in Figures (4.1 to 4.3). In these Figures, major principal strain direction, major effective stress direction and the shear stress τ_{xy} are given respectively. It can be observed that the major principal strain and the major principal effective stress directions are changed at the level of the neutral plane, furthers, the shear stress τ_{xy} is changing from positive values to a negative values at the level of the neutral plane. A typical distribution of skin friction (negative and positive friction) with the position of neutral plane is shown in Figure (4.4)

As shown in Figure (4.4) the skin friction started from zero value at the ground level and increases until it reaches a peak negative value at an intermediate depth, then it decreases down to zero at the elevation of the neutral plane, below the neutral plane the positive skin friction develops.

Figure (4.5) shows a typical distribution of the load imposed on the pile due to the surcharge loading. It can be seen that the load at the top of the pile is equal to zero and increases gradually due to the negative skin friction until it reaches a maximum value at the level of the neutral plane. Then the load decreases as a result of the positive skin friction acting below the neutral plane.

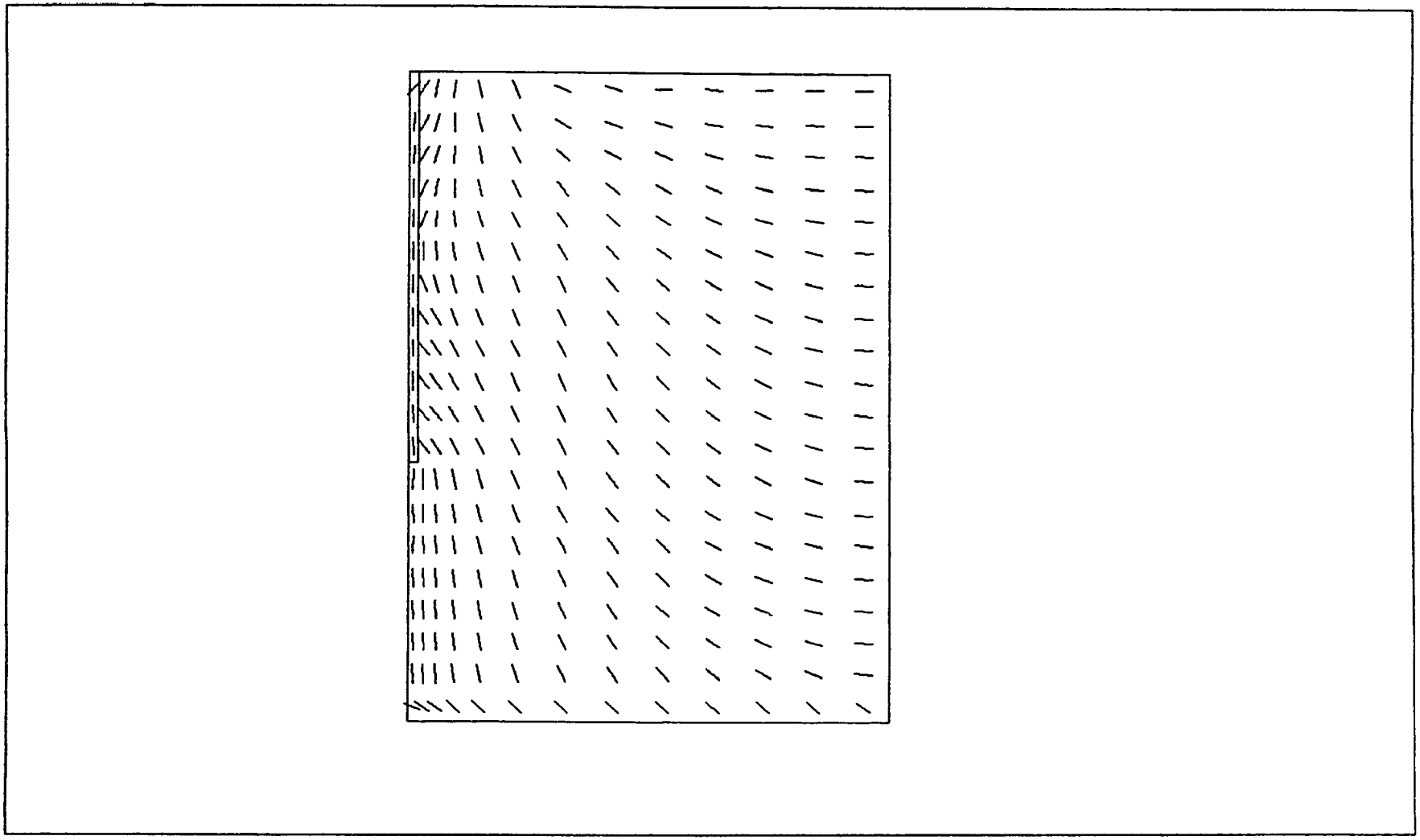

Fig. 4.1 Major Principal Strain Direction arround the Pile after applying the Surcharge Load.

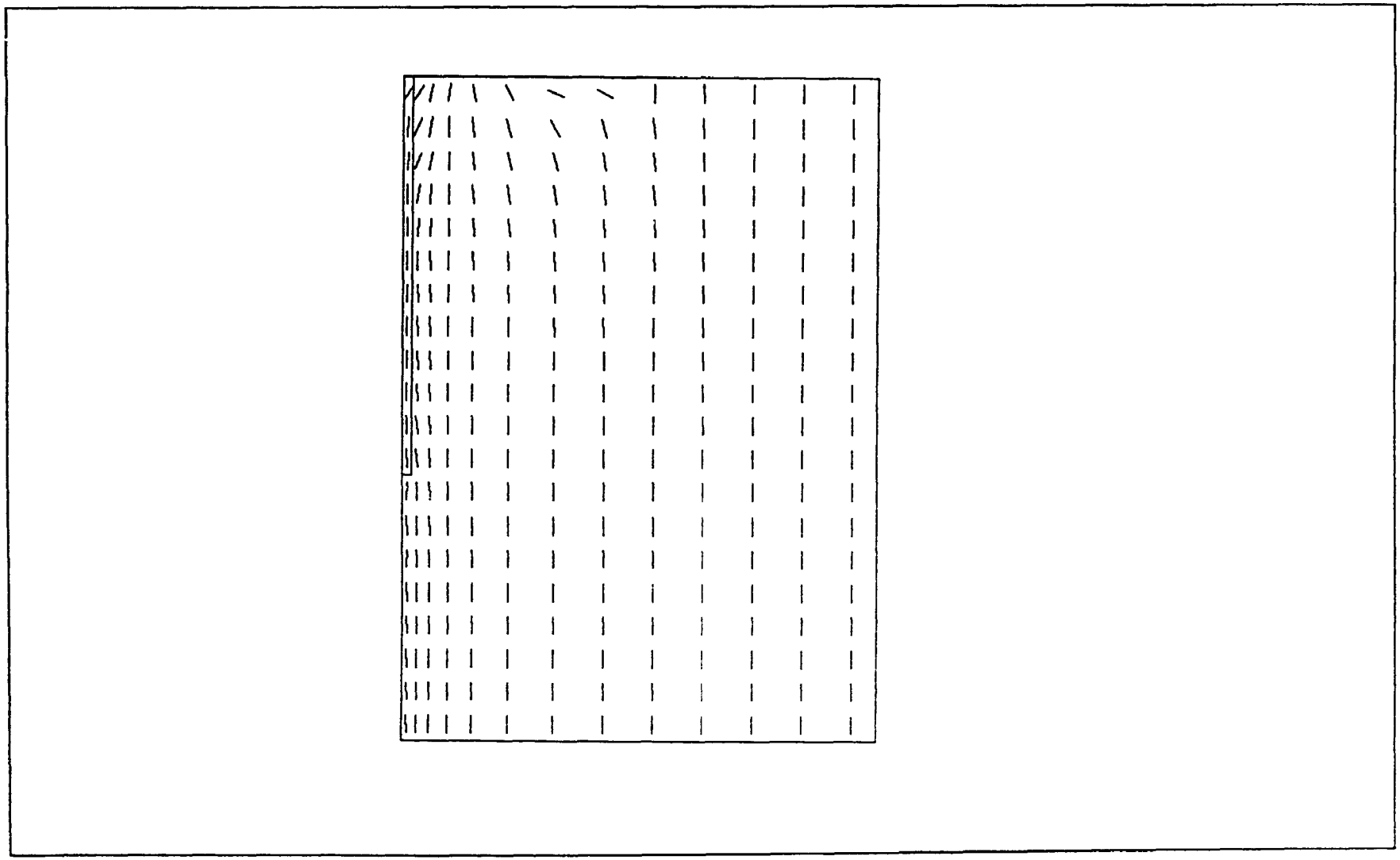

Fig. 4.2 Major Principal Effective Stress Direction arround the Pile after applying the Surcharge Load.

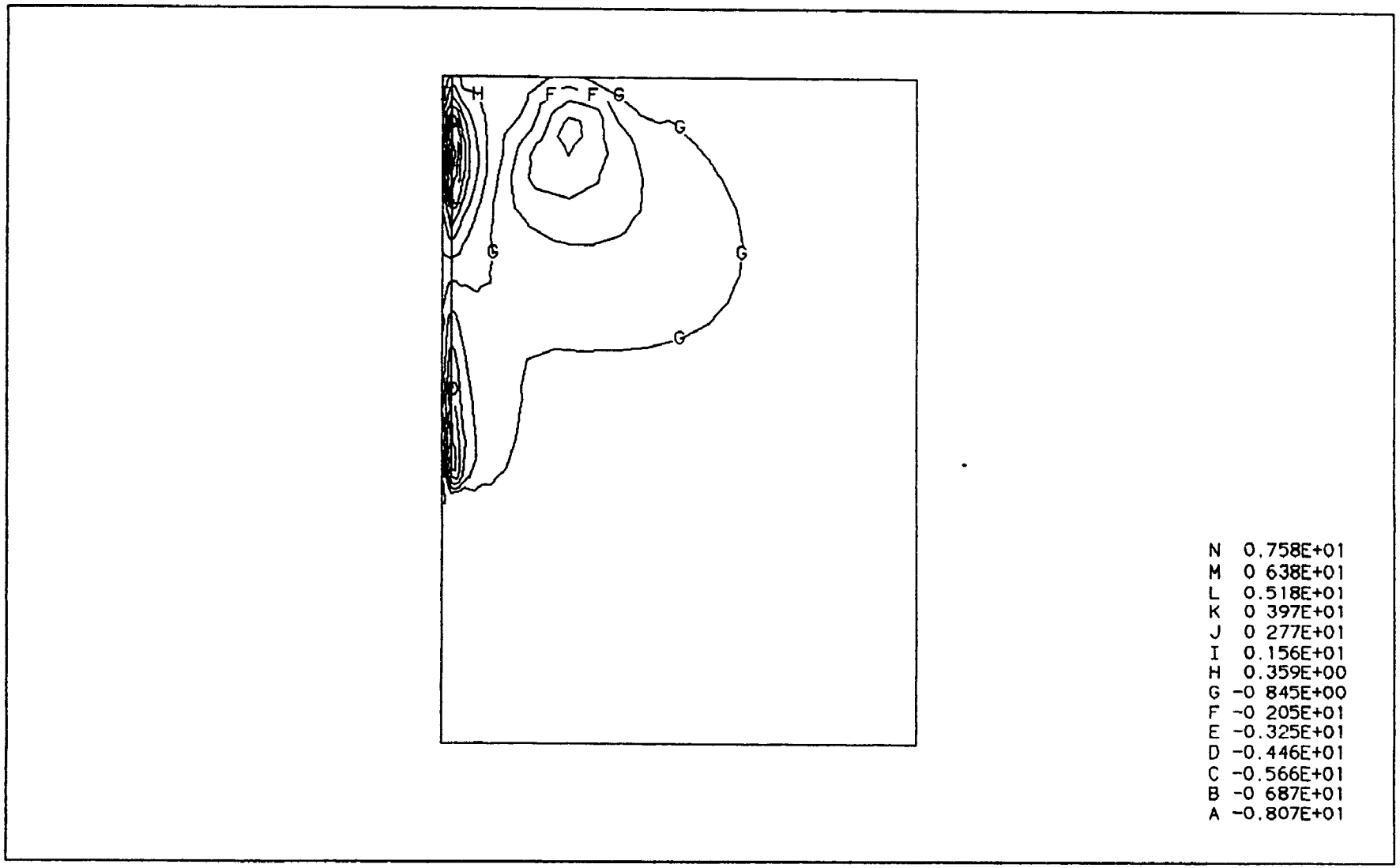

Fig. 4.3 Shear Stress arround the Pile after applying the Surcharge Load.

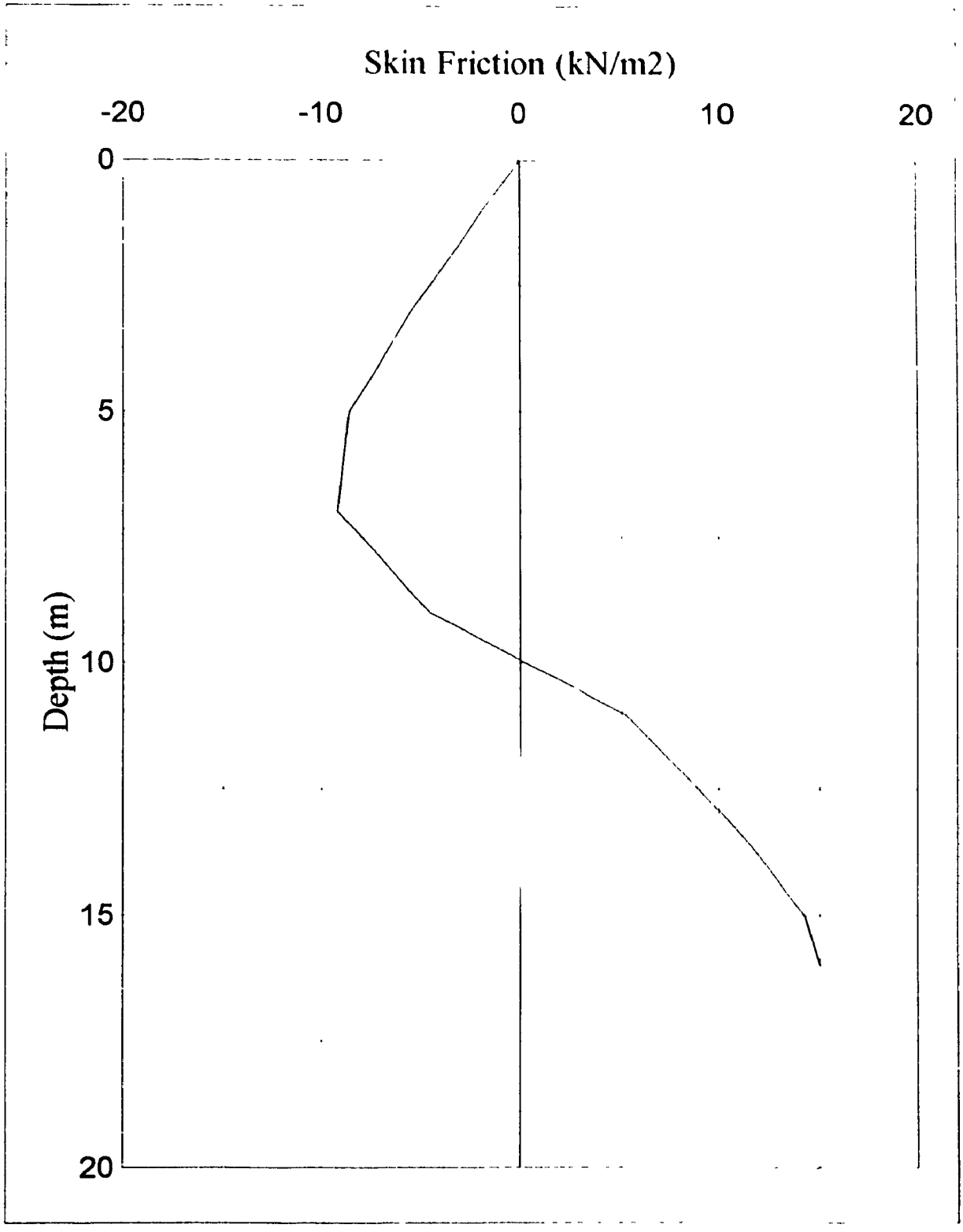

Fig. 4.4 Typical Distribution of Skin Friction and the Position of the Neutral plane.

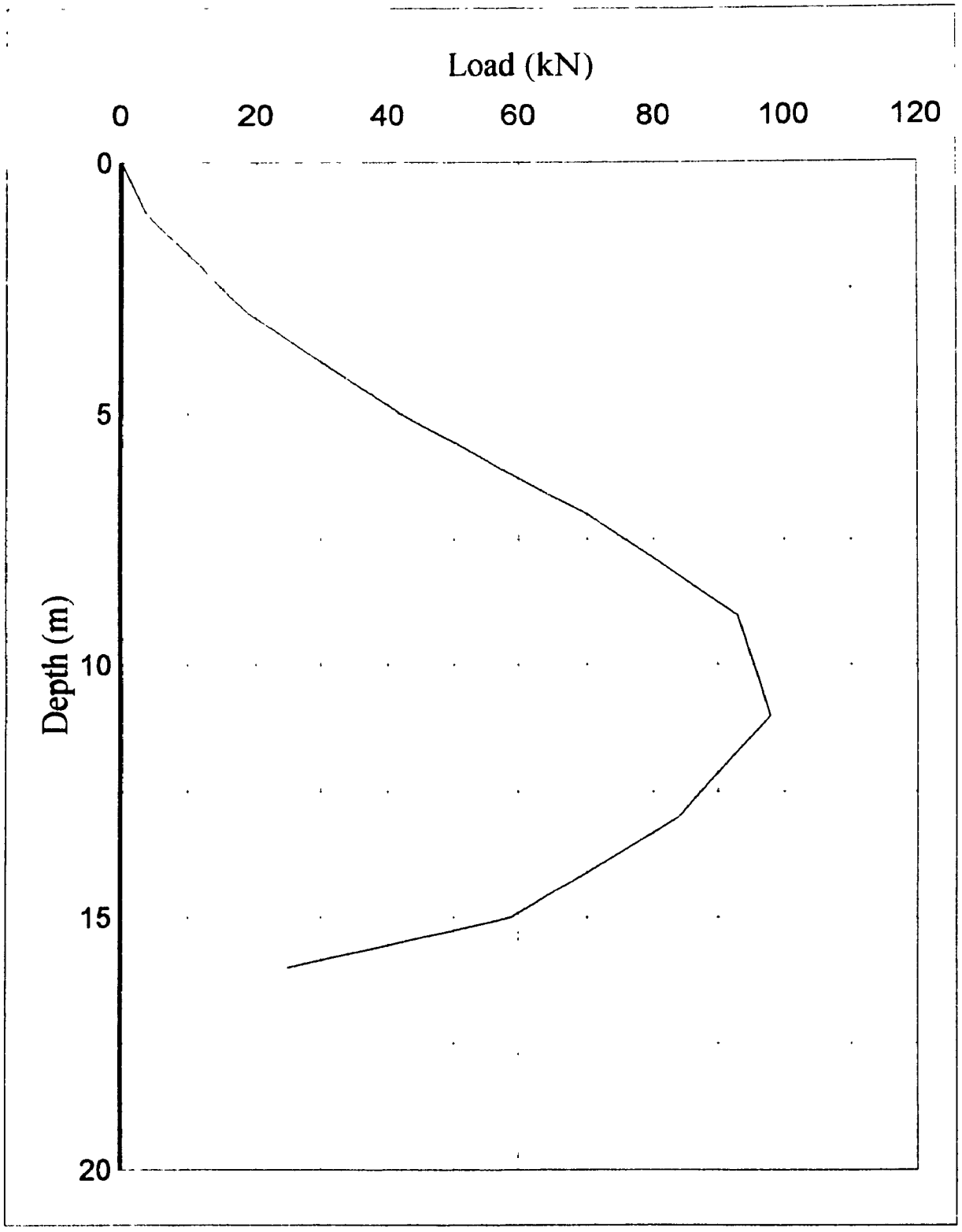

Fig. 4.5 Typical Distribution of Load in Pile in Clay Due to Surcharge Load

4.3 COMPARISON WITH FIELD DATA

The skin friction obtained from the present investigation using the modified cam clay soil model was compared with the results of a long term full-scale field test of a pile driven in Bangkok subsoil. The surrounded soil was loaded by 2 m. height embankment filling materials, the pile was driven to a depth of 25 m. below the ground surface. The embankment around the pile was constructed rapidly within 3 days. The soil parameters were as shown in Table 4.20. Figure (4.6) shows a comparison between the measured and predicted skin friction along the pile shaft, where good agreement can be found

.Table 4.20 Modified Cam Clay Parameters for Bangkok Subsoil.

Depth. m.	κ	λ	**ecs**	**M**	**G kN/m^2**	μ	γ **kn/m^3**	**Kp.E^{-5} m/day**
0-4	0.053	0.182	1.667	1.05	1666	0.33	16.66	67.6
4-10	0.084	0.514	3.052	0.97	1764	0.33	14.7	5.5
10-20	0.063	0.323	2.085	0.98	2009	0.33	16.66	2.63
20-40	0.027	0.116	1.199	0.90	3597	0.33	18.62	3.72

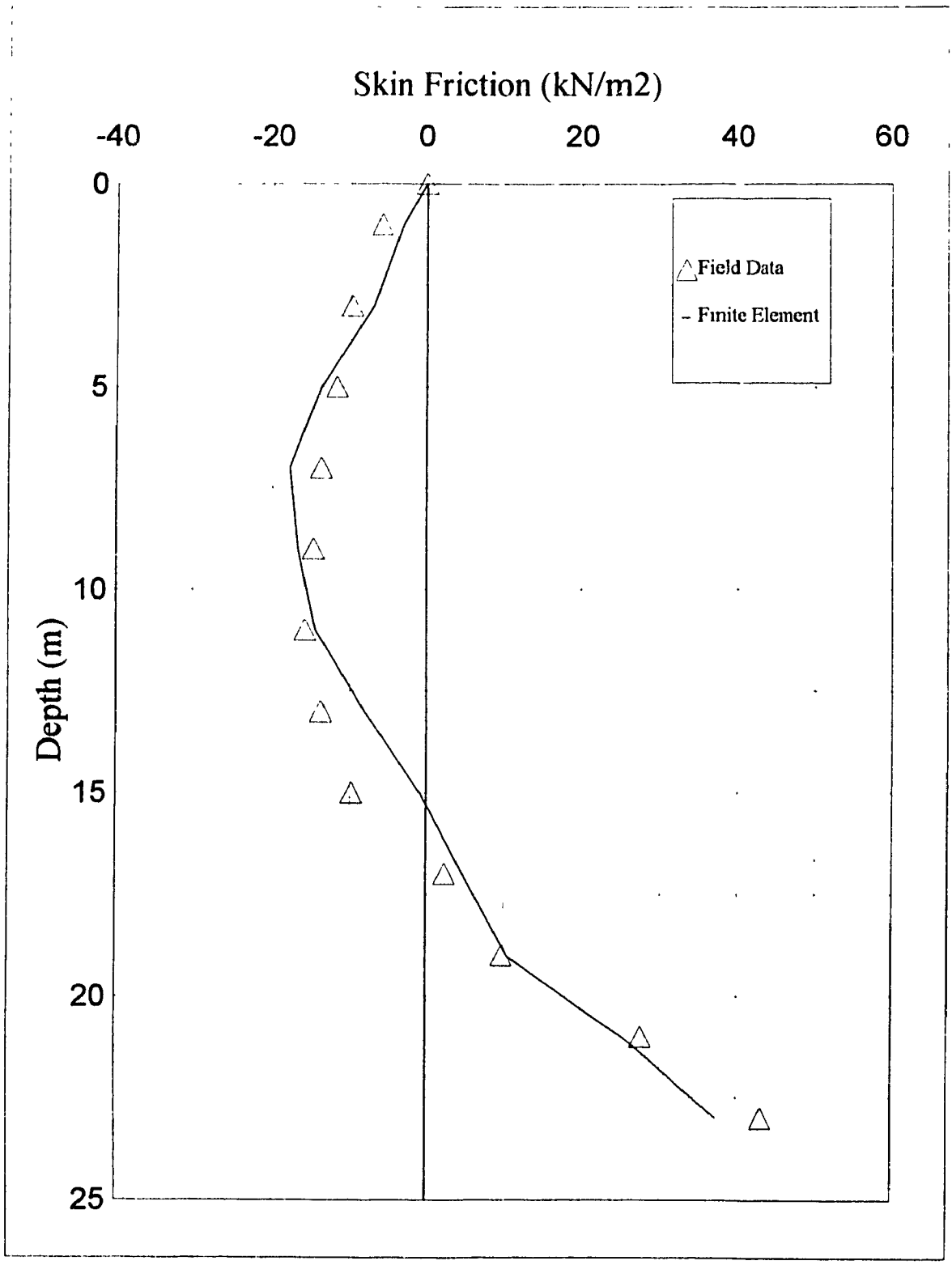

Fig. 4.6 Comparison of the Results Deduced from the Numerical Model and Field Measurments (Indraratna, 1992).

Table 4.21 presents a comparison for the case of 16 m long pile and 0.4 m diameter surrounded by soft clay loaded by a surcharge 15 kN/m^2. The negative skin friction predicted in the present investigation using the Mohr-Coulomb soil model was compared with Gralanger empirical values (Table 2.3) and Vesic equation (Table 2.4)

Table 4.21 Comparison of results of present investigation with the existing theories

Source	Negative Skin Friction
Gralanger (1973)	96 kN
Vesic (1979)	72 kN
Present investigation	73.7 kN

It can be observed that while Vesic equation gives a close result of the negative skin friction to the present investigation, the result value obtained according to Gralanger empirical formula was overestimated.

4.4. PARAMETRIC STUDY

The parameters which believed to have a direct effect on the depth of the neutral plane (ND) were isolated and examined individually for each soil model.

4.4.1 Modified Cam Clay Model

The parameters are; the pile diameter D, the pile length L, the surcharge S, the slope of the critical state line λ, the slope of the swelling line κ and the critical state frictional coefficient M.

4.4.1.1 Effect of pile diameter, D

Figures (4.7 & 4.8) show the variation of the ratio ND/L with the pile diameter, D for three pile lengths, 16, 24 and 32 m.

From these figures, it can be concluded that the pile diameter, D is an insensitive parameter which does not affect the location of the neutral plane, ND.

4.4.1.2 Effect of pile length, L

The variation of ratio ND/L versus pile length, L for different values of κ/λ, is presented in Figures (4.9 & 4.10). These figures show that the ratio ND/L decreases considerably due to an increase of the pile length, L for piles subjected to the same conditions.

4.4.1.3 Effect of the slope of the swelling line,κ

The variation of ratio ND/L versus the slope of the swelling line, κ for different

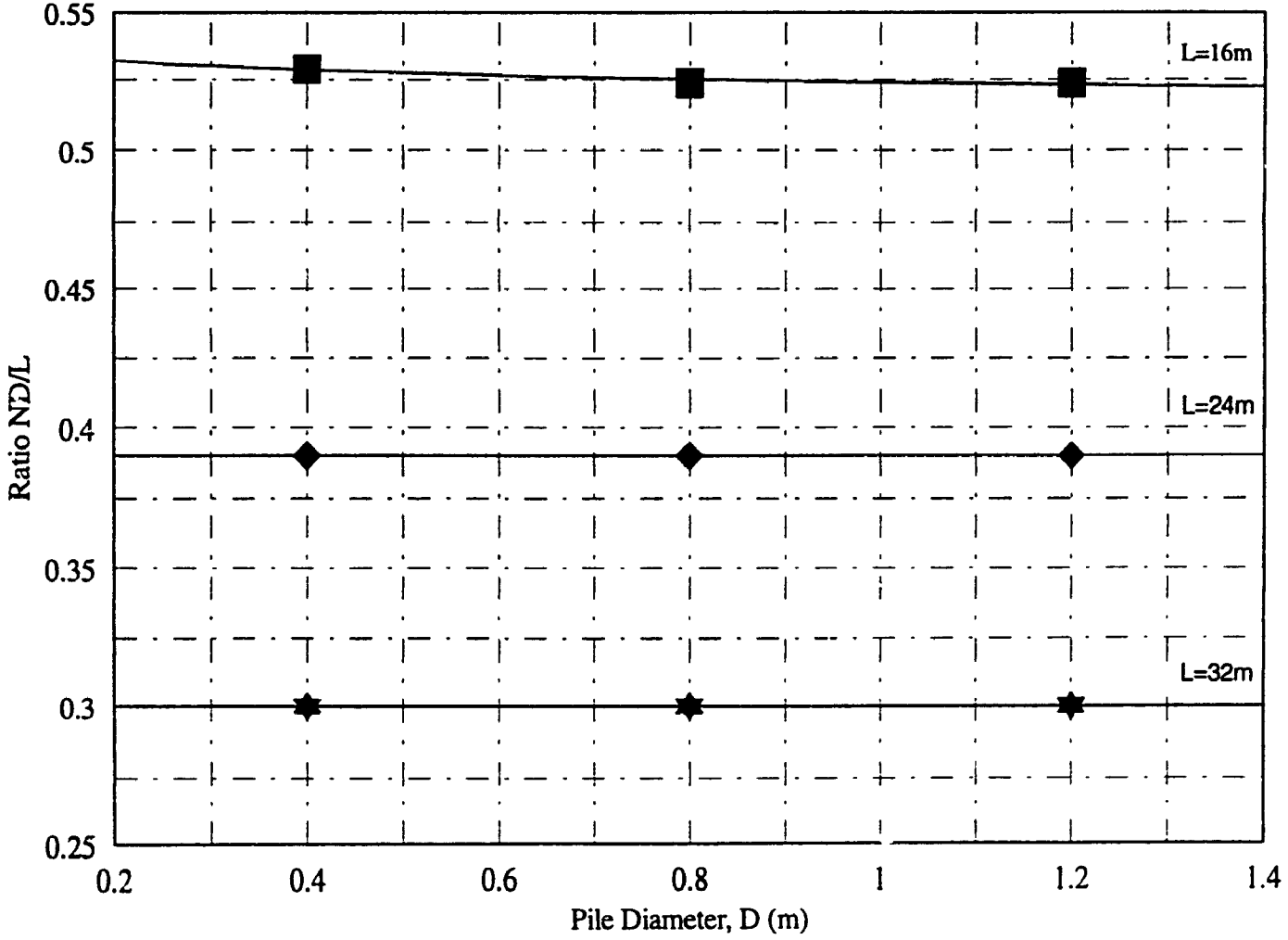

Fig. 4.7 Ratio ND/L Versus Pile Diameter,D (Surcharge = 5 kN/m2)

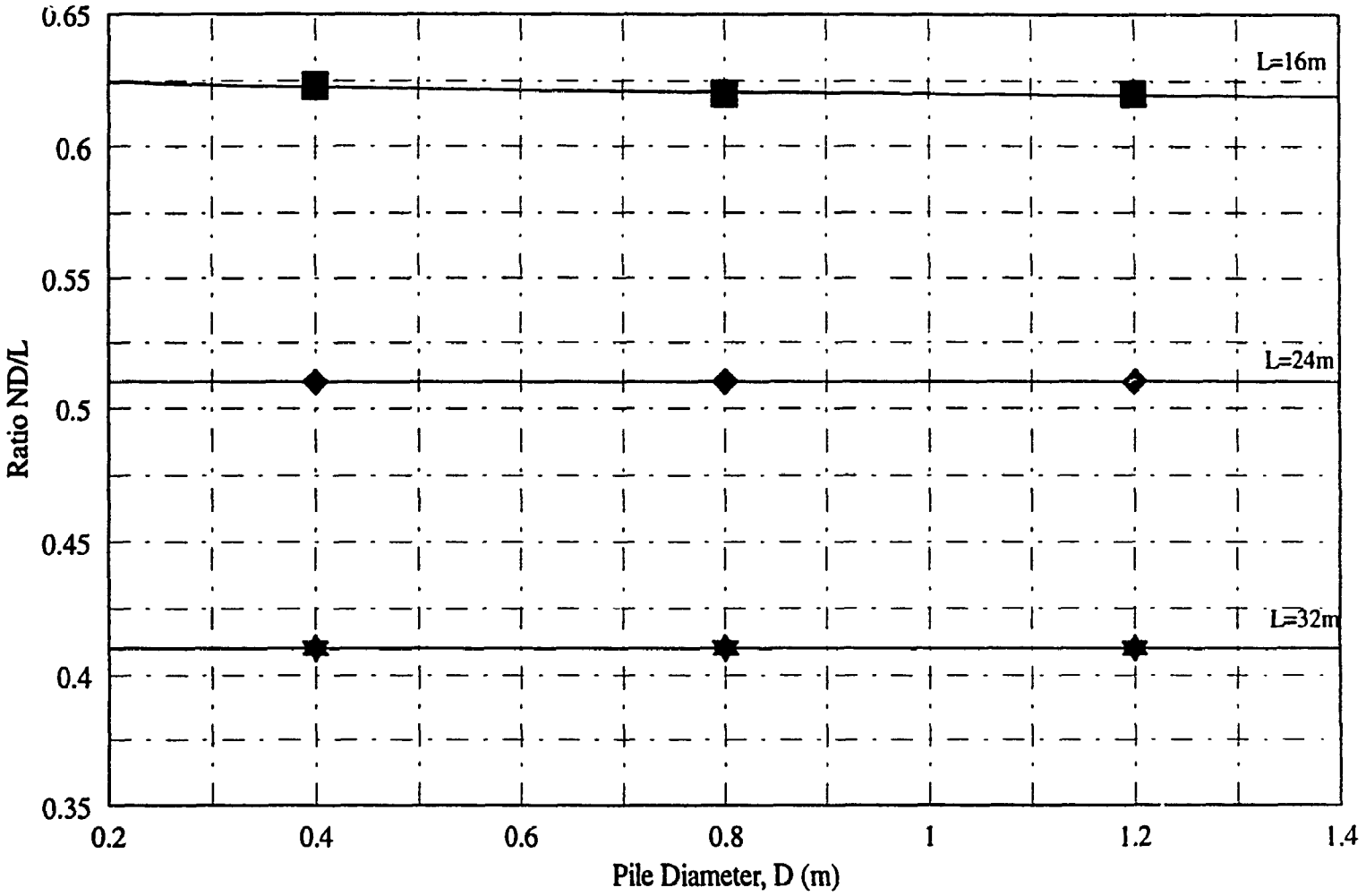

Fig. 4.8 Ratio ND/L Versus Pile Diameter,D (Surcharge = 15 kN/m2)

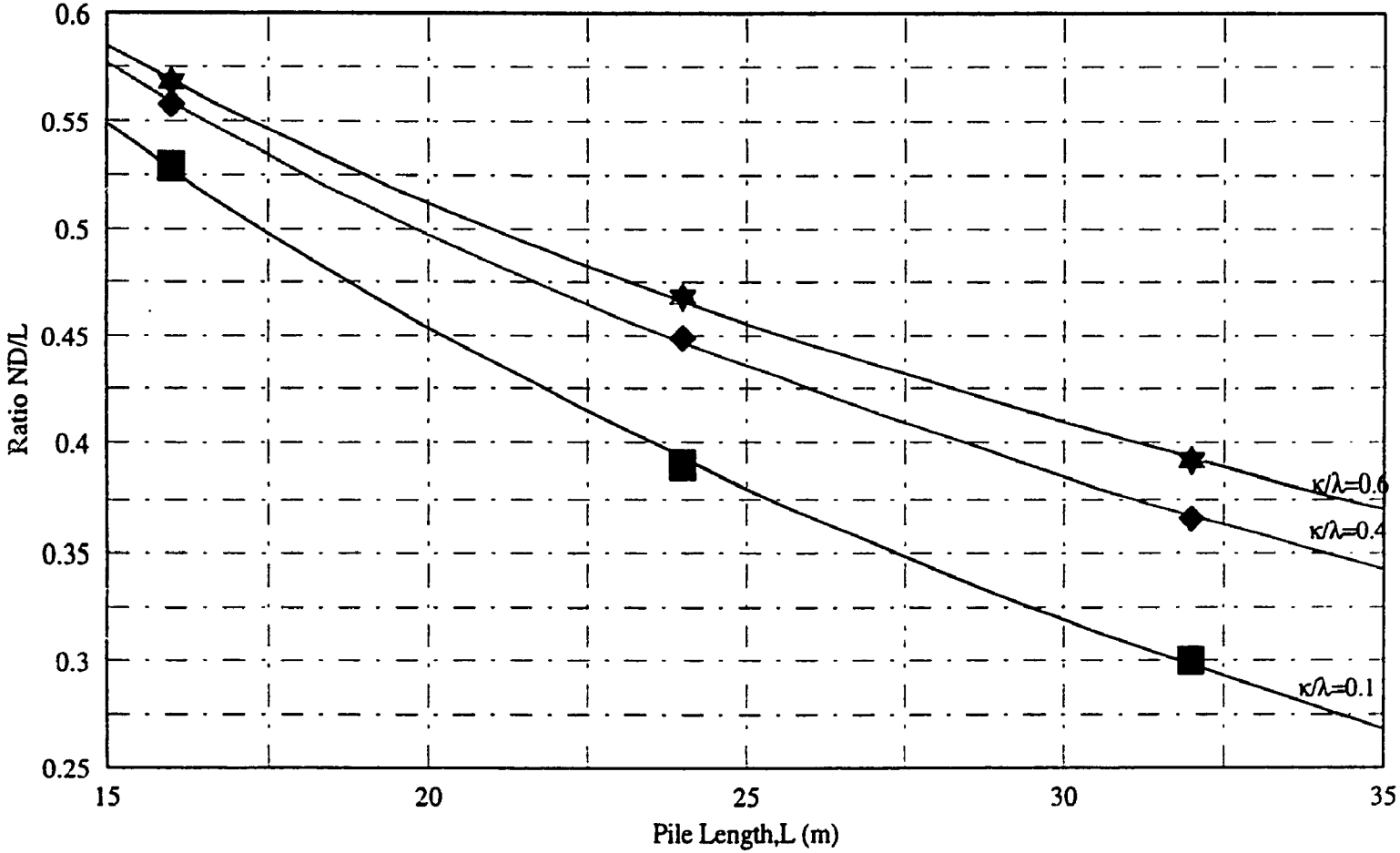

Fig. 4.9 Ratio ND/L Versus Pile Length,L (Surcharge = 5 kN/m2)

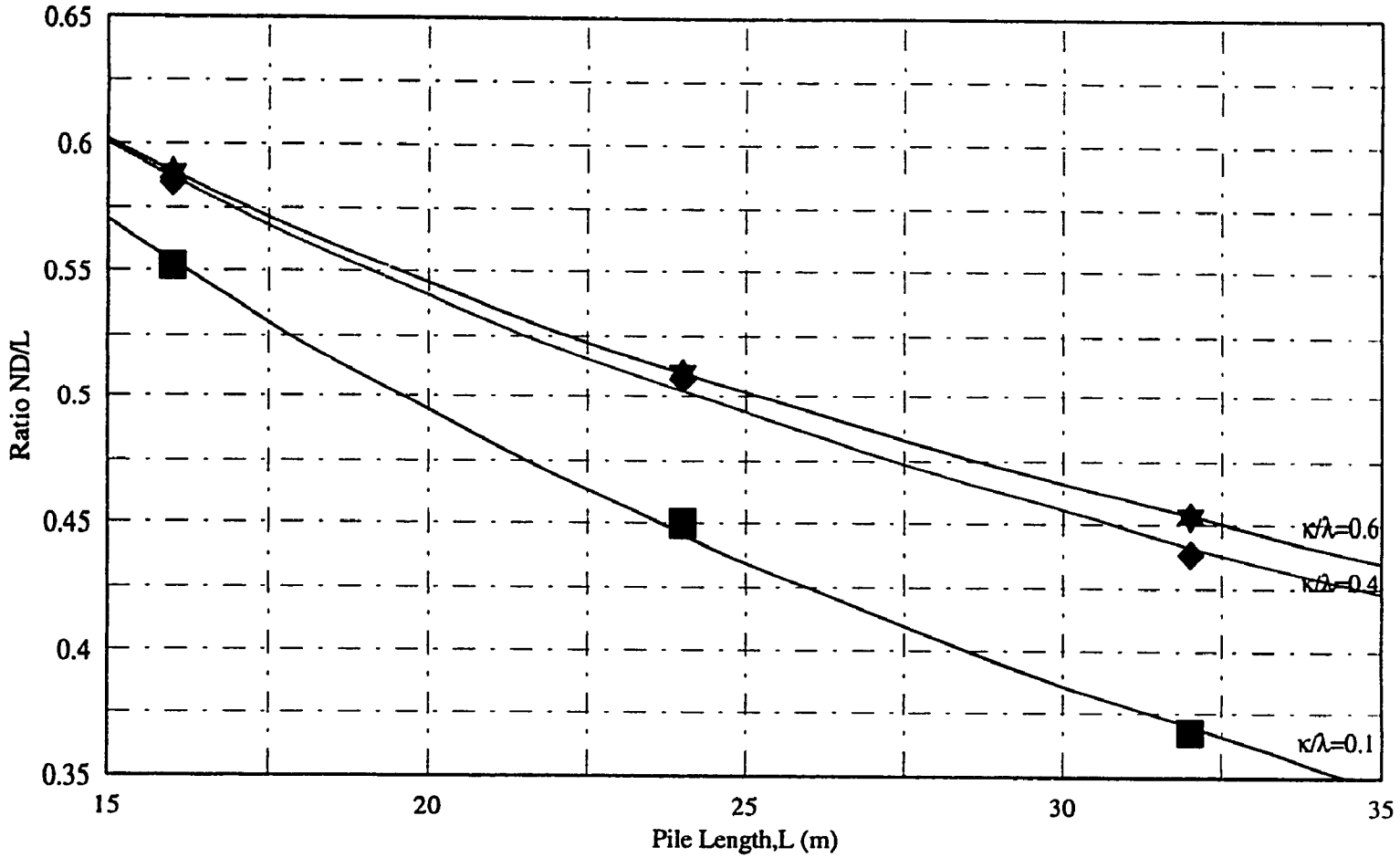

Fig. 4.10 Ratio ND/L Versus Pile Length,L (Surcharge =15 kN/m2)

pile lengths is presented in Figures (4.11 & 4.12). These Figures show that the predicted ratio ND/L increases due to an increase of the slope of the swelling line, κ. this is attributed to the fact that κ is an elastic parameter of the soil, where the stiffer the soil is, the smaller the value of κ of the soil.

4.4.1.4 Effect of the slope of the critical state line, λ

The variation of ratio ND/L versus the slope of the critical state line, λ for three different pile lengths is presented in Figure (4.13). This Figure shows that the predicted ratio ND/L insignificantly increases with the increase of λ in a slightly rate.

These increases of the ratio ND/L with the increase of λ can be explained by the fact that the higher the value of λ, the more the initial voids ratio, which means that the soil is softer.

4.4.1.5 Effect the critical state frictional coefficient, M

The variation of ND versus the critical state frictional coefficient, M is presented in Figures (4.14 & 4.15). An increase of M leads to an increase of the ratio ND/L which is expected because M is the critical state frictional coefficient and has a direct relation with ϕ as was explained in chapter three and according to the equation 3.15 and it obvious that an increase of friction leads to an increase of skin friction between soil and pile. It is noticed from these graphs that the rate of increase of ND/L at a bigger pile length is more than that for shorter piles.

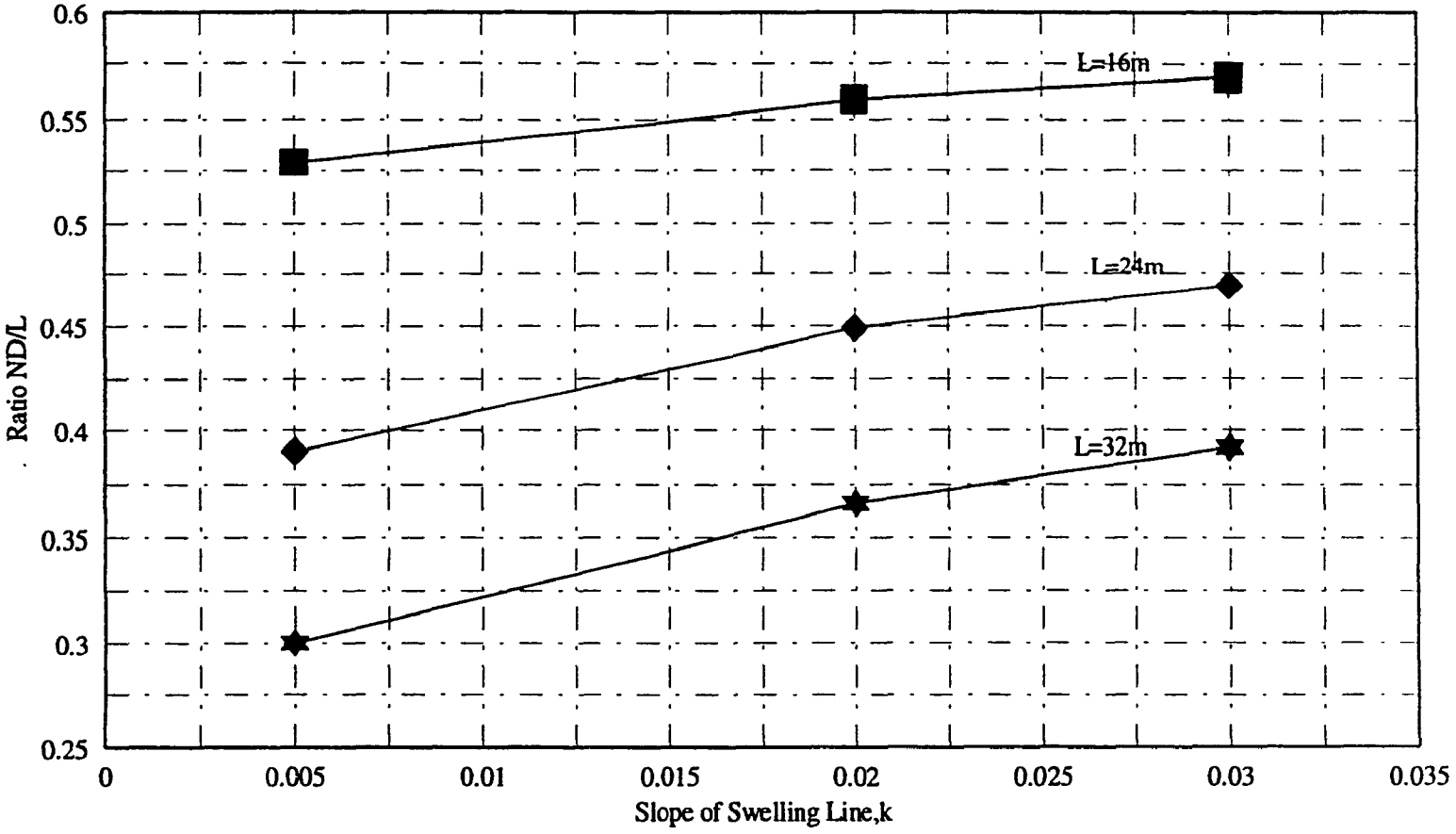

Fig. 4.11 Ratio ND/L Versus the Slope of the Swelling line, κ (Surcharg = 5 kN/m2)

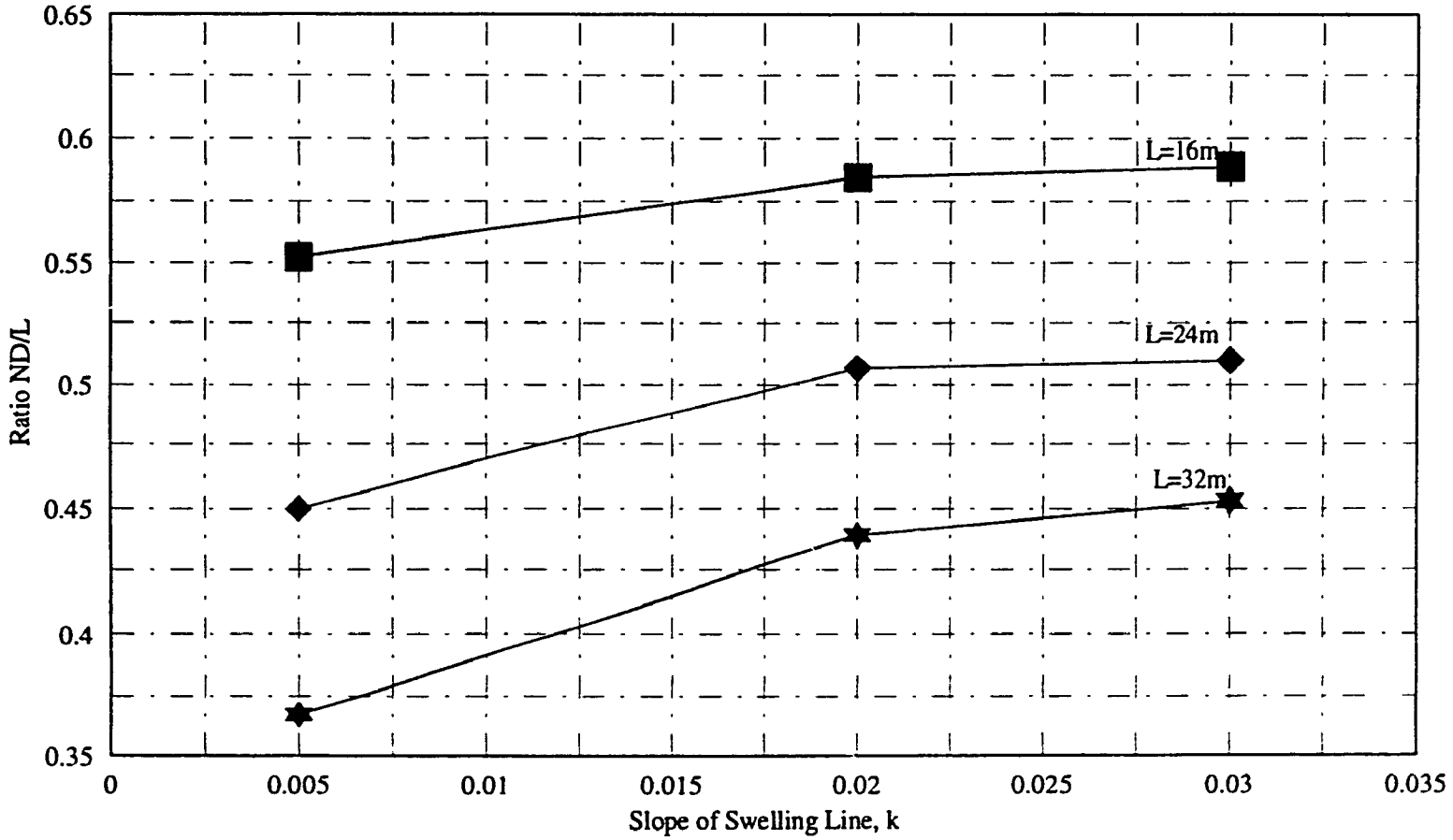

Fig. 4.12 Ratio ND/L Versus the Slope of the Swelling Line, κ (Surcharg = 15 kN/m2)

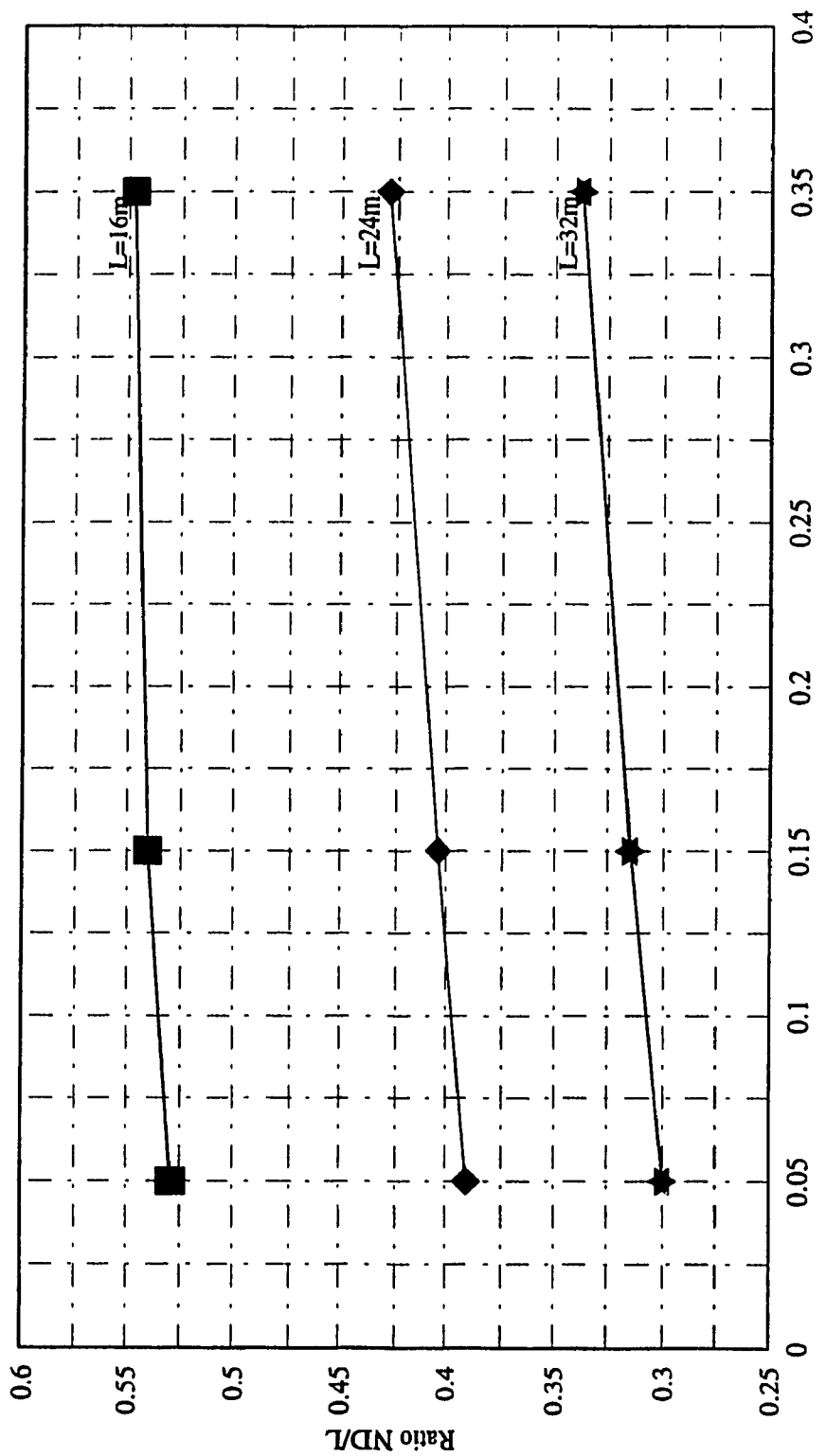

Fig. 4.13 Ratio ND/L Versus Slope of Critical State Line, λ (Surcharge = 5 kN/m2)

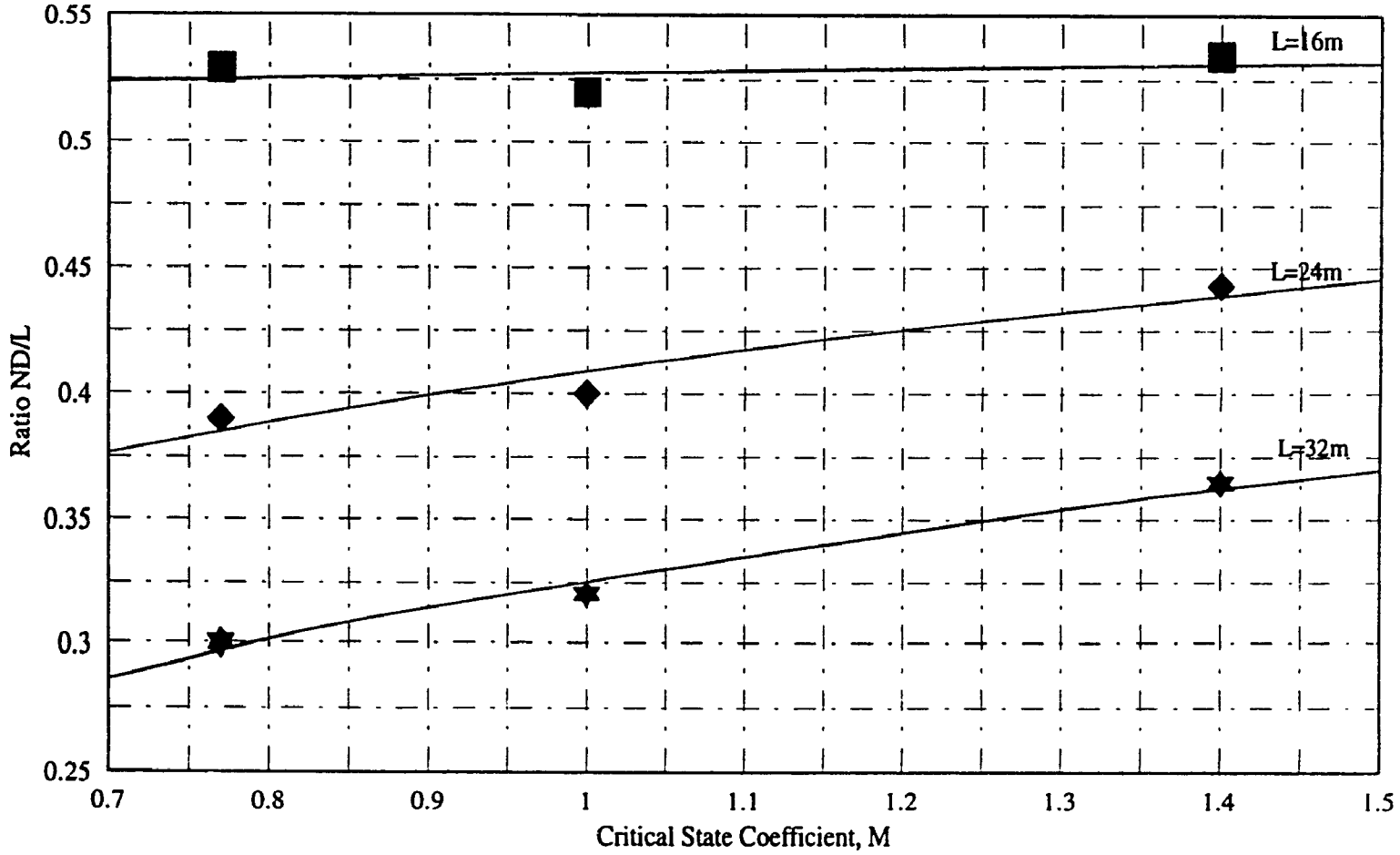

Fig. 4.14 Ratio ND/L Versus Critical State Frictional Coeffecient, M (Surcharge = 5 kN/m2)

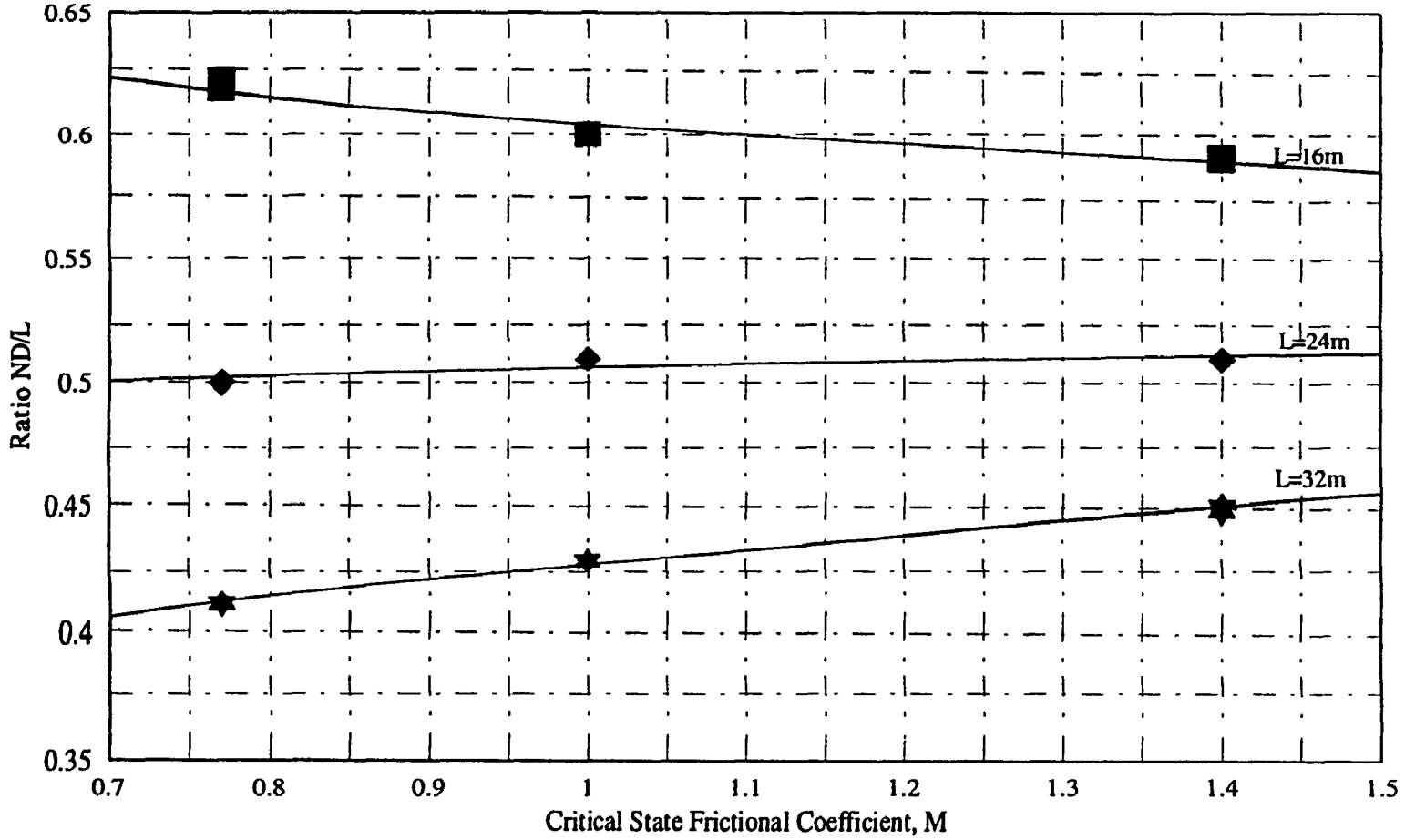

Fig. 4.15 Ratio ND/L Versus Critical State Frictional Coeffecient, M (Surcharge =15 kN/m2)

4.4.1.6 Effect of the surcharge, S

The variation of ratio ND/L versus the surcharge load, S for different pile lengths is presented in Figures (4.16 & 4.17). These figures show that the predicted ratio ND/L increases in case of weak soil due to an increase of the discharge, S, while the increase seemed to be insignificant in case of strong soil.

4.4.2 Mohr-Coulomb Model

The elastic perfectly plastic soil model Mohr-Coulomb was used in order to determine the effect of the cohesion parameter c, length of the pile, L and the surcharge, S on the depth of the neutral plane, ND.

4.4.2.1 Effect of Cohesion, c

The variation of ratio ND/L versus the cohesion, c for three different pile lengths is presented in Figures (4.18 & 4.19). These Figures show that the predicted ratio ND/L decreases with the increase of the cohesion, c, i.e. the depth of the neutral plane decreases in case of strong soil.

4.4.2.2 Effect of pile length, L

The variation of ratio ND/L versus pile length, L for different values of κ/λ, is presented in Figures (4.20 & 4.21). These Figures show that the ratio ND/L decreases considerably due to an increase of the pile length, L for piles subjected to the same conditions.

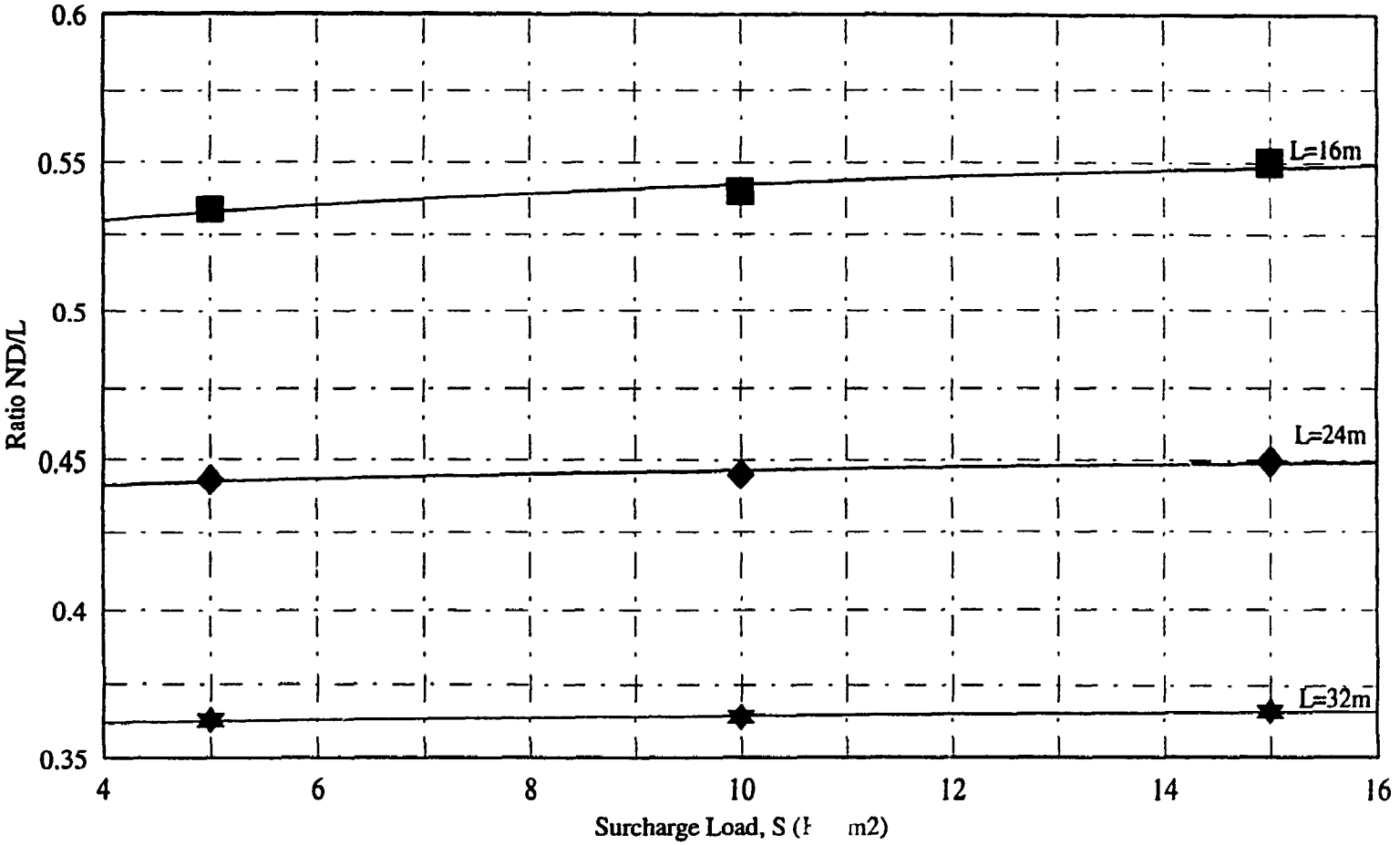

Fig. 4.16 Ratio ND/L Versus Surcharge Load, S ($\kappa/\lambda = 0.1$)

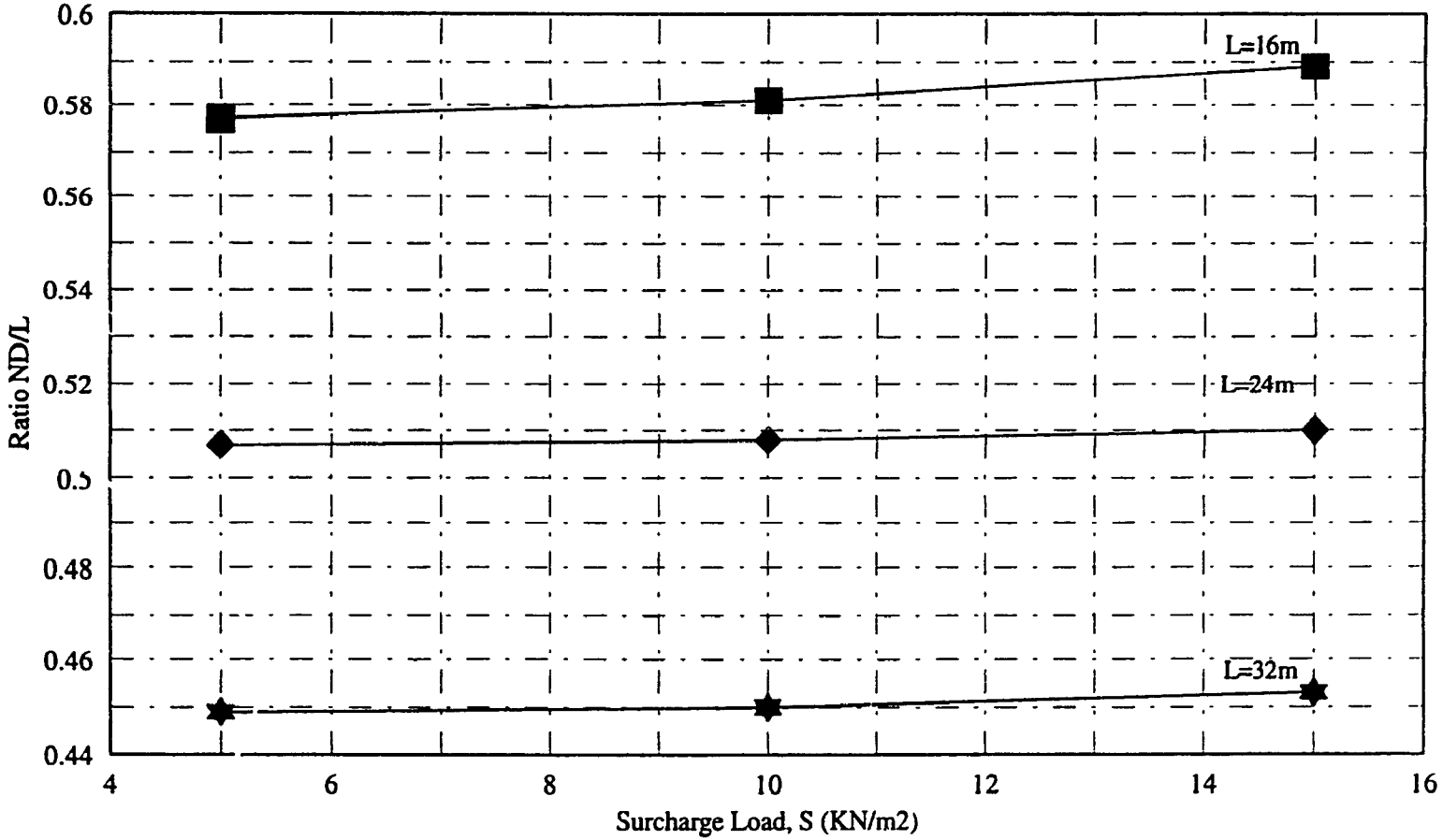

Fig. 4.17 Ratio ND/L Versus Surcharge Load, S ($\kappa/\lambda = 0.6$)

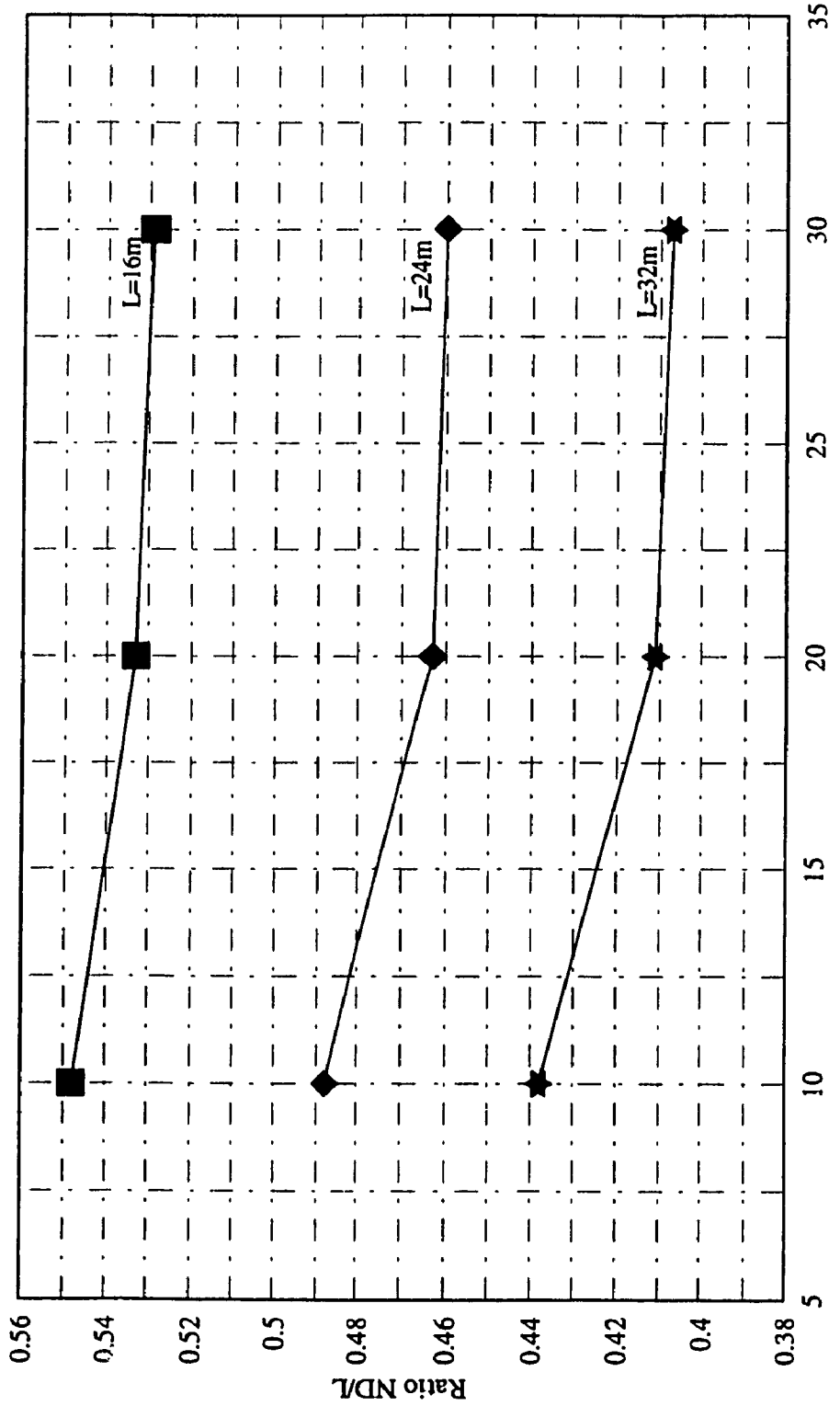

Fig. 4.18 Ratio ND/L Versus Cohesion, c (Surcharge = 5 kN/m2)

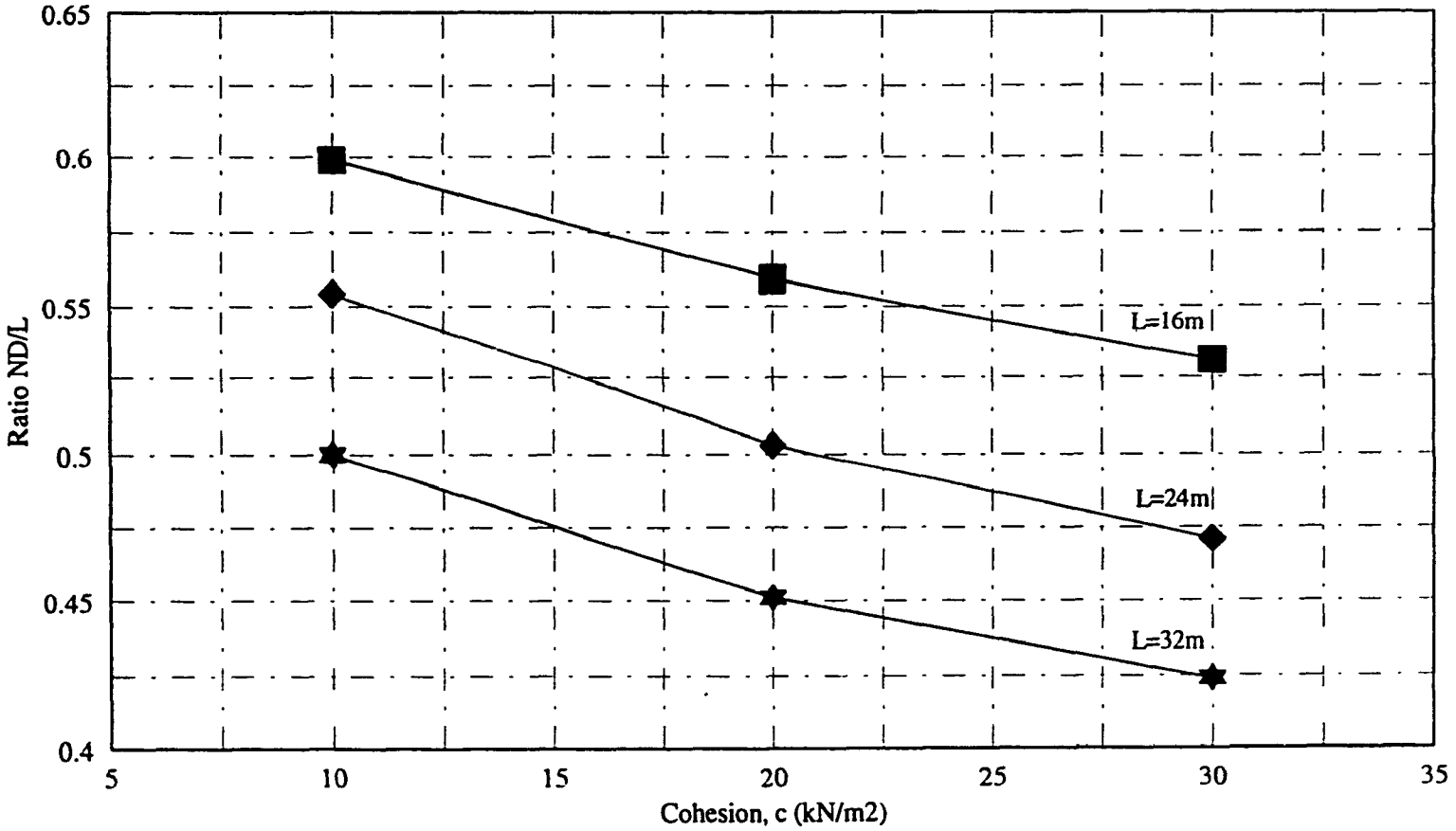

Fig. 4.19 Ratio ND/L Versus Cohesion, c (Surcharge = 15 kN/m2)

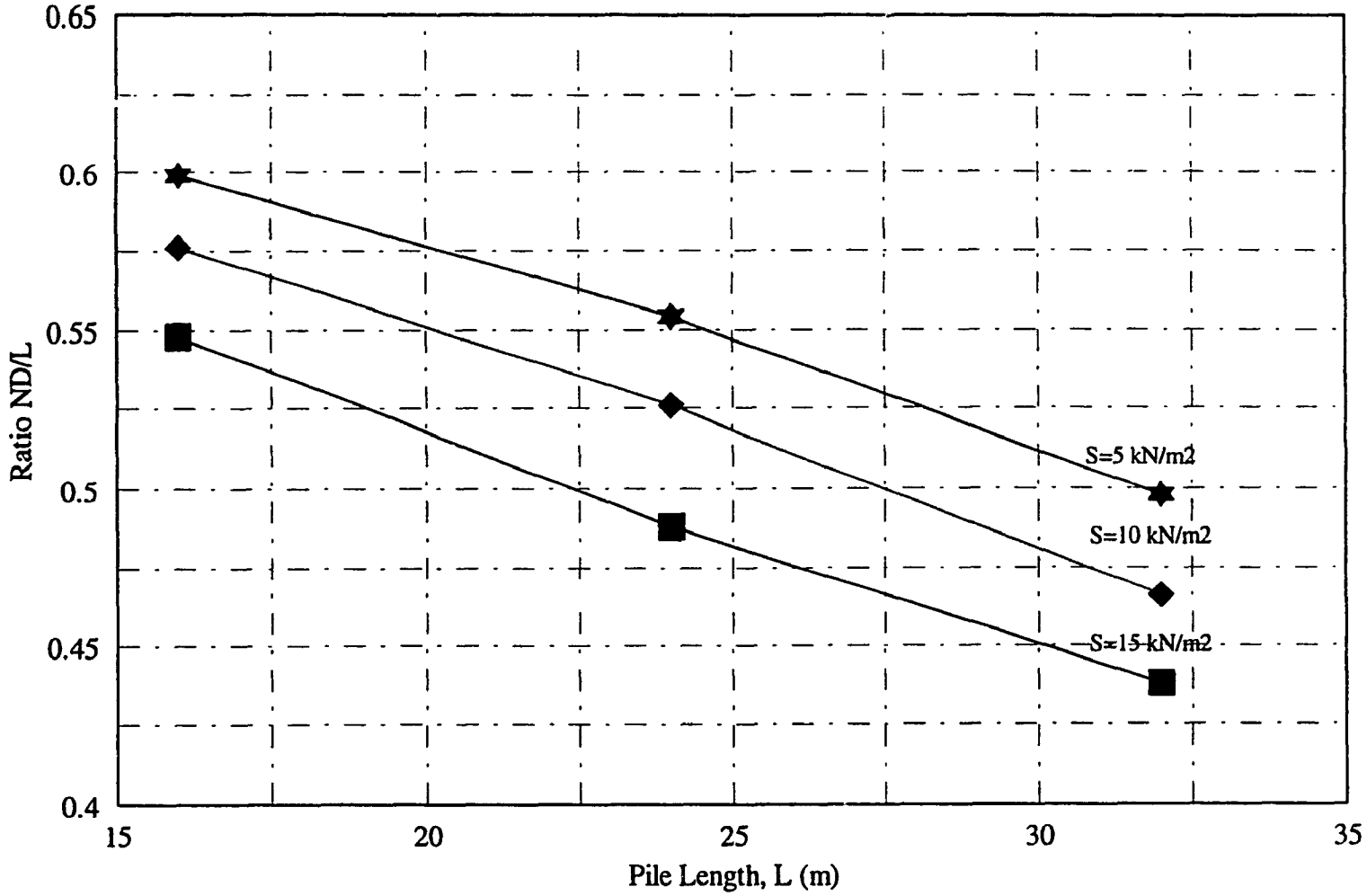

Fig. 4.20 Ratio ND/L Versus Pile Length, L (Cohesion, c=10 kN/m2)

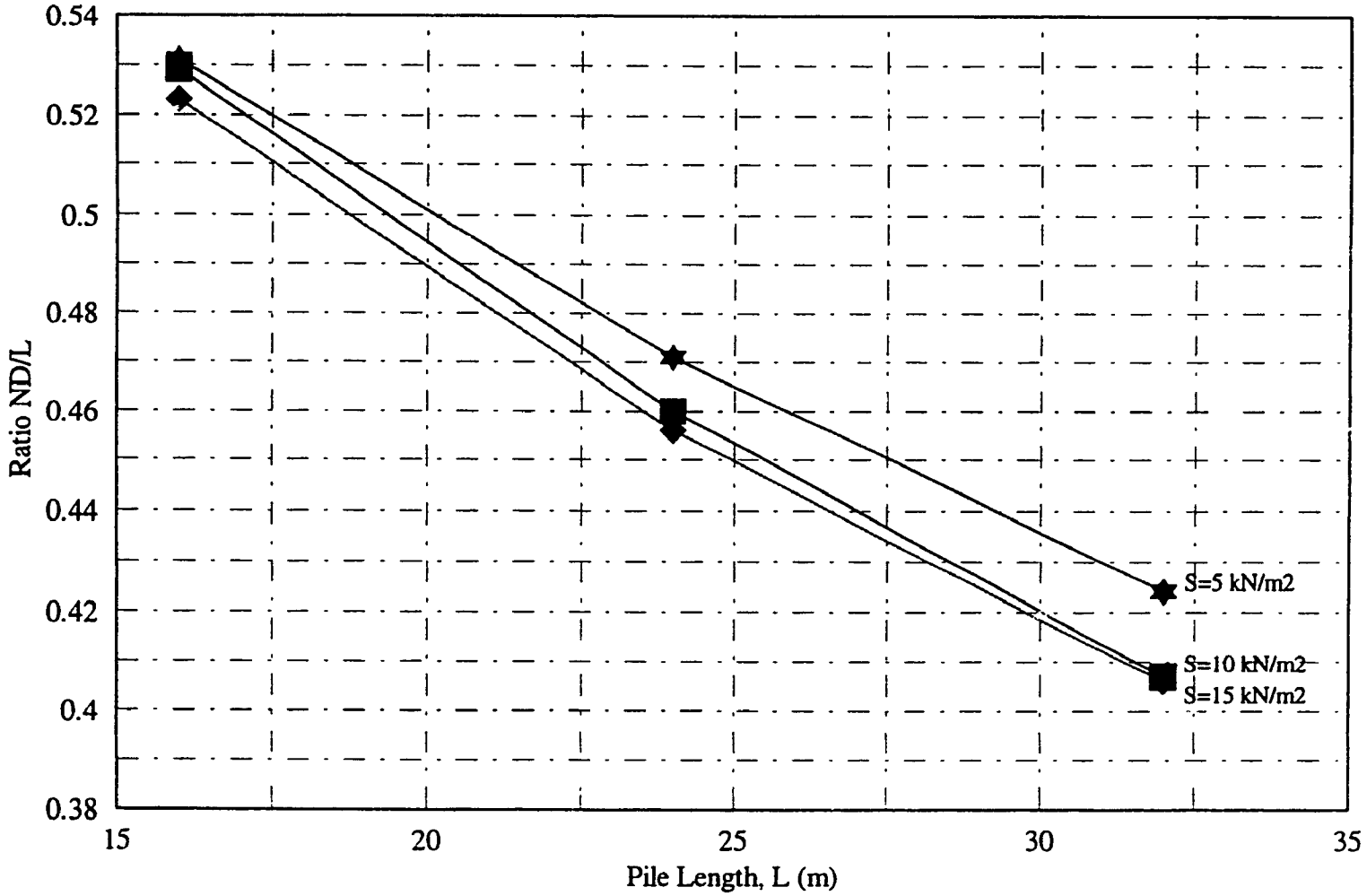

Fig. 4.21 Ratio ND/L Versus Pile Length, L (Cohesion, c=10 kN/m2)

4.4.2.3 Effect of the surcharge, S

Figures (4.22 & 4.23) show that the predicted ratio ND/L increases in case of weak soil due to an increase of the surcharge, S, while the increase seemed to be insignificant in case of strong soil.

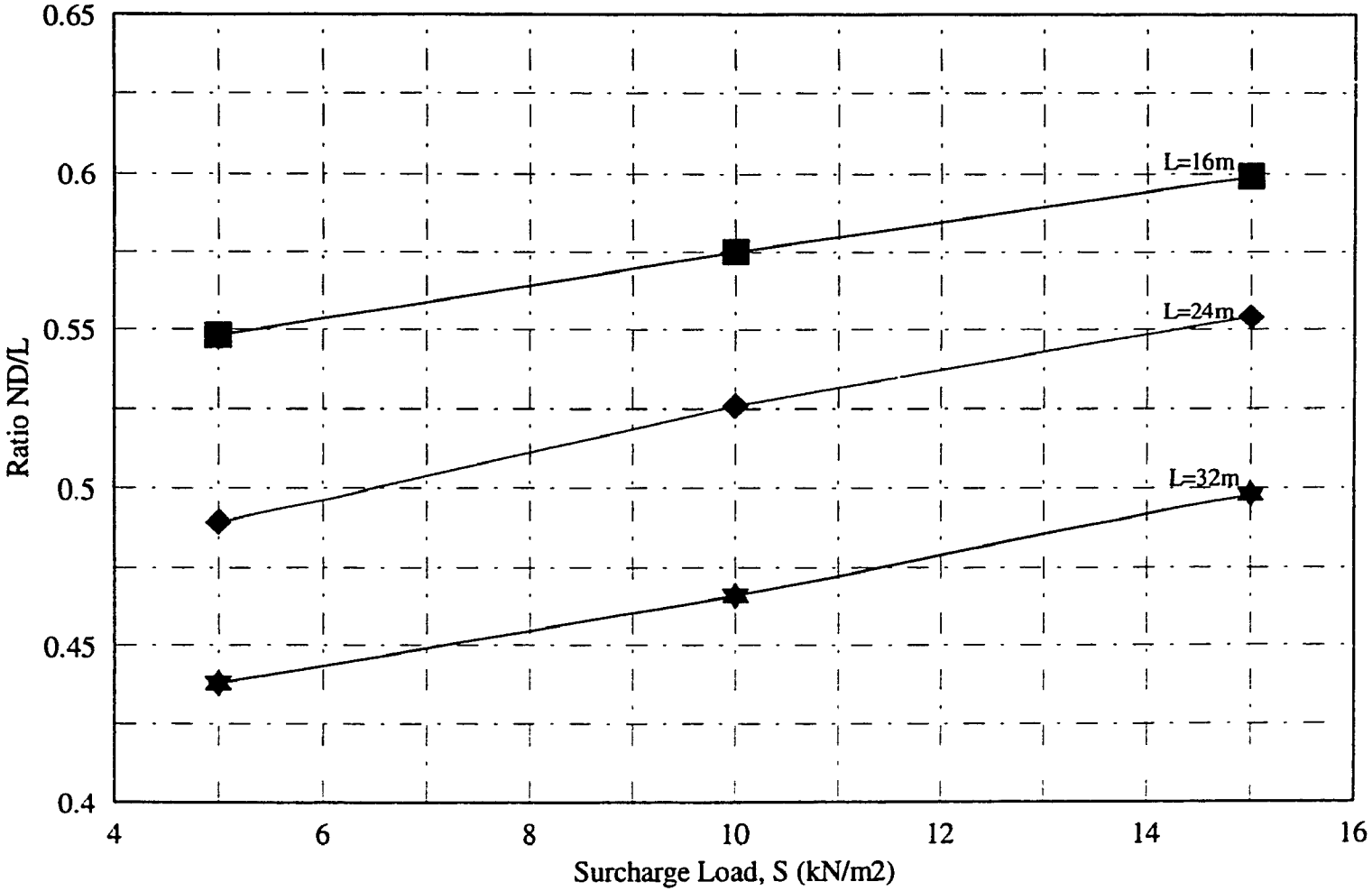

Fig. 4.22 Ratio ND/L Versus Surcharge Load, S (Cohesion = 10kN/m2)

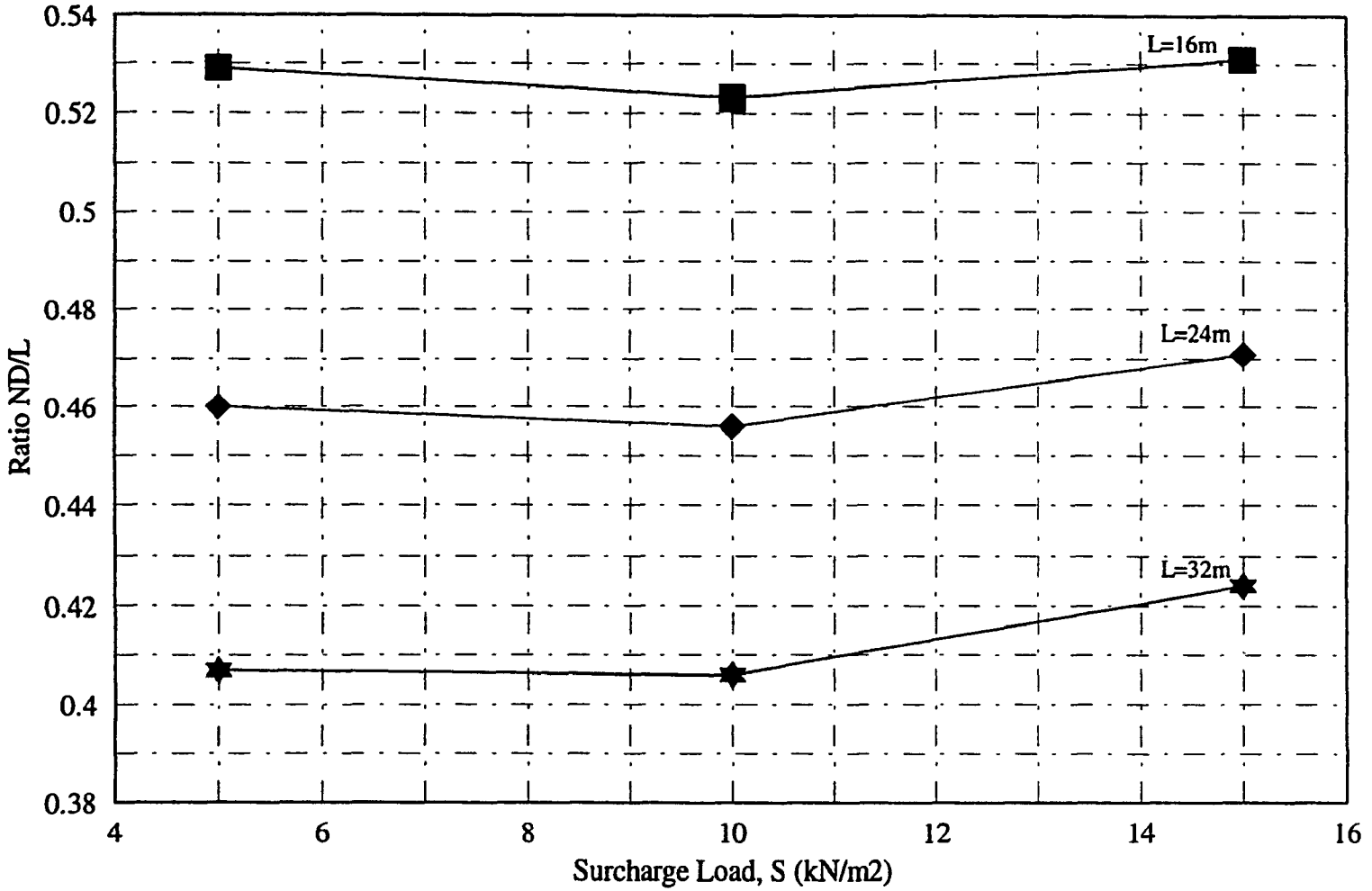

Fig. 4. 23 Ratio ND/L Versus Surcharge Load, S (Cohesion = 30kN/m2)

4.5 DETERMINATION OF THE NEUTRAL PLANE

4.5.1 Design Charts

Design charts are developed to facilitate the use of the results in the present investigation either by using critical state soil parameters as presented in Figures (4.24) to (4.26) or by using the Mohr-Coulomb soil parameters as shown in Figure (4.27).

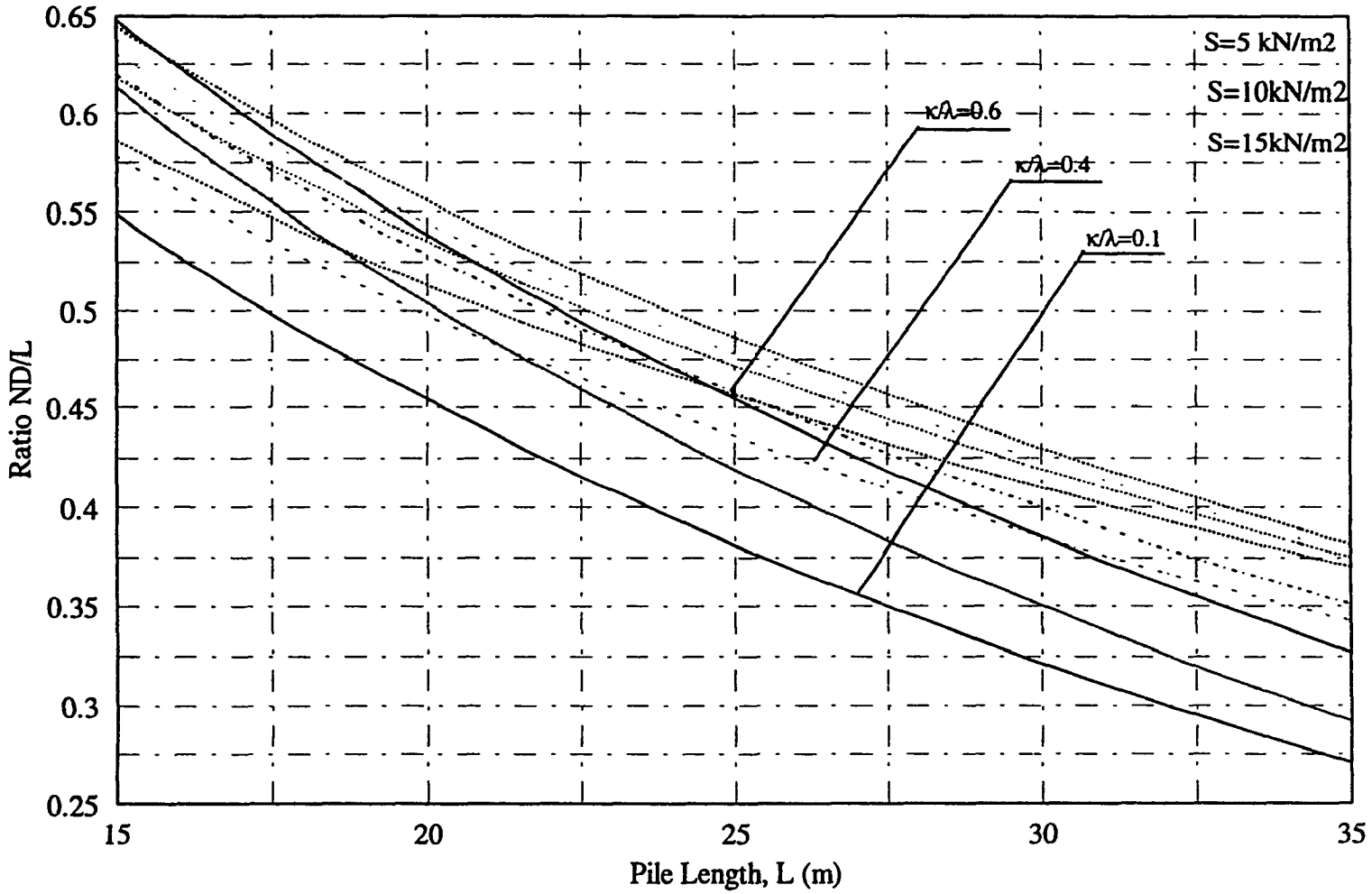

Fig. 4.24 Design Chart - Depth of Neutral Plane as a Function of Critical State Parameters. (M=0.77)

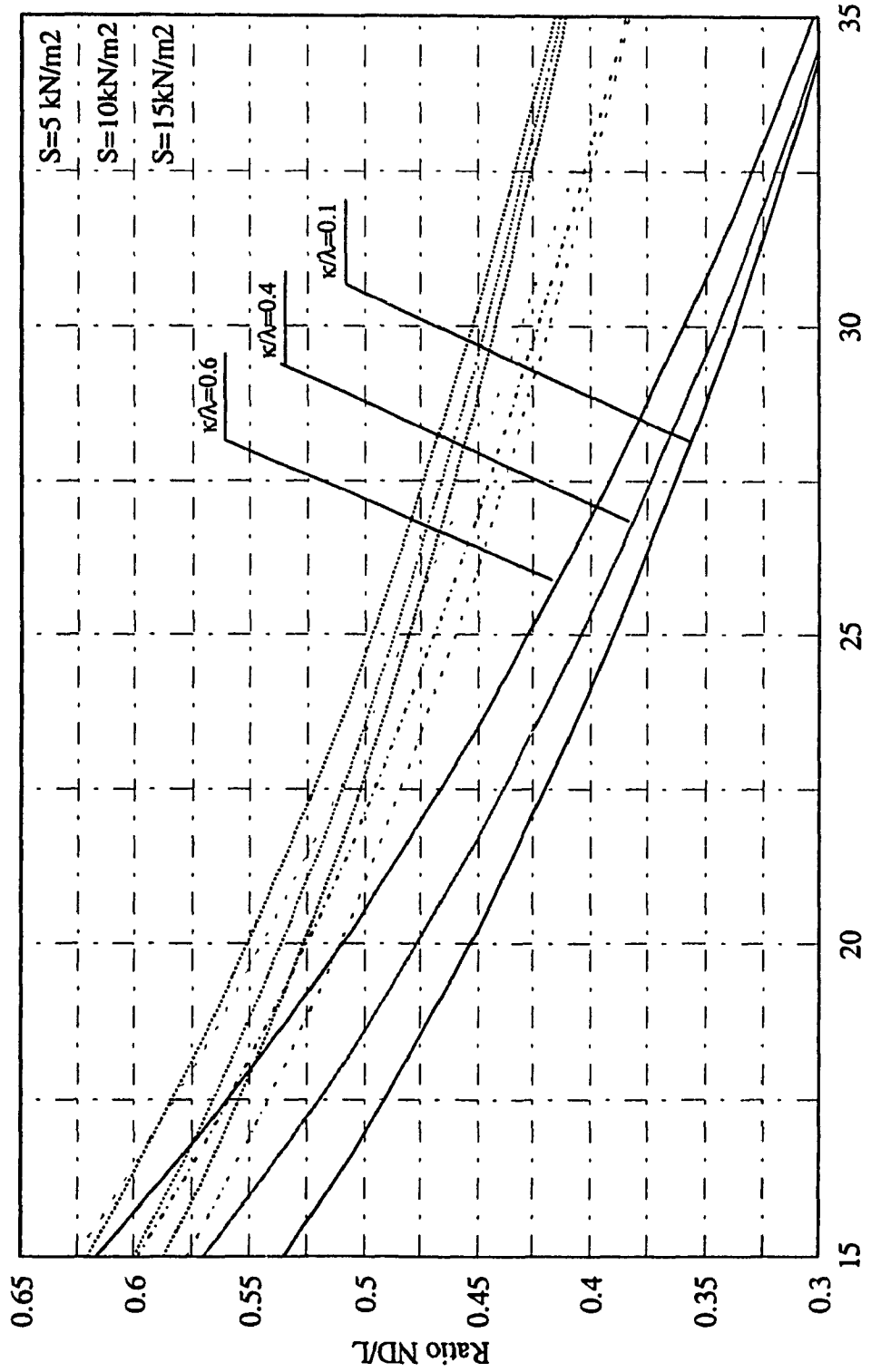

Fig. 4.25 Design Chart - Depth of Neutral Plane as a Function of Critical State Parameters. (M=1.00)

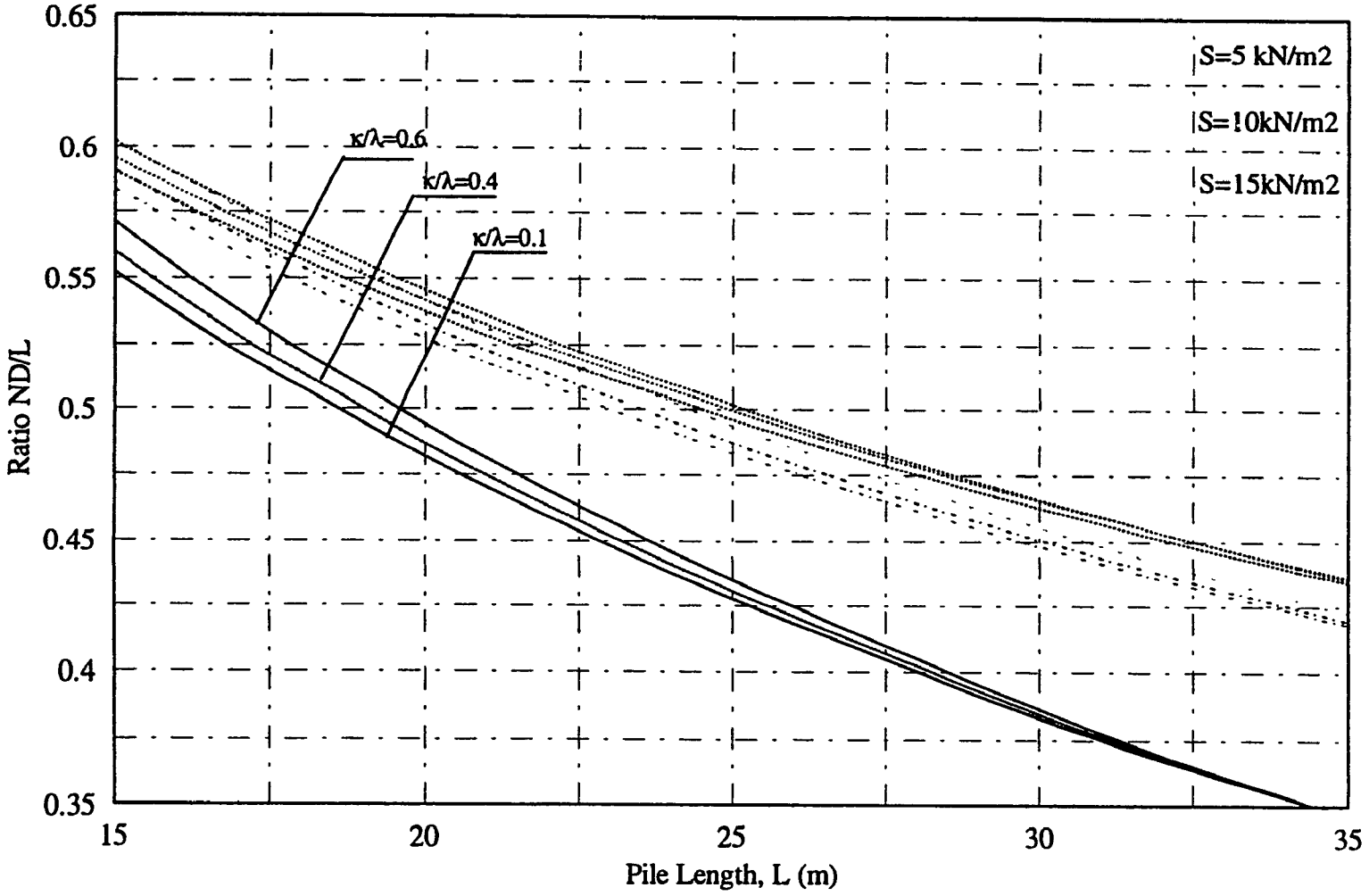

Fig. 4.26 Design Chart - Depth of Neutral Plane as a Function of Critical State Parameters. (M=1.40)

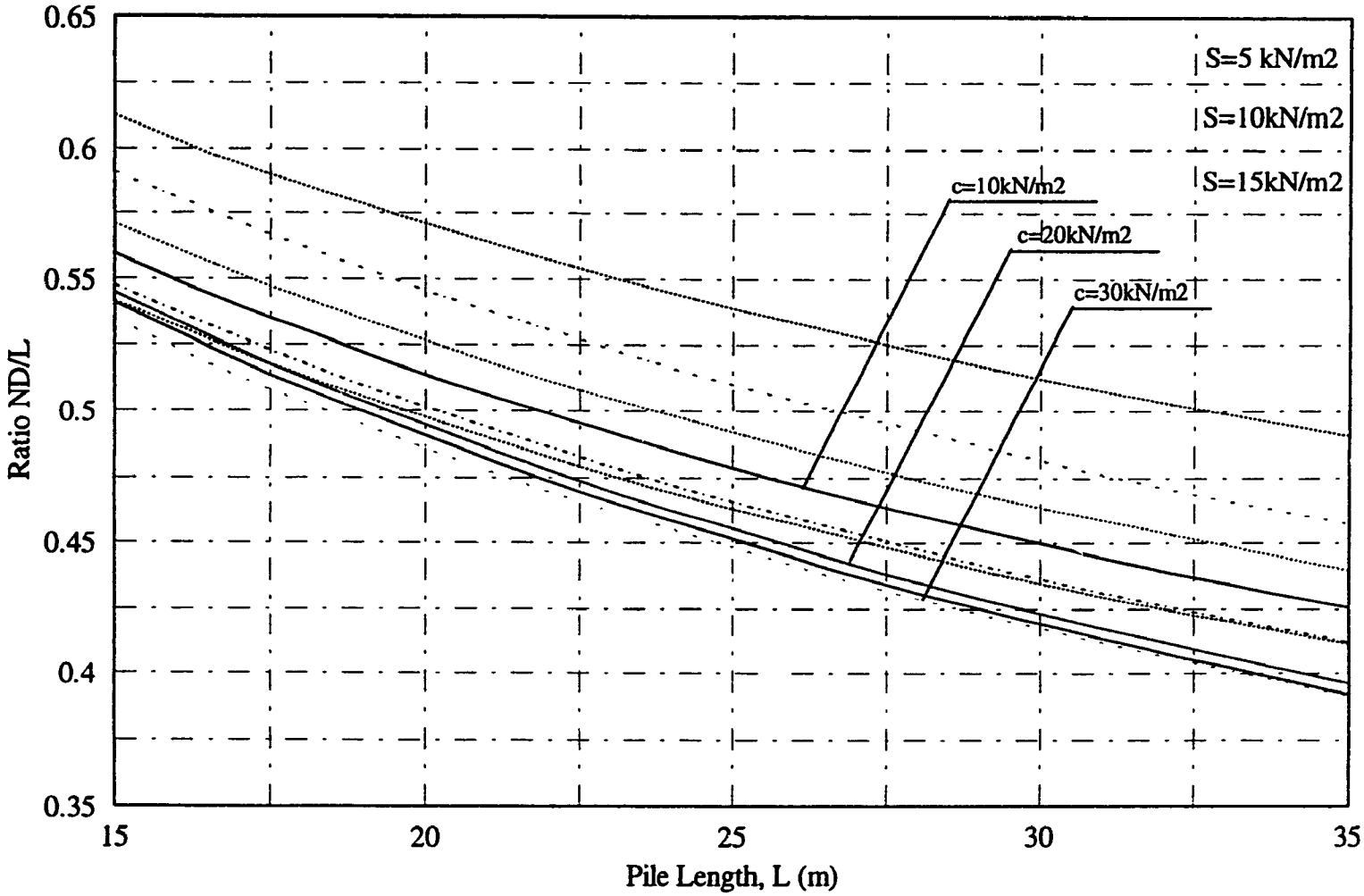

Fig. 4.27 Design Chart - Depth of Neutral Plane as a Function of the Cohesion, c.

4.5.2 Design Procedure

The proposed procedures of using the design charts are presented in the two following numerical examples:

Example no. 1, determination of the depth of the neutral plane for a case of κ/λ = 0.3, M =0.9, L=27.5 m and surcharge load, S = 8 kN/m^2, the following procedure steps is proposed in order to determine the neutral depth, ND

(a) From Figure(4.24) for S =5 kN/m^2 find the ratio ND/L for κ/λ = 0.1 and κ/λ = 0.4, these values are 0.35 and 0.415 respectively and by interpolation find the ratio ND/L for κ/λ = 0.3 which is 0.393

(b) Similarly from the same Figure (4.24) for S = 10 kN/m^2 find the ratio ND/L for κ/λ = 0.1 and κ/λ = 0.4, these values are 0.38 and 0.46 respectively and by interpolation find the ratio ND/L for κ/λ = 0.3 which is 0.433

(c) By interpolating between the two results from (a) and (b), the value of the ratio ND/L for κ/λ = 0.3 for surcharge, S=8 kN/m^2 can be found to be 0.417 which is in the case of M=0.77

(d) Similarly by repeating the procedure from (a) to (c) using figure (4.25), we predict the value of the ratio ND/L for κ/λ = 0.3 for surcharge, S=8 can be found to be 0.415 which is in the case of M=1.00

(e) By interpolating the 2 values of the ratio ND/L found from (c) and (d) find the ratio ND/L for the case of the example which is 0.416 and accordingly the depth of the neutral plane, ND = 11.23 m.

(f) Finally, apply Table (2.4) to predict the negative skin friction magnitude.

Example No. 2, determination of the depth of the neutral plane for a case of c = 15

kN/m^2, L=22.5 m and surcharge load, S = 13 kN/m^2, the following procedure steps is proposed in order to determine the neutral depth, ND

(a) From Figure(4.27) for c =10 kN/m^2 find the ratio ND/L for S = 15 kN/m^2 and S = 10 kN/m^2, these values are 0.56 and 0.525 respectively and by interpolation find the ratio ND/L for S =13 kN/m^2 which is 0.546

(b) Similarly from the same Figure (4.27) for c = 20 kN/m^2 find the ratio ND/L for S = 15 kN/m^2 and S = 10 kN/m^2, these values are 0.51 and 0.48 respectively and by interpolation find the ratio ND/L for S =13 kN/m^2 which is 0.498.

(c) By interpolating the 2 values of the ratio ND/L found from (a) and (b) find the ratio ND/L for the case of the example which is 0.522 and accordingly the depth of the neutral plane, ND = 11.75 m.

(d) Finally, apply Table (2.4) to predict the negative skin friction magnitude.

Fig. (4.28 - 4.30) show examples 1 and 2

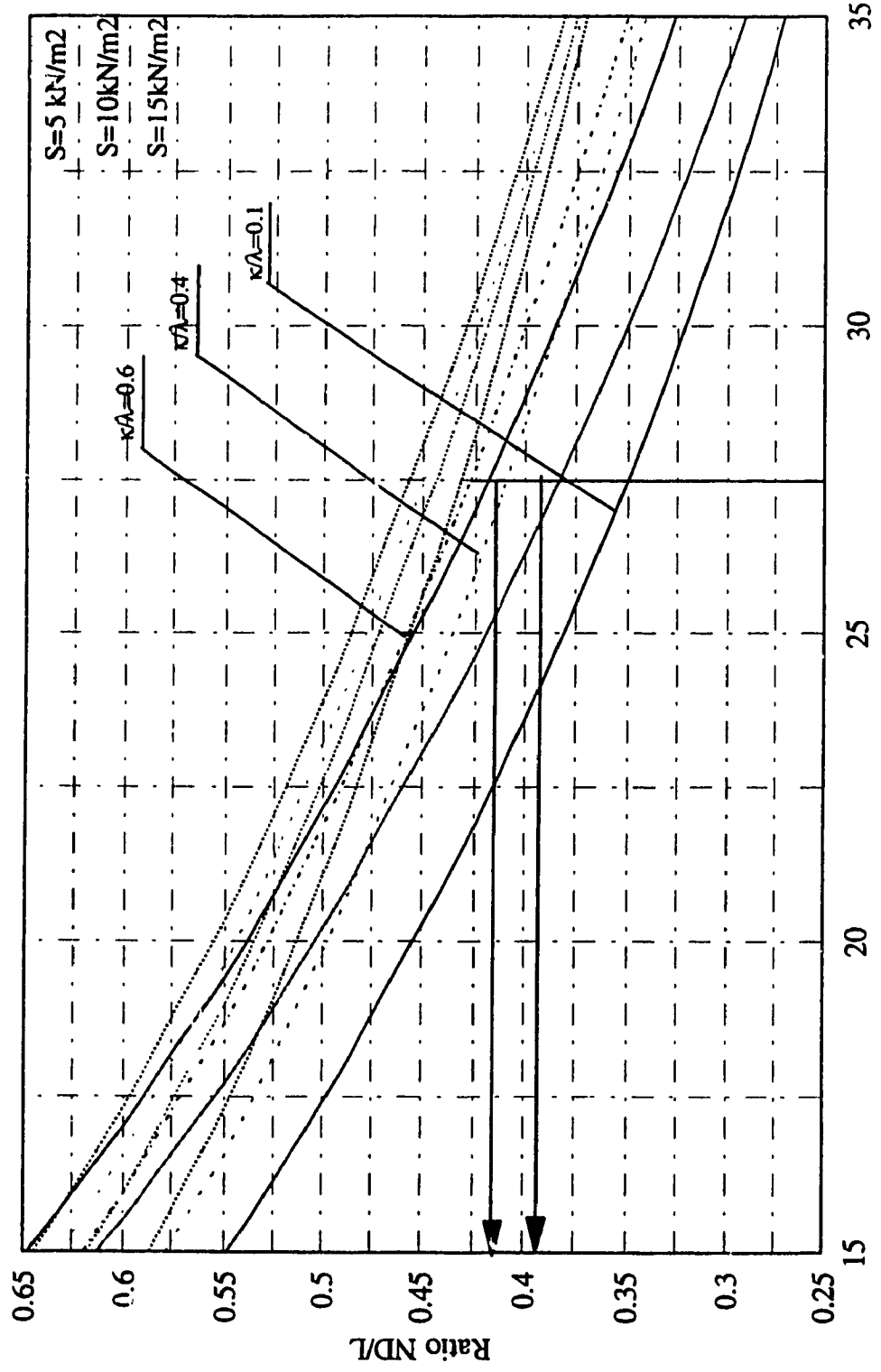

Fig. 4.28 Design Chart - Depth of Neutral Plane as a Function of Critical State Parameters. (M=0.77) (Example No. 1)

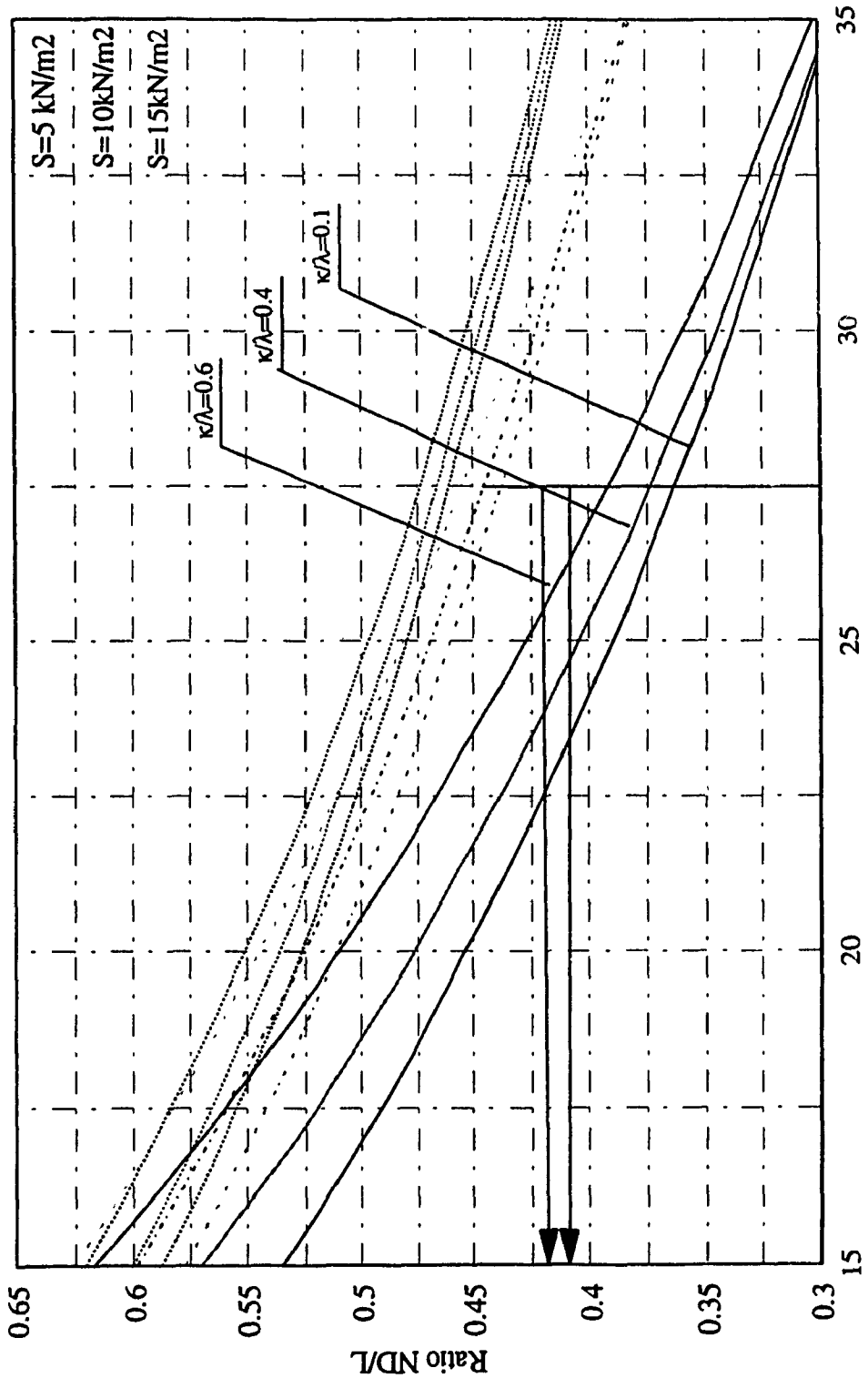

Fig. 4.29 Design Chart - Depth of Neutral Plane as a Function of Critical State Parameters. (M=1.00) (Example No. 1)

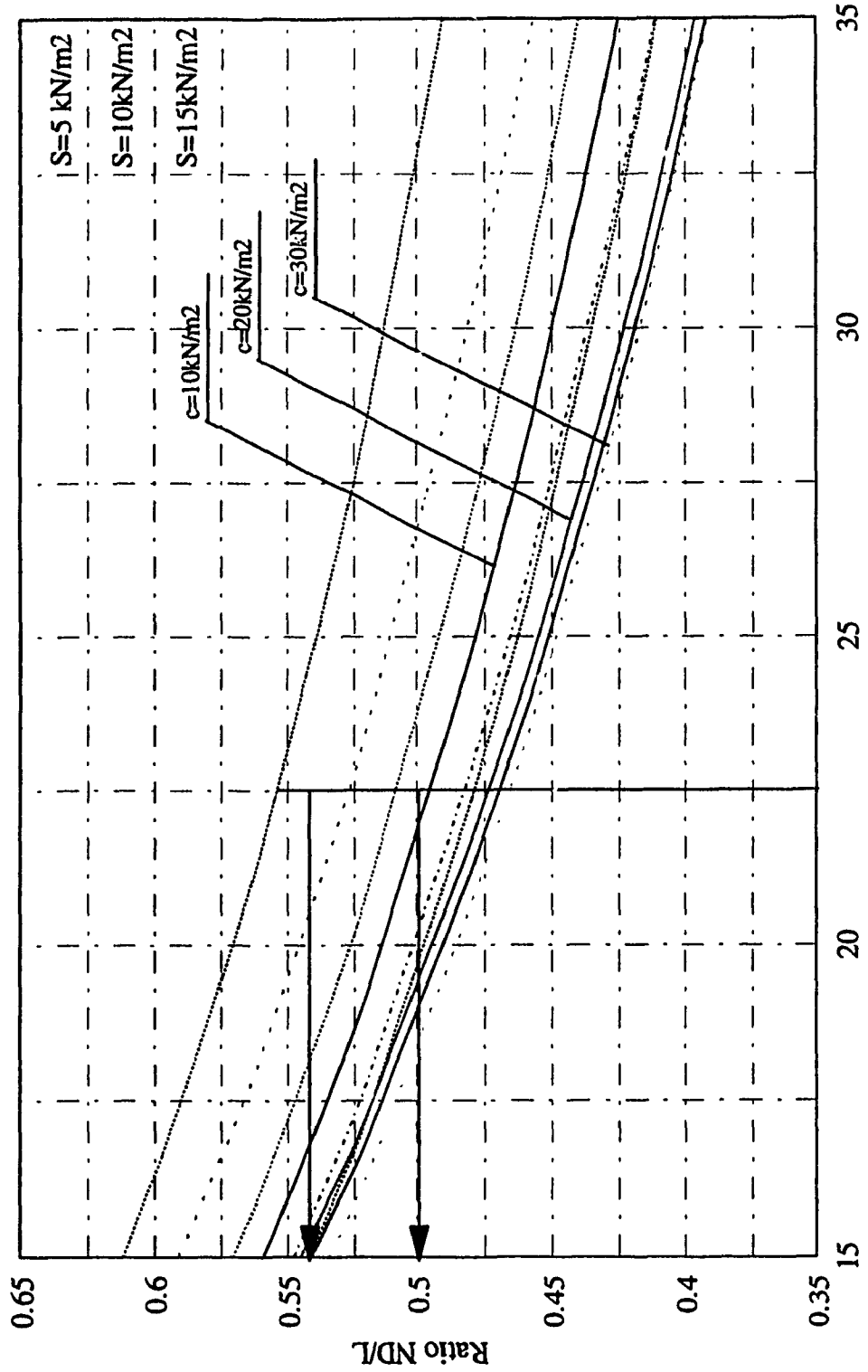

Fig. 4.30 Design Chart - Depth of Neutral Plane as a Function of the Cohesion, c. (Example No. 2)

CHAPTER 5

CONCLUSION AND RECOMMENDATIONS

5.1 CONCLUSION

Numerical investigation using finite element technique was conducted on the determination of the depth of the neutral plane of a single pile in clay, and subjected to indirect loading through the surcharge. The following can be concluded:

1- The finite element technique, together with the elasto-plastic model (Modified Cam Clay) or the elastic perfectly plastic model (Mohr-Coulomb) have provided an acceptable numerical model to solve the problem of the negative skin friction

2- Consolidation of the soil surrounding the pile due to surcharge loads induce negative skin friction on piles.

3- Based on the parametric study using the cam clay soil model:

(a) The depth of the neutral plane increase due to an increase of the pile length.

(b) The depth of the neutral plane is insensitive to the pile diameter, D.

(c) The depth of the neutral plane slightly increases due to an increase of the slope of the critical state slope line, λ.

(d) The depth of the neutral plane increase due to an increase of the slope of the swelling line, κ.

(e) The depth of the neutral plane increase due to an increase of the critical state friction coefficient, M.

(f) The depth of the neutral plane increase due to an increase of the surcharge load.

4- Based on the parametric study using the Mohr-Coulomb soil model

(a) The cohesion, c has a direct effect on the depth of the neutral plane, ND where an increase in the cohesion c leads to a decrease in the location of the neutral plane.

(b) The depth of the neutral plane increase due to an increase of the pile length.

(c) The depth of the neutral plane increase due to an increase of the surcharge load.

5- Design charts are presented to facilitate the determination of the location of the neutral plane for both critical state soil parameters and Mohr-Coulomb soil parameters, and accordingly the calculation of the negative and positive skin frictions.

5.2 RECOMMENDATIONS FOR FUTURE WORK

1- The study should be extended to investigate the effects of consolidation due to lowering the groundwater table and under the ownweight of the clay layer.

2- The present investigation should be extended to examine the effect of different variable soils.

3- Further studies are required to examine the effect of long term consolidation on the negative skin friction and the location of the neutral plane.

4- The present numerical model should be compared further with laboratory and field measurements.

5- The present investigation should be extended to examine the development of negative skin friction in a single pile subjected to direct and surcharge loading.

6-The present investigation should be extended to examine the development of negative skin friction on pile groups.

REFERENCES

1. Auvinet, G. and Hanell, J. J., 1981 "Negative skin friction on piles in Mexico clay" Proc. of the 10th Conf. SMFE, Stockholm, Sweden, vol. 2, pp.65-74.
2. Bozozuk, M. 1970 "Field Observation of negative skin friction loads on long piles in marine clay," Proc. Conf. on Design and Installation of Pile Foundation and Cellular Structures, Lehigh University, pp. 273-280.
3. Burland, J. 1973 "Shaft friction of piles in clay" Ground Engineering, Vol. 6, No.3, pp. 30-42.
4. Bozozuk, M. 1981, "Bearing capacity of pile preloaded by downdrag," Proc. of the 10th Conf. SMFE, Stockholm, Sweden, vol. 2, pp.631-636.
5. Brand, E. W. and Luangdilok, N. 1975, "A long-term failure caused by dragdown on piles," Proceeding, 4th, Southeast Asian Conf., Soil Eng., pp. 4.15-4.24.
6. Brito, A. M. 1995 'Crisp 95 user and programmer's guide" Cambridge University, Engineering Department.
7. Brito, A. M.; Gunn, M. J. 1987 "Critical state soil mechanics via finite elements" Jown Wiley & sons
8. Chellis, R. D. 1961 "Pile foundation," McGraw-Hill co., 2nd Ed.
9. Clement, F. M. Jr., 1984, "Downdrag, negative skin friction and bitumen coating on prestressed concrete piles," Ph.D Thesis submitted to the University of Tulane.
10. Desai, Chandakant S.; Siriwardane, Hemaj. 1984 "Constitutive laws for engineering materials with emphasis on geologic materials" Prenticeall, Inc., Englewood Cliffs, New Jersey.
11. Endo, M., Minov, A., Kawaski, T. and Shibata, t., 1969 "Negative skin friction act

ing on steel pipe-piles in clay," Proc., 7th.Iint. Conf. SMFE. Mexico, vol. 2, pp. 85-92.

12. Fellenius, B. H. 1972 "Downdrag on piles in clays due to negative skin friction," Canadian Geotechnical Journal, vol. 9, No. 4, pp. 325-337.

13. Fellenius, B. H. "unified design of piles and pile groups" Transportation research record 1169, department of Civil Engineering, University of Ottawa, Ontario K1N 6N5, Canada.

14. Garlanger, J. E. and Lambe, T. W. 1973, "Proceedings of a symposium on down drag of pile," Mass. Inst. Techn., Cambridge, Mass., Research Report, No. 73-56.

15. Garlanger, J. E. 1974, "Measurement of pile downdrag beneath a bridge abutment," Highway Research Board, Transp. Research Record No. 517, pp. 61-69.

16. Hansen, j. B. 1968, "A theory for skin friction on piles," Danish Geotechnical Insti tute, Bulletin No. 25, pp. 5-12.

17. Indraratra B. 1993 "Development of negative skin friction on driven piles in soft Bangkok clay" Canadian Geotechnical Journal vol. 30, 1993 pp. 887-888.

18. Matyas Elmer L.; Santamarina J. Carlos, 1994 "Negative skin friction and the neutral plane" Canadian Geotechnical Journal vol. 31, 1994 pp. 591-597.

19. Tam, Heng-Kong 1992 "Some applications of Cam Clay in numerical analysis", A thesis submitted for the degree of Doctor of Philosophy, the City University, England.

20. Trochanis, A. M.; Bielak, J. and Christiano, P. 1988 "A three dimensional nonlin ear study of piles leading to the development of a simplified model" A Technical Report of Research, The National Science Foundation, Carnegie Mellon

university, Pittsburgh PA 15213.

21. Zeevart, L. 1973, "Foundation engineering for difficult subsoil conditions," Van Nostrand Reinhold Co. New York.